"**Nematic Elastomer Nanocomposites as Electromechanical Actuators**"

Contract no: FA8655-04-1-3018

PI Dr. Eugene M Terentjev

Grant Report

This project had a pilot nature, on the one hand, exploring a possibility of active collaboration of our research group with EOARD and (via) the colleagues at Wright-Patterson AFB, on the other – making a focused attempt to explore a novel actuation system based on elastomer composite with aligned carbon nanotubes (CNT). The original proposal and the Interim Report outline the scientific background[i] and the principles behind the mechanical actuation in nanocomposite elastomers[ii]. Our main tasks have been:

(A) Develop the robust method of CNT dispersion in amorphous polymeric matrix and establish a set of quantitative methods to characterise the quality of this dispersion.

(B) Develop a technique for nanotube alignment on the dense polymer matrix, as well as the tools to characterise the degree of this alignment.

(C) Study the mechanical actuation in response to different stimuli: plain heating, IR irradiation, and electric field.

Preparation, stability and alignment of polymer nanocomposites are very significant and challenging areas. The review of key issues, materials and procedures involved, and the current state of the art in the literature is one of the main outcomes of this grant[iii]. Main results on mechanical actuation have been listed in the Interim Report and are presented in the short letter publication[iv], which is another outcome of this grant.

In all cases, for experiments on series of materials and compositions, we have used the isotropic elastomer matrix: the standard siloxane polymer (PDMS) crosslinkable into a rubber. Even though it was obvious from the outset that the nematic liquid crystal order in the matrix does have a number of particular advantages in promoting greater CNT alignment, we had to establish benchmarks for all effects and develop proper characterisation techniques.

The first stage of nanocomposite preparation is the dispersion of CNT aggregates. Figure 1a shows one of the key features of this process, characterized (among other ways) by continuously monitoring the viscosity of the mix. The jamming viscosity peak, and the onset of the subsequent plateau indicating the achieved dispersion, are functions

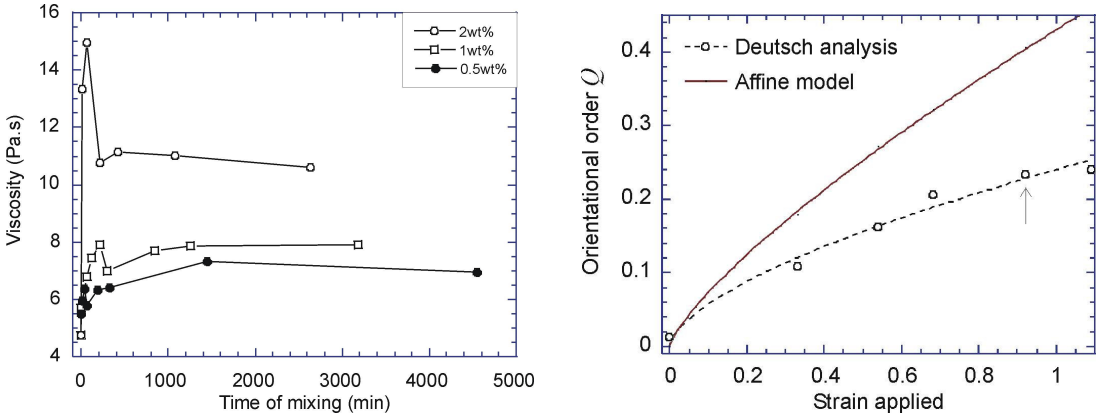

Figure 1: (a) – Viscosity of the sheared PDMS-CNT mixture, as function of time for increasing CNT loading; (b) – Orientational order parameter detected by Xray method and Deutsch analysis, compared with the maximum theoretical prediction of affine alignment.

REPORT DOCUMENTATION PAGE

Form Approved OMB No. 0704-0188

Public reporting burden for this collection of information is estimated to average 1 hour per response, including the time for reviewing instructions, searching existing data sources, gathering and maintaining the data needed, and completing and reviewing the collection of information. Send comments regarding this burden estimate or any other aspect of this collection of information, including suggestions for reducing the burden, to Department of Defense, Washington Headquarters Services, Directorate for Information Operations and Reports (0704-0188), 1215 Jefferson Davis Highway, Suite 1204, Arlington, VA 22202-4302. Respondents should be aware that notwithstanding any other provision of law, no person shall be subject to any penalty for failing to comply with a collection of information if it does not display a currently valid OMB control number.
PLEASE DO NOT RETURN YOUR FORM TO THE ABOVE ADDRESS.

1. REPORT DATE *(DD-MM-YYYY)*	2. REPORT TYPE	3. DATES COVERED *(From – To)*
07-03-2005	Final Report	23 December 2003 - 05-Apr-05

4. TITLE AND SUBTITLE

Nematic Elastomer Nanocomposites as Electromechanical Actuators

5a. CONTRACT NUMBER
FA8655-04-1-3018

5b. GRANT NUMBER

5c. PROGRAM ELEMENT NUMBER

6. AUTHOR(S)

Dr. Eugene M Terentjev

5d. PROJECT NUMBER

5d. TASK NUMBER

5e. WORK UNIT NUMBER

7. PERFORMING ORGANIZATION NAME(S) AND ADDRESS(ES)
University of Cambridge
Cavendish Laboratory
Madingley Road
Cambridge CB3 0HE
United Kingdom

8. PERFORMING ORGANIZATION REPORT NUMBER

N/A

9. SPONSORING/MONITORING AGENCY NAME(S) AND ADDRESS(ES)

EOARD
PSC 802 BOX 14
FPO 09499-0014

10. SPONSOR/MONITOR'S ACRONYM(S)

11. SPONSOR/MONITOR'S REPORT NUMBER(S)
SPC 04-3018

12. DISTRIBUTION/AVAILABILITY STATEMENT

Approved for public release; distribution is unlimited.

13. SUPPLEMENTARY NOTES

14. ABSTRACT

This report results from a contract tasking University of Cambridge as follows: The Grantee will investigate
a. Dispersal of carbon nanotubes and their alignment in a polymer/elastomer matrix
b. Characterisation of nanocomposites embedded in the bulk of insulating amorphous matrix
c. Study of electrically- and thermally driven mechanical actuation in nanocomposites
d. Understanding mechanisms of electromechanical effect

15. SUBJECT TERMS
EOARD, Elastomers, Liquid Crystals, Carbon nanomaterials

16. SECURITY CLASSIFICATION OF:			17. LIMITATION OF ABSTRACT	18, NUMBER OF PAGES	19a. NAME OF RESPONSIBLE PERSON
a. REPORT	b. ABSTRACT	c. THIS PAGE			MATTHEW MORGAN, Lt Col, USAF
UNCLAS	UNCLAS	UNCLAS	UL	132	19b. TELEPHONE NUMBER *(Include area code)* +44 (0)20 7514 4505

of CNT loading and the local shear stress (viscosity*shear rate). The required mixing time is a function of these two parameters.
Once CNT are dispersed in the polymer matrix, the only practical way of stabilization is its crosslinking. Other methods used (reviewed in [iii]) rely on surface modifications of CNT and ultimately degrade their response to electric field or photon absorptivity. This issue is often ignored in studies of composites for their mechanical properties, but is key for the actuation response.
Figure 1b shows the result of the alignment study. On stretching of the crosslinked nanocomposite elastomer the tubes acquire alignment. Its monitoring by wide-angle Xray scattering requires careful analysis. The currently most advanced analysis of the azimuthal intensity bias is based on the Deutsch approach. The description of this, and the theoretical prediction of tube alignment are detailed in [iii,iv].
The main result of the actuation study, described in greater detail in the Interim Report, and in the publications, is the dependence of its amplitude and even sign (contraction vs. extension of the material on stimulus) on the degree of CNT alignment. It is proven that IR photon absorption, and not plain heating, that is the underlying cause of actuation. Theoretical modelling of the mechanical response as function of CNT alignment, see sketch in Figure 2, indicates that tubes experience significant contortion, which then translates into the macroscopic network response. Much work remains to be done to optimize the effect and really understand its mechanism.

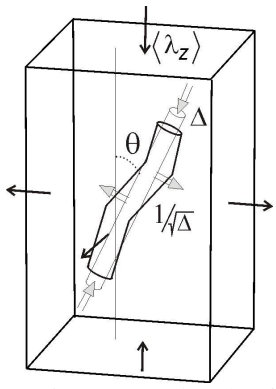

Figure 2 – Sketch of CNT response

Conclusions:

In summary, the work progressed successfully. The initial pursuit of electromechanical actuation effect has been deflected into more fundamental studies of nanocomposite formation, alignment and development of ways of characterizing their properties. The main actuation investigated in detail here was the stimulation by IR radiation. The study focused on underlying mechanism, establishing its dependence on the degree of nanotube alignment in the rubbery matrix.
The grant provided only a small support for a pilot study of preparation and actuation response of new elastomer nanocomposite systems, showing possible directions of future work. However, it enabled the work to proceed and also stimulated active collaboration between our group and that of Dr. R Vaia (WPAFB). Dr. Vaia has visited us in Cambridge this summer. We continue to have an on-going exchange of samples, tests and ideas. With the help of this grant we were able to purchase a sufficient amount of chemical consumables (to enable wider spread of chemical synthesis and material testing, pursuing broader temperature range), finance a major literature investigation and writing of a review article on polymer nanocomposites, and support several overseas visits.
The review, and the short original article outlining the results on IR-stimulated actuation are attached and form a part of this final report (the EOARD support is acknowledged in both publications). There were no subject inventions to declare as defined in FAR 52.227-13, during the performance of this contract.

---

[i] M. Warner and E.M. Terentjev, *Liquid Crystal Elastomers*, Oxford Univ. Press 2003.
[ii] S. Courty, J. Mine, A.R. Tajbakhsh, and E.M. Terentjev, Europhys.Lett. 64:654, 2003;
H. Koerner, G. Price, N.A. Pearce, M. Alexander and R.A. Vaia, Nature Mater. 3:115, 2004.
[iii] S.V. Ahir and E.M. Terentjev, Review chapter in: **"**Polymeric Nanostructures and Their Applications**"**, ed. H.S. Nalwa, Amer. Sci. Publishers, 2005.
[iv] S.V. Ahir and E.M. Terentjev, Nature Mater. *In press*, 2005.

"**Nematic Elastomer Nanocomposites as Electromechanical Actuators**"

Contract no: FA8655-04-1-3018

PI Dr. Eugene M Terentjev

Interim Report

This project has a pilot nature, on the one hand, exploring a possibility of active collaboration of our research group with EOARD and(via) the colleagues at Wright-Patterson AFB, on the other – making a focused attempt to explore a novel actuation system based on nematic (or isotropic) elastomer composite with aligned carbon nanotubes.

A brief summary of local grant administration is due. The direct interaction between individual researchers and their sponsors is now complicated by the changing internal procedures within Cambridge University. The central Research Services Division (RSD) is established to monitor and manage the IPR position and control the spending. In some cases, the contract negotiations ensuing between the RSD and the sponsor result in delays. Another aspect relates to the overhead charge, which with EOARD would stand at 70%. With a relatively small grant issued in US dollars (with a current unflavoured exchange rate), to make this effective we had to take a route bypassing the Central University administration. EOARD has offered the contract to the PI personally, which was then passed on into the group internal donation account and used in the most effective way possible. This cannot be a permanent way of business, but ought to be kept in mind as an option for the future.

Background and Aims:

Carbon nanotube composites with polymeric materials represent a surprisingly small (in relative terms) sector of the overall international research effort in nanotechnology. One of the reasons is the lack of quantitative and reproducible ways of CNT dispersion, in solvents or directly in polymer melts. The second major difficulty preventing this field from fast development is the lack of characterisation techniques that would unambiguously monitor the state of CNT dispersion and alignment in the dense matrix. Resolving this, or at least making a systematic starting point for all planned future work, has been the first and the main task of this programme.

Accordingly, our main tasks for this first year have been (and remain):

(A) Develop the robust method of CNT dispersion in amorphous polymeric matrix and a set of quantitative methods to characterise the quality of this dispersion.

(B) Develop a technique for nanotube alignment on the dense polymer matrix, as well as the tools to characterise the degree of this alignment.

(C) Study the mechanical actuation in response to different stimuli: plain heating, IR irradiation, electric field.

In all cases, we have used the isotropic matrix: the archetypical PDMS crosslinkable into a rubber. Even though it was obvious from the outset that the nematic liquid crystal order in the matrix does have a number of particular advantages, we had to establish benchmarks for all effects and develop proper characterisation techniques.

Interim Results:

A1. The main effort and time, as well as consumables, have been spent on the study of CNT dispersing. We have gone systematically through a number of classical methods, from ultrasonic bath and high-power ultrasonic tip mixing, to chemical modification of CNT surface, to plain mixing with a high-rpm shear mixer. The conclusions can be summarised in brief: (i) we decided against ultrasonic methods, whether low- or high-powered, on the grounds that one has no real control over the amount of mechanical energy supplied to system – thus making it impossible to quantify (and in some cases, almost certainly breaking CNTs up in the process); (ii) we decided against a variety of possible surface modifications, since they invariably alter the fundamental properties of CNTs (such as polarisability and bending rigidity); (iii) we decided in favour of shear mixing with a well-controlled rpm, tip radius, vessel gap and the matrix viscosity giving the accurate value of shear stress locally supplied to the CNT vicinity (which is the correct control variable for this process). We were able to generate a plot of characteristic time t* required for the CNTs to be completely dispersed, vs local shear stress. The most direct way to decrease this mixing time was to reduce the amount of solvent, making the mix of higher viscosity – in this way one can get several orders of magnitude increase in local stress, as opposed to limitations in increasing the mixer rpm. It is also important to note that the mixing time t* is relatively large in all situations (many hours even in a quite viscous PDMS melt) and that re-aggregation of CNTs is a process starting immediately after the mixing seizes.

A2. In the key plot t*(σ) mentioned above, the criterion of "complete dispersion" is hard to test. This is one of the big challenges in the field of polymer nanocomposites, with no unique solution. We used a combination of SEM/TEM of fractured surfaces (counting exposed CNT concentration), measurement of dielectric constant and of resistivity – all in conjunction with accurate theoretical prediction of the corresponding response for a given loading percentage and the assumption of uniform isotropic dispersion. In practice, this remains an ongoing work because none of the methods in isolation can even theoretically provide a quantitative method of assessing the dispersion.

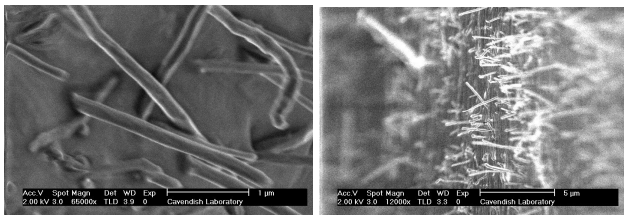

(a) (b)

Fig.1 SEM images of nanocomposite surfaces in different orientations of fracture. The apparently good alignment in (b) is an artefact of fracturing and pulling CNTs out.

B. Alignment of CNTs in a nematic elastomer has been easy and reached very high degree. In contrast, our initial expectation, that stretching the PDMS composite before crosslinking would produce a strong alignment has not been confirmed. This was the main method: after the proper mixing (t>t*) the polymer was quickly doped with the crosslinker+initiator mixture. Having previously timed the rate of the crosslinking reaction, we took the gel at about 50% crosslinking, stretched by 50-100% and then allowed to crosslink fully. This is a method of choice in producing the best monodomain nematic elastomers. However, although the

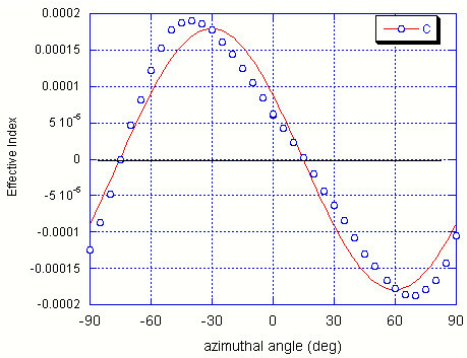

Fig.2 Variation of the effective refractive index difference Δn with the angle to analyser; the fit is to Sin 2θ: the typical birefringent response.

resulting composite PDMS rubber was very clearly birefringent (fig.2), the CNTs were not aligned to a great degree. Fig.3 shows a typical Xray image with very little azimuthal bias. The two results do not contradict each other: the birefringence is a much more sensitive technique and the value (0.0002) is very low, comparing with what one could expect for well-aligned highly polarisable CNTs. Note that Xray characterisation is also a challenge because we need to have a low CNT loading (to avoid percolation and conductivity), which gives only a weak contrast. We now plan to examine several new alignment methods (such as fiber drawing, or electric field), as well as return back to nematic elastomer nanocomposites where the alignment is assured.

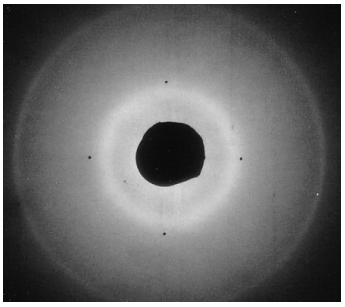

Fig.3 Outer ring (3.6nm) shows little azimuthal bias, showing only very low alignment.

C. Before proceeding to the main target of this project, the electrically stimulated actuation, we had to examine the response of PDMS nanocomposites to other stimuli. First of all – to reassure ourselves that we understand the mechanisms of CNT interaction with the matrix.

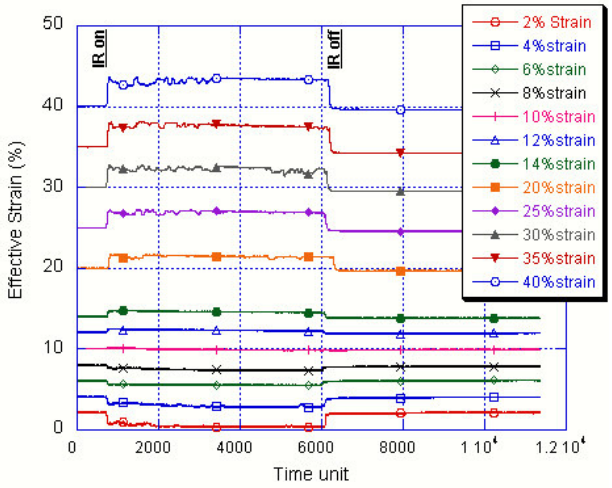

Fig.4. Response of PDMS nanocomposite (initially unaligned) to the IR irradiation. Curves show the response at different degrees of pre-strain, which we assume produces an increasing CNT alignment. Response changes at 10% strain.

Subjecting our materials to a mild IR radiation we found the first unexpected result. Fig.4 shows (for a nanocomposite with 1wt% CNT loading, initially non-aligned) that the material has a significant "thermal" expansion (of 2-3%). Thermal is in quotes because although IR induces the temperature increase (which we detect), a control experiment when the same temperature increase is provided (in the oven) gives at least an order of magnitude less response. Clearly the IR (electromagnetic) radiation interacts with CNTs directly, and not via random molecular motion of heat. Needless to say that a control sample (with no CNTs) had no noticeable response to IR.

The second remarkable aspect of the data shown in Fig.4 is that when the same nanocomposite is subjected to a certain pre-strain before IR irradiation, the response changes qualitatively. After a crossover (at ~10% pre-strain), we begin to see the increasing uniaxial contraction of nanocomposite along the axis of pre-strain. The magnitude of this relative contraction reaches 5-10% in different materials. This crossover effect is reproduced, albeit with a much lower amplitude, on plain heating. Our current assumption, which goes into the theoretical model that describes this phenomenon, is that on pre-straining we induce an increasing degree of CNT alignment. Aligned nanotubes respond to IR (and other excitations) in a certain coherent way – effectively reducing their length by a significant factor (~30-50% is required for each tube to produce the macroscopic effect shown in Fig.4). We believe the startling results

of nematic nanocomposite response to electric field were due to this good alignment as well.

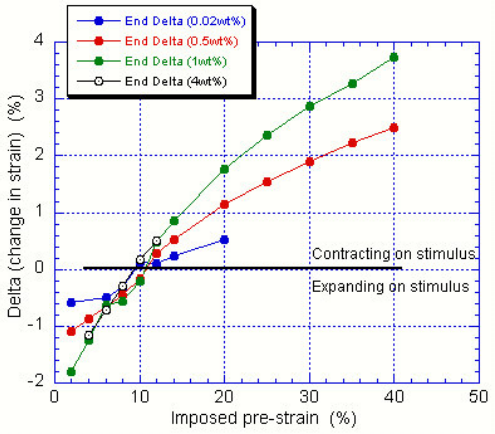

Fig.5 Aggregate plot of response at different pre-strain and CNT loading. Clearly the composite is more sensitive at higher loading, but also note the crossover universality.

To quantify this effect, Fig. 5 shows the collection of data for a series of PDMS nanocomposites. Two things become obvious: that on increasing the CNT loading the effect is enhanced and that the crossover from stimulated expansion to contraction occurs at the same pre-strain of the order 10%. The first fact seems natural, but in practice one cannot increase the loading too much: on high loading above percolation threshold the response changes dramatically once again. The universal crossover is a good new, supporting our idea that the induced alignment (tubes rotate affinely with the imposed macro-deformation) is the explanation. Apparently there is critical value of (low) induced CNT order above, which the material behaves as a contractile actuator while below which it is expanding on IR stimulus.

Conclusions:

The work progresses successfully. The current grant provides only a small support for a pilot study of nanocomposites showing possible directions of future work. However, it enabled the work to proceed and also stimulated active collaboration between our group and that of Dr. R Vaia (WPAFB). Dr. Vaia has visited us in Cambridge this summer. We continue to have an on-going exchange of samples, tests and ideas. The final report will probably give more information than in this interim report, with perhaps certain parameters improved. We hope to derive a model of what happens to each nanotube on the stimulus signal and also have the electric field stimulation investigated. However, it is clear that a longer and more involved research is needed to achieve a qualitative breakthrough we hope for. Two figures below indicate how much we do not understand (and do not expect) in CNT nanocomposites, even on a basic level of PDMS.

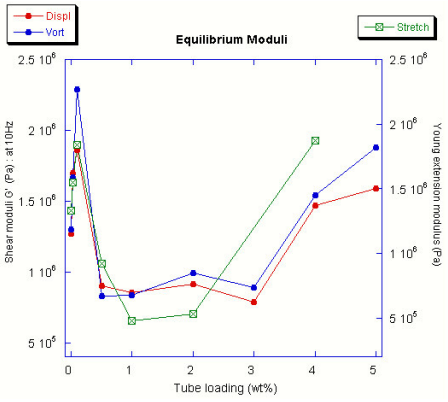

Fig.6 Young and Shear moduli of PDMS nanocomposites as function of loading. We associate the non-monotonic behaviour with the spontaneous CNT alignment into the Onsager nematic phase, cf. Fig.7.

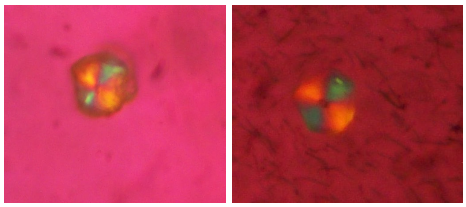

Fig.7 Spontaneously ordered nematic "droplet" seen in an initially homogeneous composite (with no crosslinking), when the tendency to phase separate and re-aggregate creates regions of higher CNT concentration (exceeding the Onsager threshold).

Polymers containing Carbon Nanotubes: Active Composite Materials

S. V. Ahir and E. M. Terentjev*

Cavendish Laboratory, University of Cambridge,
Cambridge CB3 0HE, U.K.

*To whom correspondence should be addressed; E-mail: emt1000@cam.ac.uk

31 January 2005

Abstract

We review the current state of the polymer-nanotube composites field. The article first covers key points in carbon nanotube preparation and physical properties, then focusing in greater detail on questions of dispersion, alignment and stabilization of nanotubes in a polymer matrix. Particular attention is paid to the types and quality of nanotubes used in composites. Physical properties of such materials are summarized along with possible production routes. We then focus on the emerging trends in polymer-nanotube actuators, in particular, electrically and photo-stimulated, and discuss their possible actuation mechanisms.

Contents

1 Introduction

The concept of nanoscience is older than many would otherwise think. It was Richard Feynman, who first suggested in the celebrated lecture in 1959 that there is no fundamental objection to manipulating matter on the atomic scale, making for "plenty of room at the bottom" [1]. The now fashionable word *nanotechnology* was conceived by Norio Taniguchi in 1974. A number of excellent monographs, over the years, have formulated the key ideas of this field [2, 3, 4]. So what exactly is nanoscience? An initial thought might be the science of very small objects, about a billionth of a meter dimensionally. Interestingly, size alone is not enough. Control of the properties at this length scale is also important. A very good example of such a system is the carbon nanotube. This review will explore some properties and dimensional dependence of such tubes, as well as explain their role when added to a continuous polymer matrix to form polymer-nanotube composites.

Composites as a class of materials have existed for many millennia and are prevalent in both nature and among engineering materials. Basically, a definition of a classical composite is a continuous system with inhomogeneity on the length scales that are much larger than atomic (to allow us to use the equations of classical physics), but are essentially homogeneous macroscopically. A number of substantial monographs illuminate this field of study, e.g. [5, 6].

The practice of creating synthetic polymer based composites originates from pioneering work undertaken in the 1970's, mostly in military-based research, on carbon fibre reinforced thermosets and thermoplastics. Perhaps the most famous of these materials is carbon fibre composite; it has been in use for more than three decades and many reviews and books have appeared in the field [7, 8, 9, 10]. There has always been an interest in carbon in its fibrous form due to its covalent in-plane bonding, considered amongst the strongest in

nature, imparting a great deal of structural strength. It is essentially the same bonding regime as found in individual graphene sheets within graphite. Carbon fiber is an ideal reinforcing agent in aerospace composites due to its strength to weight ratio and currently leads the way in advanced composites in service.

But what would make an ideal fibre? Issues of processability and cost effective production aside, the perfect fibre would have to be free of defects and posses a structure akin to single-crystal graphite. Carbon fibres currently in use contain large amounts of structural defects and impurities along the surface which largely disables their ability to achieve strength, toughness and conductivities approaching their theoretical limit.

An ideal nanometer sized fibre would also raise the possibility of having a quasi-one-dimensional structure embedded in the continuous elastic matrix, which would be of immense benefit to fundamental scientific research, for example, testing a multitude of physical phenomenon that are dimensionally correlated [11]. Normal carbon fibre are much greater in size, rendering them less than perfect for idealized structural studies. Additionally, other types of fibres and devices can be fabricated to create semi-one-dimensional systems using semiconductor nanolithographic techniques (amongst others) but even these processes are limited to making structures $\sim$50nm in width [11]. Compare this length-scale with that of an sp^3 hybridized carbon bond which is an order of magnitude less and can thus create structures which truly approximate one-dimensional topologies. The discovery of fullerenes [12] certainly made this a reality and paved the way for more exotic nanometer scale structures based around the C-C sp^3 and sp^2 hybridized bonds.

The most celebrated of these exotic nanometer scaled structures is a tube made of carbon with a acicular single crystal structure much like a tubular version of fullerene, termed carbon nanotubes. The seminal paper by Iijima [13] in

1991 is widely regarded as having introduced and started the nanotube revolution. However, it is interesting to note that the first patent regarding nanotubes was registered as early as in 1987 by Hyperion [14]. Furthermore, the first images of a nanotube were produced by Endo back in 1975 [15] though at the time, it was not given any thought or focus. Clearly, nanotubes were discovered before 1991 but it was only after Iijima's work that global scientific attention was rightly turned to these curious allotropes of carbon.

Multi-wall carbon nanotubes (MWNTs) were first reported in 1991 [13] but the single-wall variety of nanotubes was theorized in 1992 [16] with experimental confirmation of its existence following soon after [17, 18, 19]. Single-wall carbon nanotubes (SWNTs) can be thought of as a single graphene sheet rolled up to form a hollow cylinder, see Fig. 1, with diameters ranging from 0.3 to around 10nm. Concentric cylinders, each one wrapped around the tube before it, form the MWNTs. The properties of the tubes border that of a perfect graphite fibre and the dimensions bridge the length-scales from individual Buckminster fullerene to the more widely used micron-sized fibres.

A prudent question arises at this point – why are carbon nanotubes so important both for fundamental research and industrial applications? The unique structure (discussed in greater depth in section 2) leads to some remarkable properties which have only reached a more mature understanding in the last five years. For example, the individual mechanical strength of a nanotube is greater than Fe, while its density is lower than Al, but it retains thermal stability at 1400°C in vacuum [21]. The tubes can have different crystallinities which in turn decides whether they are superconducting [22], conducting, semiconducting or insulating [23]. The crystal structure, diameter and defect geometry also affects the mechanical properties of the tubes. Current literature is divided as to the exact Young modulus value (nor can there be an unambiguous defi-

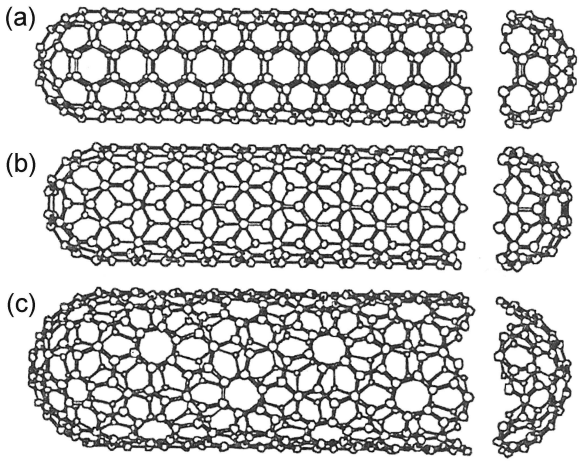

Figure 1: **Classification of carbon nanotubes:** (a) armchair, (b) zigzag, and (c) chiral nanotubes. From the figure it can be seen that the orientation of the six-membered ring in the honey-comb lattice relative to the the axis of the nanotube can be taken almost arbitrarily [20]. Reproduced with permission from Imperial College Press.

nition of the modulus and quasi-continuous elasticity for such a small object). However, carbon nanotubes are widely regarded as having modulus values in the tera-Pa range and a tensile strength $\sim$ 150GPa (cf. steel $\sim$1.5GPa).

The actual arena of nanotube-polymer composites was first introduced by Ajayan *et al.* in 1994 [24]. Though that work was initially directed toward aligning the tubes in any given medium, it proved an important milestone demonstrating the proof of concept and together with other early work [25, 26, 27, 28] showed that the remarkable properties indigenous to the tubes could be transferred to the local polymer matrix. Another interesting avenue of research involves manipulation of the tube chemistry which also presents the opportunity to develop multifunctional composites with tailored physical properties. By the end of 2003, 59 out of 152 nanotube patents existed in relation to nanotube composites, their processability and production [29].

Since the early work from 1994-98 and thereafter, an explosion of literature and scientific debate has surfaced. Much has been garnered from nanotechnological (nanotech) research, especially in the period 1999-2004, with around 10 papers a week currently appearing in relation to polymer-nanotube composites alone. This chapter deals with some of the fundamental information discovered in the last 10 years. It is an attempt to distill the collected knowledge/information into a useable format and should prove useful for beginners as well as more experienced scientists and engineers who would like to have all the works collected in one place.

For this purpose, we explore the nanotube fundamentals in depth before embarking on a survey of their properties, both electrical and mechanical. Additionally, fabrication techniques for production of individual nanotubes are briefly reviewed. However, our main focus is on the behavior and properties of nanotubes dispersed in polymer matrices. Therefore we also review aspects of pro-

duction and processing of polymer-nanotube composites along with nanotube dispersion and alignment in the matrix. Having discussed how to make good quality composites, the final section focuses on the emerging field of polymer-nanotube actuator materials. We use this opportunity to demonstrate an exciting example of what is possible with active nano-composites, above and beyond improvements in existing carbon fibre technologies. It is hoped that this chapter will provide stimulating insight into the nanotube composite field and furthermore, motivate researchers in academia and industry toward improvement of existing materials and discovery of innovative new ones.

2 Carbon Nanotube Fundamentals

It is worth spending some time discussing the basic science and characteristics of carbon nanotubes. What is it about these carbon structures which makes them so special? Let us first take the more simple theoretical case of a single wall carbon nanotube pictured in Fig. 1. It can be thought of as a layer of graphite, a graphene sheet, that has been rolled up to form a cylinder with axial symmetry along the long axis of the tube. Diameters can range from 0.3nm [30] to around 10nm [20]. By comparison, the length of the cylinder can reach into the millimeter scale thus harnessing aspect ratios of $\approx 10^5 - 10^6$. Many research scientists thus use SWNTs to approximate 1-dimensional systems for use in dimensionally constricted experiments.

The other general class of nanotubes is the multi-walled variety (MWNT). For a MWNT one should try to envisage the conformal mapping of a finite number of graphene layers onto themselves [11, 13], much like Russian dolls, each one containing smaller versions of itself. The graphene layers are coaxially arranged around the central axis of the tube with a constant separation between the layers of 0.339nm [31]. Generically, we see that two general classes

of nanotubes exist which are not mutually exclusive but rather one is the natural evolution of the other (SWNT becoming MWNT by incorporation of more shells around the primary/1^{st} hollow core).

A further and more useful distinction can be made when closer attention is given to the arrangement of the carbon hexagons. (By hexagon, we mean the 6-membered carbon ring.) The hexagons of carbon are themselves completely intact except for distortions brought by the curvature of the nanotube as can be seen in Fig. 1. This highlights an important characteristic of nanotubes – the 'helicity' of the honeycomb lattice with respect to the tube axis [13, 32].

Within each graphene plane, the carbon atoms have a hexagonal symmetry due to the six-membered ring. When the lattice is curved to form a tube, the edges of the plane which carry unoccupied bonding sites (so-called dangling bonds) need to pair with available sites.[1] The way in which the edges pair up leads to a wide selection of possible crystallographic orientations of the surface hexagons. Thus, the *helicity* of a tube refers to a crystallographic parameter which in itself is a measure of the departure from 'normal' orientation of the ring arrays with respect to the tube axis [11].

In a SWNT, helicity is observed using electron diffraction techniques to register the signature (*hk0*) spots that originate from the top and bottom of the tube. For a multi-walled tube, constant inter-layer separation of continuous tubes is an additional constraint requiring each cylinder to have its own helicity. Though different (*hk0*) spots appear for differing helicities, MWNTs generally show a smaller number of sets of observed spots than the number of layers. This suggests a number of layers in a MWNT have the same helicity [11].

Armed thus with an understanding of the helical property of nanotubes, we can look at the periodic arrangement in structure *along* the tube axis and more

[1]The argument presented here is simplistic at best – one must always be mindful of the delocalized nature of electron distributions in σ and π-bonded systems such as these.

efficiently character ize our nanotubes. A single tube can primarily be classified as achiral (symmorphic) or chiral (non-symmorphic). See [33] for the review of chirality, formally defined by Pasteur and Kelvin as the difference between an object and its mirror image, from the physics and engineering standpoint. Only two kinds of achiral nanotubes are found to exist - 'armchair' and 'zigzag' tubes. The names refer to the arrangement of hexagons around the circumference of the tube, Fig. 1(a,b). In practice, it is believed that most carbon nanotubes do not form these highly symmetric achiral structures, instead preferring to form chiral formations whose mirror image cannot be superimposed on the original tube. It is the inherent chirality of the nanotubes which leads to such a range of geometries and thus properties of the individual tubes and the subsequent composite they make up. Understanding the chirality fully can help characterize composite behavior from the nanoscale through to the macro-scale properties.

To this end, one needs to define a chiral vector, $\mathbf{C}_h$. This is a Bravais lattice vector defined in terms of two primitive lattice vectors[2] ($\mathbf{a}_1$,$\mathbf{a}_2$) and a pair of integer indices, (n,m).

$$\mathbf{a}_1 = (\frac{\sqrt{3}}{2}a, \frac{a}{2}),\ \mathbf{a}_2 = (\frac{\sqrt{3}}{2}a, -\frac{a}{2}) \tag{1}$$

$$\mathbf{C}_h = n\mathbf{a}_1 + m\mathbf{a}_2 \equiv (n, m), \quad \text{where} \ \ 0 < |m| < n \tag{2}$$

Figure 2 contains the vector representation leading to the definition of the chiral vector. Consider the tube axis denoted by the vector $\overrightarrow{OB}$ and the section perpendicular to the tube axis denoted by $\overrightarrow{OA}$. By trying to 'roll-up' the honeycomb sheet so that the crystallographic equivalent sites O and A coincide (and B and B' coincide) a model tube can be constructed. Therefore, it can be seen that an armchair nanotube corresponds to the case where n=m, i.e. $\mathbf{C}_h$=(n,n).

[2]Remembering that a the C–C bond is 1.44$\mathring{A}$ for nanotubes

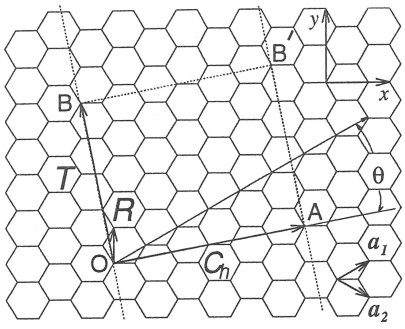

Figure 2: **The unrolled honeycomb lattice of a nanotube.** When we connect sites O and A, and B and B', a nanotube can be constructed. $\overrightarrow{OA}$ and $\overrightarrow{OB}$ define the chiral vector $\mathbf{C}_h$ and the translational vector $\mathbf{T}$ of the nanotube, respectively. The rectangle $OAB'B$ defines the unit cell for the nanotube. The vector $\mathbf{R}$ denotes a symmetry vector. The figure corresponds to $\mathbf{C}_h = (4, 2)$, $d = 2$, $\mathbf{T}$= $(4, -5)$, $N = 28$, $\mathbf{R}$= $(1, -1)$ [20]. Reproduced with permission from Imperial College Press.

A zigzag tube will be denoted by $\mathbf{C}_h$=(n,0) (the case where m=0). All other (n,m) chiral vectors denote chiral tubes. Furthermore, the diameter of a carbon nanotube (given by $\pi d_t = L$ where L is the circumference of the tube) can be calculated by:

$$d_t = \frac{|\mathbf{C}_h|}{\pi} = \frac{\sqrt{\mathbf{C}_h \cdot \mathbf{C}_h}}{\pi} = \frac{a\sqrt{n^2 + m^2 + nm}}{\pi} \tag{3}$$

For a more detailed treatment of the translational and rotational vectors, the reader is directed towards [20]. Matters can be slightly more complicated if one considers nanotubes with changing helicity along the tube axis [34]. Generally, SWNTs remain straight and relatively defect free for most of the tube length until the ends are reached where cones and polyhedral cap structures occur due to the presence of pentagonal defects [11]. Nanotubes with diameters <2nm tend to be more structurally perfect (fewer defects) then tubes with d_t >2nm. Thus, MWNTs which always have larger diameters are relatively

more densely populated with defects along the tube axis as has been experimentally observed [35, 36]. As will be discussed in section 3, it should be noted that defects can be removed with suitable heat treatments.

As it stands, knowledge of $\mathbf{C}_h$ and thus d_t are enough to derive many if not all the properties of individual SWNTs and to some degree, MWNTs. The helicity information contained in $\mathbf{C}_h$ can be used as an indexing scheme for different nanotubes and it is this unique feature, indigenous to carbon nanotube structures, which in part makes them so special.

What are the physical properties of the nanotubes, that secure their special place (and early entry) into the Hall of Fame of material science, and how do they arise?

2.1 Electronic Properties

Transport properties of nanotubes widely vary depending on the type of tube, its chirality and method of production. The problem of variation in electrical property values is compounded by non-standardized measurement methods and poorly defined material in the literature. However, this sections attempts to give an idea of current theoretical and experimental understanding of the electronic properties of nanotubes with an emphasis on qualitative understanding as oppose to quantitative numbers.

Though it may seem academic, understanding the different types of transport phenomenon is also of considerable importance so that a better appreciation of nanotube behavior can be garnered. This becomes especially evident when nanotube-polymer composites are manufactured - the electrical behavior of the composite can be strongly non-linear or even quantized in differing situations.

Let us first consider a normal every-day electric wire. This would be a classical conductor that obeys Ohm's law. The material properties, such as resistivity

and conductivity, do not vary with physical properties of the macroscopic system such as length or applied voltage. However, as the size of the wire is reduced to the nanometer scale, quantum effects become more significant. At this scale, the characteristic length of electron motion is suppressed, leading to quantization effects on conductivity. At the nanoscale, electrons demonstrate more of their inherent wave-like qualities, thus classical theories break down and a more detailed quantum picture is desirable. Three main characteristic lengths arise:

- The mean free path or momentum relaxation length, (L_m)
- The Fermi wavelength, $\lambda_F = 2\pi/k_F$
- The phase relaxation length[3], (L_φ)

Detailed theoretical discussion of these terms can be found elsewhere (see for example monographs [7, 37]) - what is important to remember is that in transport experiments, only electrons that exist near the Fermi energy contribute to the transport phenomenon. Thus, along with other characteristic lengths (not mentioned here, but listed in [20]) three characteristic transport regimes can be identified;

- Ballistic transport: single electron conduction with neither phase nor momentum relaxation. L_m and L_φ are large relative to the physical dimensions of the system.
- Diffusive transport: in this regime many elastic scattering events occur but $L_\varphi \gg L_m$ hence the wavefunction is localized.
- Classical transport: momentum and phase relaxation occur more often as L_m and L_φ are small relative to system dimensions. Electron is considered to behave as a particle.

[3]This term refers to the length over which an electron will retain its coherence as a wave.

With the basic transport phenomenon defined, we can turn our attention to single-walled carbon nanotubes - a good approximation of a one-dimensional system. The first electrical measurements were made in 1997-1998 [38, 39, 40, 41] with a host of papers following thereafter, including useful review articles [42, 43, 44]. Theoretical reasoning which has since been reinforced with experimental data concludes that SWNTs can be either superconducting, metallic or semiconductors. Their electrical properties are known to exceed the best metals or semiconductors known given the right conditions.

These extraordinary electrical properties originate from the unique electronic structure found in graphene. If we model the graphene structure as a two-dimensional (2D) system and roll it up to form a nanotube as described in section 2, it can be seen that the wave vectors along the circumferential direction become quantized due to periodic boundary conditions ($\mathbf{k}_\perp = 2\ell/d_t$, where d_t is the tube diameter and ℓ an integer) while wave vectors along the tube axis remain continuous [45]. This results in a one-dimensional (1D) metal or semiconductor structure being created. Predominantly metallic or semiconductor properties are decided by how the electron momentum states compare with the preferred directions for conduction. In essence, SWNTs and MWNTs are metallic or semiconducting depending on their helicity indices (n,m). If n-m is a multiple of 3 (e.g. (6,3), (18,9) etc) then the tube is said to be metallic [46]. All other permutations of the (n,m) indices represent semiconducting nanotubes. Statistically, for a random sample, one in three tubes are metallic with the rest being semiconducting. Recent reports claim to be able to bias this production probability as briefly discussed in section 3. The SWNT has an associated bandgap in most directions in **k**-space, but due to it vanishing in certain directions, creates a zero-bandgap semiconductor [47]. A significant property of semiconducting nanotubes is that their bandgap, E_g is proportional

to the outer tube diameter and found to scale with it, $E_g \sim (0.9eV)/d_t$ [48]. A metallic nanotube will differ due to two 1D subbands spanning the gap that have a low but constant density of states at the Fermi level. This is why SWNTs in particular are regarded as 1D metals and are the subject of ongoing research.

Having discussed some of the more theoretical aspects, it is worth focussing on the experimental observations of electrical properties of nanotubes. The first transport property measurements were actually made on bundles of MWNTs by Langer *et al.* in 1994 using gold contacts attached by lithographic techniques [49]. The experimental data suggested, for the first time, a temperature dependence of the resistance that fitted a simple two-band semi-metal model. This was followed by other works confirming the thermally activated electrical behavior with E_g ranging from 6 to 240meV [50]. Electrical conductivity experiments on aligned multi-walled bundles have also demonstrated that the structures behave as conducting rods exhibiting anisotropic transport properties in respect to different alignment formations [51, 52, 53, 54].

However, it should be noted that in the early days of reporting electrical properties of both single and multi-walled nanotubes, huge variations in reported numbers would exist. For example, metallic SWNTs were quoted as having resistances ranging from $\sim$6kΩ to many MΩ. This variation is in large part due to the differing contact resistances between measurement electrodes and the tubes themselves. As experimental techniques have evolved, conductance values have approached the theoretical limit (G=4e$^2/h$) predicted for a ballistic nanotube [55, 56, 57]. (The best contacts are thought to involve evaporating Au or Pd over the tube followed by an annealing step [47].) The 1D ballistic conductor effect has been directly observed in defect-free arc-produced metallic MWNTs and catalytically produced SWNTs at room temperature [55, 29]. The accompanying minimal resistance is around 6.5kΩ, which is thought to be unavoidable

– a product of the coupling of the two conducting subbands in the nanotubes with the leads [29]. Doping may affect resistance by biasing subbands near the Fermi level but it also has knock-on affects on the scattering properties. In arc-produced MWNTs, the current flows over the outer layer only. This is because when the top layer is metallic the next layer underneath is statistically more likely to be semiconducting (in two out of three cases). Additionally, transport properties perpendicular to the tube axis is strongly suppressed due to the reciprocal space arguments outlined above. It is also worth noting that catalytically produced MWNTs are diffusive conductors with resistance per micron length $\sim$ 1MΩ due to disordered behavior originating from the higher number of defects this processing technique imparts [58]. A detailed assessment of processing of the tubes themselves is found in section 3.

A reasonable and widely accepted method to determine the conductivity mechanism (and therein all associated electrical phenomenon) is by using direct 4-probe measurements as outlined in [59]. Dai *et al.* and Thess *et al.* were amongst the first to show that geometric differences such as the chiral vector ($\mathbf{C}_h$) and thus tube diameter (d_t) as well as surface defects all directly effect the electronic response of a nanotube [58, 60].

Indeed, the presence of defects can vastly change the electronic behavior of both single and multi-walled tubes. For nanotubes, surface defects occur in the form of additional pentagon or heptagon configurations in an otherwise dominantly hexagonal network. This can cause an otherwise metallic nanotube conductor to behave as a semiconductor as the bend caused by the presence of the defects can transform a tubes network arrangement from zigzag to armchair. Terrones *et al.* were the first to demonstrate 30°-bent MWNTs [61]. This can be clearly seen from Fig. 3. These bent structures were theoretically investigated and found to have metal-metal as well as metal-semiconductor junctions due to

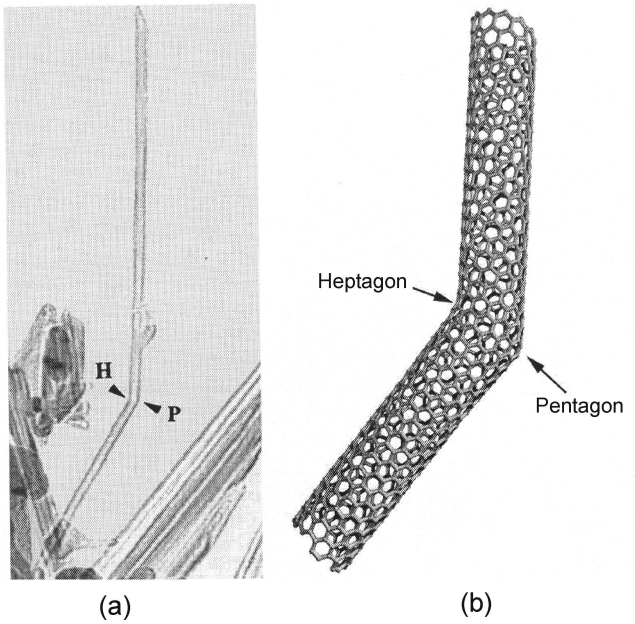

Figure 3: **Structural defects that occur in nanotubes:** (a) TEM image of a 30°-bent MWCNT produced using arc-discharge techniques; (b) molecular model of a 30°-bent nanotube - two different electronic properties (e.g. semiconductor and metallic conductor) are possible [66]. Reproduced with permission from Annual Reviews.

single pentagon-heptagon pairs within the tube [62, 63, 64, 65]. These properties give rise to the possibility of constructing nano-switches [43, 66]. Gathering data on defects is a field unto itself but very recent strides have been made in directly imaging defect structures on nanotube specimens which adds weight to the growing body of evidence regarding the role of defects on the electronic behavior of the tubes [67].

It is clear that electrical properties and the electronic response of nanotubes still needs further development but a clear underlying understanding of the physics has been achieved over the last twelve or so years. The important mechanisms for transport in these systems has been outlined here. A good appreciation of transport phenomenon in individual and bundled tubes allows for

a better understanding of the electrical behavior of tubes in polymer matrices which is addressed in subsequent sections of this chapter. Other exciting subjects, not mentioned here, include the photon emission from nanotubes leading to the development of field-emission displays [29], as well as new mechanisms of superconductivity in nanotubes – see the review [66].

2.2 Mechanical Properties

After the experience in other composite materials, briefly mentioned in the Introduction, there is widespread interest in using nanotubes for the reinforcement of composites due to the apparent excellent mechanical properties they themselves posses. We have seen that carbon nanotubes have some curious electronic properties which range from classical to non-linear quantized responses. However, questions arise about what mechanical properties could develop from such unique 1D structures? Can these mechanical properties be modified and what role do defects play in such structures?

There is no developed answer to any of these questions as it remains the focus of intense ongoing research at the time of writing. However, if we first investigate the bonding regime found in nanotubes, a better understanding of their mechanical behavior might be gleamed.

The C=C sp^2 hybridized covalent bond in graphite and nanotubes is one of the strongest bonds known to man. It forms due to the hybridization of the available $2s^1$, $2p_x^1$ and $2p_y^1$ orbitals, thus creating the σ-bonded skeleton of the honeycomb lattice. The $2p_z^1$ orbital is left unhybridized allowing formation of the π-bond structure leading to the well-known delocalized π electron arrangement. The stability of the delocalized π-system along with the σ-bonded honeycomb provides a rich territory for theoreticians and experimentalists to investigate.

It should be clear that three fundamental forces exist in this type of bonding

regime: the σ-bonding force and the π-bonding force between the carbon-carbon bonds, as well as additional weaker interlayer van der Waals forces. The three forces differ by orders of magnitude but are nonetheless important in describing the full elastic properties of nanotubes.

Let us first consider a single graphene layer and treat it as an elastic sheet. Rolling it up to form a single-walled nanotube allows us to see that the total energy of the nanotube is increased by the strain energy, E_σ, due to curvature of the tube. SWNTs with very small diameters are known to be less stable than larger diameters due to an increasing strain energy term with decreasing tube diameter ($E_\sigma \propto 1/d_t^2$) [68]. This does not mean however that tubes with certain chirality will form more readily over others, as the abundance of nanotubes is controlled by the initial formation of the end cap of the tube [36]. There is only a weak dependence of the strain energy on chirality (i.e. the fine topology of the sheet rolling) and this is probably due to the chirality-dependent directions of the σ and π bonds [68, 20]. Hence, a simple linear continuum model treatment of the mechanical behavior of nanotubes is used throughout the literature. To this end, single-walled tubes have been modelled as simple cantilever beams, with varying success, to determine the the intrinsic Young modulus, Y (see [69, 70, 71]). A more rigorous and direct approach has been adopted by Treacy *et al.* involving the measurement of thermal vibration of individual tubes as a function of temperature [72] and statistically weighting the data using the Boltzmann distribution. They find $Y \sim$1TPa.

Nanotubes are essentially strong and resilient like their carbon fibre and other larger graphitic cousins, but only in specific directions. As mentioned, SWNTs have a $Y \sim$1000GPa while tensile strength is thought to be around 150-180GPa c.f. steel$\sim$1.5GPa ([73, 29, 72]. Additionally, and perhaps not so obviously, is the ability of single-walled tubes in particular to reversibly buckle

under a load applied perpendicular to the tube axis. The load need not be very large. They are in essence flexible structures because of their hollow core thus large and mostly reversible bending is observed while the σ-bonded skeleton remains unbroken when stress is applied perpendicular to the long axis of the tube. [69, 71, 74]. This is not to be confused with the presence of defects along the tube axis which have their own set of implications for the mechanical behavior of SWNTs. Defects can arise during straining of a SWNT: in this instance, nanotubes are thought to be able to elongate by $\sim$30% [75, 76] with a breaking strength of 55GPa [77] due to the formation of Stone-Wales pair dislocations [78]. What is important to remember is that the σ-bonded hexagonal lattice, which is further deformed due to the inherent curvature of the tube, provides one of the most mechanically stable structures. The Stone-Wales defects seemingly prompt the fracture of nanotubes [78]. Experimentally, it has been shown that the defects can lead to the breakage of the outer shells only in MWNT specimens [79].

It must be noted that the σ bonds do not provide high strength alone – they act in conjunction with the delocalized π-system originating from the $2p_z^1$ unhybridised orbital. The π-system does not in itself contribute vastly to the overall strength of a single-walled nanotube. However, the effect of the π electrons on the elastic properties do need to be considered. In a single-walled nanotube (and thus in an individual shell of a MWNT) the π electrons occupy only half the valence energy band. This is thus analogous to a 1D metal with only half the valence band occupied. The energy bands are unstable should a distortion be applied causing the unit cell to increase by a factor of 2. In **k**-space, this amounts to halving the reciprocal space available. This leads to the formation of an energy gap at the Fermi energy at the zone boundary of the reduced Brillouin zone. This phenomenon is known as the Peierls instability. It occurs

predominantly for partially filled bands which have been distorted causing the lower energy bands to become occupied and the higher bands to remain empty. This ultimately leads to a lowering of the energy of the system. The Peierls instability manifests itself as the bond alternation or Kekulé structure in neutral nanotubes [80, 81, 82]. In essence, a Peierls instability will cause the transition of a metallic nanotube to become semiconducting.

However, for the instability to exist, a distortion has to occur to cause it. The distortion only appears if the electron-phonon coupling constant is strong enough [83, 84, 85]. It is found that, in theory, an energy gap does form when a Peierls distortion is placed on the shell of the nanotube due to the π electrons experiencing the Peierls instability effect. The energy gap scales with the strength of the electron-phonon interaction. This would have some significant effects on the electrical and mechanical properties of the tubes. However, it is also found that the energy gap approaches zero quickly as diameter is increased. Direct experimental observation has not been possible to date but recent indirect measurements of electron-electron interaction have successfully shown that Peierls instability plays a significant role on the properties of nanotubes when d_t $<\sim$1.5nm [86, 87]. In most situations, the energy gap formed due to the Peierls instability is very small. Hence, the number of metallic and semiconducting tubes is chirality dependent (as outlined in section 2.1) and almost independent of lattice deformation [20, 88].

Having discussed a single shell in some detail, we now turn to the elastic properties of multi-walled nanotubes. The behavior of MWNTs is very different to their single-walled variety, because we now have concentric cylinders wrapped around a central core with each cylinder interacting with the others around it. Load transfer from one shell to the next has to be accounted for. Inter-wall cohesion may also have a strong influence on the stiffness properties of

the MWNT [89]. Theoretically, this becomes a much more difficult system to model, and computationally expensive as well.

The Young modulus for MWNTs with d_t <5nm is around 1000GPa [90]. Tensile strength is reported around 150GPa [29, 89, 91]. Fracture toughness of nanotubes has yet to be unambiguously determined. Quantitative values of mechanical properties listed in the literature fluctuate due to the various types of testing regimes used, many of which have been created for the unique conditions of a particular experiment. Thus, it is difficult to compare modulus values from various reports. The numbers listed here are guideline values at best.

As the diameters of MWNTs become larger relative to the central hollow core, the tubes begin to exhibit the mechanical properties of graphite. As the outer diameter increases beyond 10-20nm, the multi-walled tube takes the shape of a hexagonal pillar, similar to faceting in carbon fibers [7]. (However, this is not generally found in pyrolytically grown MWNTs [20].) For MWNTs with d_t <12nm, the effective bending modulus is very large, ∼1TPa [73]. This figure drops considerably to ∼100GPa as diameter increases. Electron microscopy images of larger multi-walled tubes have also shown buckling/rippling distortions along the inner arc of bent nanotubes suggesting a possible strain relaxation mechanism [71, 73]. These experiments suggest MWNTs can reversibly withstand large lateral deformations and are thus easier to bend then they are to elongate [92]. The shape of the stress-strain curve for MWNTs is complex and still requires a deeper theoretic understanding [79, 90].

It is clear that nanotubes posses some outstanding mechanical properties due to the nature of their σ-bonded hexagonal lattice and the geometry inherent in their formation. For very small tubes ($d_t < 5$nm), the delocalized π electrons can participate in the Peierls instability, but on the most part this is a very small effect and has little significance to the mechanical stability of the tube.

A good review of the most up to date mechanical analysis can be found in [92] and [93], but it is clear that the exact numbers have yet to be decided due to inconsistencies and difficulties in experimental techniques due to the length-scales upon which the experiments need to be conducted.

3 Forming/Production of Carbon Nanotubes

It is important to look at the available production routes of nanotubes as the method of production has a drastic influence on the properties of tubes, as has been seen in section 2, and hence the composite. The methods outlined here are suggestive at best and the reader is also reminded that there currently exists an ever-growing number of commercial outlets from which to acquire nanotubes. A word of caution here: carbon nanotubes, like their diamond allotrope cousins, can range in price from the prohibitively expensive to the reasonably cheap. The more expensive nanotubes will often be research grade materials with very few defects. Contrastingly, cheaper tubes will be littered with defects and may not even have hollow cores [29]. The variety of production techniques leads to a range in quality of the nanotubes. With no approved set of standard practice guidelines, this is an issue the nanotechnology industry has yet to resolve at the time of writing. It is also one of the key reasons that quantitative experimental measurements produced from different labs are sometimes difficult to compare with any real precision. Because of these difficulties, it is increasingly important to have at least a basic grasp of the synthesis routes used in nanotube formation. Summarized below are the main techniques currently used for production of single and multi-walled nanotubes.

There are three primary synthesis routes for nanotube formation; electric arc-discharge [94], laser ablation/vaporisation [95], and chemical vapor deposition (CVD) [96]. All of these umbrella techniques are discussed in limited detail

below. Other methods such as electrolysis and solar production are not considered as they are not thought to be commercially viable and there also remains a general lack of information in the literature on these methods. The reader is directed toward [66] for some insight on these techniques.

It should be noted that the arc-discharge and laser vaporization methods have limited application for the manufacture of nanotubes in *composites*. This is because the manufacturing of nanotube-polymer composites requires large quantities of nanotubes. It is *not* economically viable to manufacture large quantities using such techniques due to their inherent scale-up shortcomings [97]. Arc-discharge and laser ablation are only suitable for laboratory scale production because of the equipment requirements and large energy consumption. In contrast, gas-phase methods (i.e. CVD) have become a very important, if not primary, source of SWNT and MWNT commercial production. The technique allows scaling up to industrial production levels possible. It is also a tried and tested technology in industry with carbon films [98], fibers [99, 100] and composites [101] all being manufactured using CVD for over twenty years [102]. CVD techniques are widely regarded as the key methods with which to pursue commercial nanotube production.

Electric Arc-Discharge

Historically, this technique was instrumental in developing nanotube understanding as it was the production method used by Iijima when he first observed multi-walled tubes [13]. In general, the technique involves the use of two high-purity graphite rods (5-20mm diameter) as the anode and cathode. Under a He- or Ar-atmosphere, the rods are brought together with a voltage applied ($\sim$20-25V with DC$\sim$50-120A). Once a stable arc is obtained, nanotube growth begins with the anode being consumed in the process. The gap between the

anode and cathode is maintained at ∼1mm by adjusting the anode position. The nanotubes deposit on the cathode in soft fibrous form, surrounded by a shell of fused material. The technique can be modified to produce SWNTs by the incorporation of electrodes doped with a small amount of metallic catalyst particles (examples include Co, Ni, Fe, Y and Gd) [18, 19, 94, 103, 104].

Laser Vaporisation/Ablation

This technique also has some historical significance – Buckminster fullerenes were first synthesized using it [12]. It has since been modified to produce nanotubes [95]. Like the arc-discharge process, it also requires a significant temperature to operate, around 1200°C. A laser is set-up to vaporize a graphite source/target in a controlled atmosphere oven. Flowing argon gas sweeps the condensed product from the hot-zone in the oven to be collected on a water cooled target downstream [60]. Formation of single-walled tubes is facilitated by doping of the graphite target with Co and Ni catalysts [95, 60].

Control over temperature along with catalyst composition gives some scope in controlling tube diameter distribution and therefore chirality. However the distribution is relatively broad compared to other techniques.

As mentioned before, both arc-discharge and laser ablation techniques are difficult to scale-up as the carbon source is essentially fixed prompting the need to have start-stop production runs with carbon replenishment in-between. These processes yield entangled nanotubes with differing chirality leading to various properties as outlined in section 2. Different types of nanotubes coexist necessitating further and more rigorous purification schemes. For these reasons, the methods are not viable contenders for commercialization and bulk production of nanotubes.

Chemical Vapor Deposition

By contrast, gas-phase techniques are more amenable to continuous production as the carbon source is continually replaced by the flowing gas [97]. A variety of sub-techniques have been developed on the general CVD principle. The idea is to react hydrocarbons such as CH_4 or C_6H_6 in the presence of certain catalysts in a reaction tube at around 1000±200°C with the nanotubes deposited on a substrate. Many groups have had great success in forming SWNTs with the use of CO as the carbon source reacted with organometallic catalysts introduced into the reactor. The organometallic species breaks down at high temperature to form a metal cluster on which SWNTs nucleate and grow [105]. The high-pressure CO (HiPCO) process has been an important milestone in the commercial development of high quality nanotubes. Some members of the original development team have since founded Carbon Nanotechnologies Inc., or CNI, which is one of the leading global producers of nanotubes. Other groups have also had success with methane based CVD [106, 107] and more recently, alcohols such as methanol or ethanol have been used as the carbon source [108, 109]. The methods have shown promising results for the commercial production of nanotubes with the potential to form aligned arrays of individual tubes but their detailed discussion remains outside the scope of this review. Further work has also shown that the gas-phase methods allow for controlled diameters and orientation [97, 102]. To some degree, chirality can also be controlled with a recent development using plasma-enhanced CVD preferentially generating semiconducting nanotubes (>85%) [110]. One very interesting recent development achieved the production of SWNTs with a length of ∼4cm leading to an aspect ratio of 6 million using CVD techniques [111]. Even more exciting is that this process suggests an almost limitless ability to grow the length of the tubes which in itself has very significant ramifications for many industries including

nanotube-polymer composites.

What is clear from the last few years of research is that vapor-phase methods for nanotube synthesis are the obvious route for large scale production of tubes. This is an important hurdle crossed with regard to composite applications, as it underlines the ability of industry to produce polymer-nanotube composites with greater economic and technical flexibility. Indeed, as commercial production of nanotubes matures and the optimum conditions are found, it is hoped that the cost of producing composites will decline concurrently allowing polymer-nanotube composites to directly compete with established technologies.

Quality of a Nanotube Batch

Purification

Unfortunately, nanotube processing does not end once the tubes are produced in bulk form. Impurities in the form of catalyst particles, amorphous carbon and non-tubular fullerenes (amongst others) also form. Thus, the necessity for purification becomes apparent so that the tubes may be separated. To this end, there are a number of techniques available at the laboratory scale with the number of methods available industrially much more limited.

Let us first outline a multi-stage procedure. Once the tubes are produced, catalytic particles, amorphous carbon and other impurities must be removed. The next step is to begin *sorting* the tubes by a) length, b) metallic/semiconducting properties and c) chirality [112]. It should be emphasized that none of these steps have been completely solved and that purification is still seen as a major industrial bottleneck during nanotube processing and production. Indeed, it is doubtful that a full purification procedure will have such clearly defined stages, rather a more indistinct set of criteria will likely evolve to solve purification problems.

Considering the first step, nearly all purification procedures involve either one of the following or a combination of the following techniques [112]:

- gas/vapor-phase oxidation
- wet chemical oxidation/treatment
- centrifugation
- filtration and/or chromatographic techniques

One example of a proven purification technique is the use of wet chemical oxidation in refluxing diluted nitric acid (2.6M) thus digesting the carbon crosslinks. The crosslinks serve to entangle carbon-coated metal catalysts as well as carbonaceous impurities. The impurities are functionalized by the carboxylic acid surface-functional groups and can then be washed out in a suitable base in which they are soluble [95, 113]. Larger quantities, for example 10g of material, require more complicated procedures involving acid decanting, centrifugation, filtration, ultrasonication and use of surfactants. The process has shown good high quality yields but has yet to be proven outside the laboratory setting. Additionally, the treatment can be considered as rather harsh and hence questions arise as to the damage caused to the local nanotube architecture.

For MWNTs, a more simple process has proven highly successful in purifying the multi-shelled tubes. High temperature oxidation in air, first described by Ebbesen *et al.* [114], has been a long-standing method by which purification of nanotubes can be achieved. Amorphous carbon and materials with pentagonal defects have a much lower stability than the graphene sheets making up single and multi-walled nanotubes, hence they are removed in this process much quicker. Modification of the technique to purify SWNTs has been more difficult due to the presence of metal catalysts particles which catalyze low-temperature oxidation of carbons chaotically, thus destroying the SWNTs [115, 116]. How-

ever, as this has become better understood, great strides have been made in purifying SWNTs using the gas-phase oxidative purification regime. Chiang *et al.* subsequently developed the method involving 18 hour low-temperature (225°C) cracking of the carbonaceous shells encapsulating the metal particles in a wet oxygen atmosphere. Stirring in HCl gave the normally clear acid a yellow color, indicative of Fe dissolution. Finally, they filtered off the acid, dried the product and repeated the procedure along with an oxidative bake at 425°C. Though this method has proven successful, scalability remains an issue [112].

Another novel and perhaps more scalable purification method has been developed by Eklund *et al.* [117] whereby SWNTs are microwave heated in air followed by a mild HCl acid treatment. However, any and all acid treatment based methods should be viewed with caution, especially for SWNTs, as it invariably leads to varying degrees of surface alterations. The affect of this is not well understood at this time but it is thought that mechanical and electrical properties will be degraded. It is well documented in the literature that certain types of chemical functionalization of nanotubes introduces sp^3 defects that lead to degradation of the mechanical strength [118, 119].

There are many purification methods employed in the literature. The ones outlined here are amongst the most popular and thus the most proven. No one procedure is said to be better than another with all having advantages and drawbacks. What has been mentioned above are very general techniques which can easily be modified and thus optimized.

Separation

Another stage requiring consideration is the length separation of the tubes once formed and purified. The general methods of separation such as chromatography, capillary electrophoresis and field-flow fractionation, are not new and have been available to chemists investigating other fields for some time now.

Chromatographic techniques are thought to be important for length fractionation of SWNTs<300nm in length [120]. Electrophoresis [121] and field-flow fractionation [122] are more applicable to longer SWNTs [112].

Separation of nanotubes has also been successfully achieved with the use of acid treatments, fluorination and bromination processes. The further use of surfactant allows the tubes to be suspended in various organic media [123, 124, 125, 126].

The separation of metallic and semiconducting nanotubes has also received widespread research focus as the successful separation of the two types would hail huge benefits for many industries. However, only laboratory scale successes have been reported and even then to limiting effect. The details of such methods falls outside the remit of this review, hence the reader is directed toward [112] and references therein for the most up-to-date information on these techniques.

A brief mention of economy here. It is worth considering the balance between time spent manufacturing the tubes using CVD techniques and the time spent purifying them. There are reports suggesting that the production technique alone can output very high quality tubes given careful control of the carbon source and process variables (see for example [108]). To all intents and purposes, this removes the necessity for extensive purification, but can involve costly procedures in doing so. On the other hand, purification can be lengthy and costly in itself. At the time of writing, no one method is dominant in producing high quality nanotubes of a specific type. It is envisaged that preferential growth techniques such as CVD based methods coupled with post-growth treatment and purification is the production route of choice for the foreseeable future.

Testing the Quality

Many commercial outlets have appeared within the last two years offering 'as-produced' nanotubes of both the single and multi-walled variety. Little, if any, purification has taken place and yet the tubes will have a purity >95%. (See for example the range offered by Nanostructured and Amorphous Carbon Materials Inc. at *h*ttp://www.nanoamor.com/products.) This grade of material may be acceptable for many composite applications. However, if more stringent requirements are raised, higher quality tubes are undoubtedly required. Composite specialists must be careful to choose the correct type of nanotube for their needs. At the time of writing, there are no approved standards by which the quality of a nanotube batch can be measured and hence many looking to build composites will need to test the quality of the nanotubes they have themselves.

We can in essence define two parts to the measurement of purity. The first is relatively straightforward - measuring the percentage of transition metal catalyst left over from nanotube production. Thermogravimetric analysis (TGA) is the technique of choice here. A nanotube batch has its weight measured at the start of the experiment. The nanotube sample is then burnt in air at ∼1000°C so as to remove *all* carbonaceous material. The final weight measures the remaining oxidized metal particles. With this information, a measure of the percentage purity as a function of the original sample mass can be calculated.

The second part poses more of a problem – the quantitative measure of carbonaceous material purity i.e. the quantity of nanotubes, as opposed to other carbon-based products such as amorphous and graphitic carbon. Chemically, they are virtually identical thus a probe is needed to scan their physical makeup and distinguish them through their material properties. Historically, the nanotube field has been founded by pioneers in electron microscopy [13, 17] and it is SEM/TEM (scanning and transmission electron microscopy) techniques

which have led the way in confirming nanotube structure and material purity. However, measuring the purity and thus quality of a nanotube batch requires a flexible technique able to measure the bulk specimen and not picogramm quantities within it, as is the case with microscopy techniques [112].

A standard measure of purity has yet to be developed. Haddon *et al.* argue that it is necessary to achieve a standard measure and to do this, a characteristic nanotube signal that differentiates it from other carbon impurities needs to be identified by spectroscopic methods. In so doing, a method would be widely available to most research labs which would allow the *bulk* purity to be analyzed [112]. To date, the only viable technique that fulfils the criteria involves the use of solution (dispersion)-phase near-infrared (NIR) spectroscopy, the details of which can be found in [127, 128, 129]. However, although spectroscopy of batch samples is widely regarded as the best route forward for industrial quality control, spectroscopic purity testing of nanotube batches still requires further development to move beyond the laboratory.

4 Dispersion Techniques

So now the nanotubes have been processed and purified to an acceptable level. The next stage in production of a composite is to homogenously disperse the tubes into the polymer matrix. There are many benefits of completing such a procedure. Primarily, one needs to ensure the properties of the composite are homogenous throughout. Additionally and perhaps more appropriate to nanotubes, a homogenously dispersed filler in the polymer matrix reduces the possibility of nanotube entanglement which can lead to significant changes in composite behavior. The nanotube aggregation within a polymer system would certainly have a negative impact on its stiffening ability [130]. As yet, the nature of these entanglements and their influence on the composite properties is a little

understood area still requiring a great deal of investigation.

But what actually is *dispersion* and how exactly does one achieve it with nanotubes? In itself, dispersion is a spatial property whereby the individual components (in this case nanotubes) are spread with the roughly uniform number density throughout the continuous supporting matrix. At very low concentrations, the conditions of an ideal-gas may occur, when the dispersed objects do not not *see* each other (i.e. experience the electrostatic or mechanical influence of neighbors). As is well known from the Onsager treatment of anisotropic suspensions [131], the crossover concentration when, e.g. the rod-like objects start interacting and significantly biasing their pair correlation is inversely proportional to the aspect ratio – and so can be very low indeed for nanotubes. Additionally, the nanotubes must *remain* in this uniformly dispersed state, and not re-aggregate in spite of the almost inevitable attractive interaction between them. This is an important and delicate point. Early reports in the literature often claimed homogenous dispersions had been achieved, when in truth only dispersions of aggregates of tubes had been established. True dispersion of individual tubes still required greater experimentation.

There are many routes of initial tube dispersion that can be explored. We present here a summary of the work to date. To disperse something, an initial 'aggregated' condition must exist. The nature of nanotube aggregates is different for single and multi-walled varieties. With SWNTs, crystalline ropes of individual tubes form a rich tapestry which has proven difficult for researchers to unwind. MWNTs essentially form much larger bundles of material, the physics of which proves different to its SWNT brother. Thus, differing strategies need to be implemented depending on wether single or multi-walled tubes are to be used in the composite. It is believed that no single method will dominate but rather a recipe or cocktail of techniques will serve to fully disperse the tubes

into a given media.

Dispersion broadly falls into two main categories; mechanical/physical and chemical methods. The mechanical techniques involve physically separating out the tubes from each other, but can also fragment the tubes and decrease their aspect ratio [132]. Chemical methods often use surfactant or chemical functionalization of the tube surface, which in turn can affect surface energies, wetting and/or adhesion characteristics leading to prevention of aggregation and/or re-aggregation. However, certain types of aggressive chemical treatment can lead to the key nanotube properties being compromised. This defeats the purpose of undertaking polymer-nanotube design but many in the field have, in the past, felt it a necessary concession to achieve homogenous dispersions.

4.1 Physical Methods of Dispersion

To physically separate tubes that are bundled together, and tightly held by van der Waals forces, requires a mechanical force – as opposed to a force arising from chemical potentials between different species. To this end, three main mechanical processes have been partially successful in dispersing tubes in various media: ultrasonication, milling and shear mixing.

Ultrasonication

This is a rather ubiquitous technique. However, overexposure to ultrasonication is known to lead to tube rupture which may have negative consequences for the polymer-nanotube composite properties. Clearly, due care is required with all mechanical processes.

For ultrasonication, the nanotube specimens are first mixed with a solvent and then placed into an ultrasonic regime. Two main instruments are used:

- Ultrasonic bath

- Ultrasonic horn/tip

The ultrasonic process delivers high levels of vibration energy to the system and is thought to create expansion and peeling/fractionation of the graphene layers making up a multi-walled tube. The process starts from the outside and works its way in with each layer fractionating independently from preceding and subsequent layers. So the process has the potential to make the tube thinner as well as shorter [133].

The ultrasonic process has three particular mechanisms: bubble nucleation and subsequent implosion (cavitation), localized heating and the formation of free radicals [132]. It is the cavitation mechanism that causes much of the dispersion but also much of the tube damage. Low frequencies (∼20kHz) produce larger bubbles which lead to a larger energy distribution as they collapse. Increasing the frequency leads to lower energy dissipation as the bubble radius is smaller and cavitation is thus reduced.

When an ultrasonic horn is used, the mechanical tip oscillates, normally at lower frequencies compared to a bath, leading to high-energy cavity formation (which can result in rapid sample heating if due care is not taken). In this case the dispersive energy is very high and localized around the oscillating tip. Prolonged exposure to such techniques is not recommended. An ultrasonic bath works in much the same way except that the cavitation zone is not well defined and the frequencies of oscillation are normally higher (∼40-50kHz). The dispersive energy is lower than an ultrasonic horn.

The use of an ultrasonic horn leads to the formation of a conical field of high energy around the oscillating tip [132]. Solvent within this 'dispersion zone' experiences fierce cavitation (mentioned above) which in turn induces a flow that moves material away from the tip and then recirculates inside the conical field again. The size of the dispersion zone depends on a number of

factors including solvent properties, mixture phase viscosity and the geometry of the system. However, it is *wrong* to think that by increasing the viscosity of the solvent, overall dispersion would be linearly improved due to higher stress transmission. It is an attractive idea, since many monomer solvents could have purified nanotubes directly added to them so that the ultrasonic regime would disperse them directly in the monomer before the final polymerized matrix is formed. A higher viscosity solvent, in addition to the beneficial higher levels of shear energy in the matrix, also may result in poor recirculation of the material – only a local region within the mixture will be well dispersed. Overall, beyond a certain optimum viscosity, the dispersion quality is reduced as solvent viscosity is increased. The optimum viscosity at which to operate the ultrasonic tip is a matter of experimentation. The exact value will vary for different systems and will be a function of container and tip geometry, as well as the operating frequency applied. This list of variables is by no means exhaustive.

Milling and Grinding

This method uses a rotating cylinder (or several, such as in the 4-mill mixer) filled with grinding media such as iron balls to wear down the aggregated tubes. Ball-milling can be used to break up multi-walled nanotube aggregates and reduce nanotube length & diameter distributions [134]. There is also good evidence in the literature that the ball-milling technique is amongst the most destructive toward nanotubes and produces a large amount of amorphous carbon [135, 136]. At a laboratory scale it is not a favored route toward dispersion because of the difficulty in controlling amorphous particle build-up. However, industrial scale dispersion techniques might employ ball milling of a polymer-nanotube viscous fluid as a 'cheap-and-fast' physical dispersion alternative, given the right criteria.

On a laboratory scale, a gentler route to break up large nanotube aggregates

is to use the traditional pestle and mortar before more aggressive physical or chemical treatments are employed.

Shear Mixing

High shear mixing is another dispersive option with which nanotube aggregates can be mechanically forced apart in a viscous monomer or polymer solvent. A relatively high shear regime needs to be applied. The benefits of this technique are clear:

- Direct dispersion into the host matrix
- No chemical modification is required
- Nanotubes are prevented from re-aggregation by viscous forces

However, this technique is only applicable to MWNTs as the physics behind SWNTs-entwined aggregates is different and requires more careful treatment. Additionally, shear-flow dispersion is limited to viscous fluids within a finite range of viscosities between, say, $\eta \sim 10^{-3}$ and 20 Pa.s. If the viscosity is too low, separated aggregates are able to overcome viscous forces and re-aggregate driven by their attractive Wan Der Vaals potentials. If the viscosity is too high, dispersive mixing is not efficient and greatly impeded. There are indications of successful application of melt mixing for SWNTs [28, 137, 138], but this will inevitably only disperse large aggregates and not solve the inter-tube tapestry formed between single tubes.

Results illustrating the effect of shear mixing multi-walled tubes in a viscous matrix are shown in Fig. 4. The host polymer PDMS (polydimethylsiloxane) is shear mixed with MWCNTs. The real part of composite viscosity (η) is recorded at intervals during the mixing process. Variations in inter-tube spacing (dispersion) are accompanied by corresponding changes in viscosity. Measuring viscosity changes as a function of nanotube-polymer mixing time gives

some quantitative understanding of dispersion in the bulk specimen. For all concentrations tested, some underlying universal effects seem to occur. An initial viscous peak is observed suggesting an internal structure forming, which is consequently broken down. This is analogous to the effect observed in lyotropic liquid crystal systems, which form yield structures [139]. The level to which the liquid crystal model, widely available in the literature, can be applied to nanotube-polymer systems has yet to be determined. There are suggestions that nanotubes exhibit genuine liquid crystalline behavior [140, 141], but more information is required to establish whether these reports deal with equilibrium phase structures. Whether the jamming phenomena observed in the results is universal for all rigid rod approximated systems is a another obvious question requiring much greater research.

Generically, the viscosity increases with time of shear mixing and then reaches a plateau, which could be regarded as a point in the process at which the maximal dispersion is achieved. The time to reach this plateau is less as the nanotube concentration is increased. This is very significant. The power transferred from the rotating mixing blade to the viscous polymer with the viscosity η in terms of the shear rate ($\dot{\gamma}$) and shear stress ($\eta\dot{\gamma}$) is $\dot{W} = \sigma\,\dot{\gamma} \sim \eta\dot{\gamma}^2$. This is the energy delivered to the system per unit time. For higher concentrations (higher overall viscosity η), more energy is delivered quicker, thus resulting in shorter mixing times. The mixing time required to achieve a homogenous dispersion reduces with higher concentration of nanotubes. The results in Fig. 4 demonstrate this unambiguously.

Other work has added weight to the findings presented in Fig. 4. Potschke *et al.* [142] indicated an interesting relation between nanotube connectivity and the onset of non-Newtonian nanotube-polymer solution behavior. There are also suggestions that non-linear inelastic instabilities can form, associated with flow-

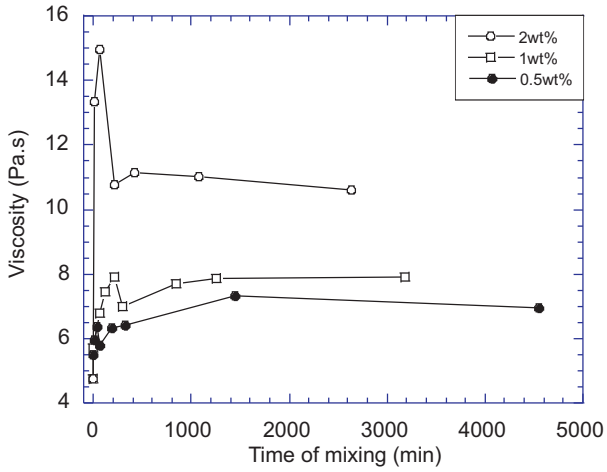

Figure 4: **Viscosity variation on shear-mixing the polymer melt.** The plot illustrates the evolution of the MWNT-polymer mixture composition, for different levels of tube loading (labelled in the plot), as function of time spent in the shear mixer at approximately constant rate $\dot{\gamma} \sim 100\,\mathrm{s}^{-1}$. The plateau approach after a long mixing time is an indication of the complete dispersion. The viscosity peak at short times is discussed in the text.

induced clustering in semi-dilute nanotube-polymer suspensions [143]. These conclusions are reached when a correlation was found between the transient rheological behavior and the formation and evolution of highly elastic nanotube aggregates aligned in the shear vorticity direction. As in other similar complex fluids under flow [144], the MWCNTs are flexible enough to deform under high flow rates but readily inter-lock to form coherent structures under weak shear. Simulation work further suggests that friction leads to aggregation in the absence of attractive interactions. Further experimental evidence for the negative normal stress difference has also recently and independently appeared [145]. The viscosity peaks seen in Fig. 4 may be indicative of a similar domain ordering process taking place within the system, analogous to liquid crystal systems. Further experimental work is needed to confirm this.

The use of shear mixing to disperse MWCNTs has also been used by Andrews *et al.* [146]. Using polystyrene as the host matrix and mixing MWCNTs

under severe conditions (180°C and 80rpm using a twin blade mixer), the authors monitored tube attrition by regular TEM analysis of sample aliquotes to quantify the effects of shear mixing. While the tube length did diminish with increased mixing energy, the rate of breakage was reduced as the nanotubes were better dispersed and tube lateral separation distances increased. We conclude that shear mixing is a useful approach in dispersing multi-walled nanotubes within a viscous polymer matrix and although tube breakage does occur, it may not be a serious problem as it takes place less often as dispersion improves. Further experimental studies make similar conclusions on the usefulness of shearing MWCNT-polymer blends [147, 148].

It should be noted that measuring tube attrition is notoriously difficult, especially using surface probing techniques such as TEM and AFM (atomic force microscopy). The reason is that often, only parts of the wall are exposed above the polymer surface leading to a false conclusion that aligned tubes with reduced lengths are present as detected by TEM/AFM. This problem is much more common in hard composites where part of the curved nanotubes can be cut during sample preparation and thus appear as separate tubes [149].

4.2 Chemical Methods of Dispersion

Why explore the route of chemical functionalization at all? It should be remembered that the sp^2 hybridized structure of nanotubes makes them insoluble in common organic solvents. While a physical technique such as the shear flow method is a viable route for scalable dispersion, local inhomogeneities may occur if careful application of the method is not followed. The technique also only applies to MWNTs due to their closer proximity to rigid-rod behavior. Additionally, functionalization of the tube surface influences the interaction between the tube and its local matrix environment in a polymer-nanotube composite.

Choosing the right level/type of functionalization, summarized in Fig. 5 [150], can have a very positive affect on composite behavior.

There has thus been much interest in mastering chemical functionalization of the nanotube surface to make the tubes more soluble and/or separable in a given solvent. A chemical route toward dispersion would be scalable by default. It would also ensure homogenous dispersion throughout the solvent and thus a host matrix, giving much technical flexibility to polymer-nanotube composite manufacture. Two general classes of chemical dispersion methods are considered – covalent and non-covalent.

Covalent Methods

Lessons learnt from fullerene chemistry demonstrate that reactivity in addition reactions has a strong dependence on the *curvature* of the fullerene species [151]. By increasing the curvature, pyramidalization of the sp^2-hybridized network becomes more pronounced leading to a greater tendency to participate in addition reactions [150]. In the case of SWNTs, the diameters tend to be larger than fullerenes thus their curvature is lower. Hence their willingness to participate in reactions is reduced.

Covalent methods refer to functionalization treatments involving covalent bond breakage across the nanotube surface which disrupts the delocalized π-electrons and σ-bonds and hence incorporate other species across the exterior of the shell. The mechanisms may preferentially occur at defect sites, Fig. 5, or where tube curvature is highest i.e. tube-ends.

A functionalized tube is more soluble in an organic solvent hence spectroscopic characterization in the liquid phase is much more amenable [152]. It is the sidewalls of a nanotube which tend to experience chemical attack during oxidative workup [124, 152], Fig. 5(a). A classical example of nanotube treatment is by refluxing in 2.6M nitric acid [113]. The acidic attack forms defect

sites which are in turn saturated with -COOH groups. These side groups are what functionalizes the tube and makes it more receptive to further treatments such as attachment of long alkyl chains via amide formation [153]. Covalently attaching alkene groups to nanotubes has been shown to increase solubility in organic solvents such as THF [124, 154, 155, 156], chloroform, methylene chloride [157] and DMF [158]. Other studies have shown that acid/oxidative treatments enable stable aqueous solutions of catalytically produced MWNTs to be produced by way of introducing oxygen containing surface groups, leading to the formation of viscoelastic gels forming at high concentration [159].

Fluorination has also proven a popular functionalization method for nanotube surfaces. Treatment with F_2 gas at temperatures between 150-600° results in C-F covalent bond formation [60]. However, fluorination of SWNTs causes any metallic character to be lost and hence electrical properties of the bulk batch of nanotubes will change drastically. A fluorinated tube dissolves in alcohol more readily (especially if ultrasonicated) and subsequent 'wet-chemistry' procedures with nucleophiles will substitute the fluorine with alkyl groups [157], e.g. by treatment with alkyl lithium.

Stable solutions of SWNTs can be formed when nucleophilic carbenes are added as described by Holzinger *et al.* [154]. Each added group is bound through just one covalent bond and is positively charged. The configuration leads to electrostatic repulsion between the nanotubes hence higher solubility.

Though many of these techniques seem initially attractive in dispersing nanotubes into a given matrix, consideration needs to be given over to the amount of defects and thus damage the tubes experience. Mechanical strength appears to be lowered [118, 119] due to surface functionalization, and electrical properties can be severely affected [150]. Because these are surface dependent effects, a multi-walled tube may not be as drastically affected as single-walled varieties.

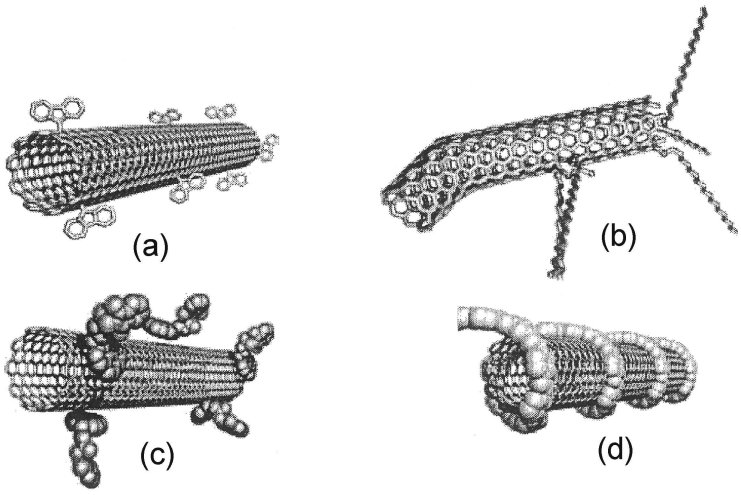

Figure 5: **Chemical methods for dispersing nanotubes:** (a) covalent sidewall functionalisation; (b) defect group functionalisation; (c) noncovalent exohedral functionalisation with surfactants; (d) noncovalent exohedral functionalisation with polymers [150]. Reproduced with permission from WILEY-VCH Verlag GmbH & Co.

All shells below the outer few remain un-reacted. However, much of the properties with MWNTs are still dependent on the outer surface, especially in a composite where the interface is a key limiting factor in the properties of the material. Covalent surface modification of MWNTs may or may not affect a composites performance depending on the system being constructed. Further investigations are underway in this area.

For SWNTs, though surface modification is popular for certain uses, better functionalisation control is still required to ensure its outstanding properties are transferred to a polymer matrix and not lost due to defect saturation on the nanotube surface.

Non-Covalent Methods

Non-covalent functionalization generally involves the use of surfactant to bind ionically to the nanotube surface and prevent the tubes aggregating, Fig. 5(c). This can be a much less destructive route toward dispersion than covalent bonding/acidic boiling. Surface active molecules such as sodium dodecylsulfate (SDS) or benzylalkonium chloride have proven successful in dispersing nanotubes into an aqueous phase [160, 161, 162]. The mechanism is thought to involve the nanotubes residing in the hydrophobic interiors of the micelles [150]. If the hydrophobic region of the amphiphile contains an aromatic group, π-π stacking interactions occur with the nanotube sidewalls as demonstrated by Chen *et al.* [163]. Interestingly, they went on to show that parts of the amphiphile can be substituted with amino groups from proteins causing immobilization of the biopolymers – a useful development in biosensor research [163].

Non-surfactant mediated dispersion has been carried out using anilines [164], amines [165] and more recently DNA [166] to name just a few. For anilines and amines interacting with nanotubes, it is thought that donor-acceptor complexes are formed. Strong curvature of the tubes imparts acceptor character to the corresponding macromolecular carbon networks [150, 167].

Supra-molecular complexes can also be formed between SWNTs and certain polymers such as poly(m-phenylene-co-2,5-dioctoxy-p-phenylenevinyllene) (PmPV). The polymer wraps around the tube when in solvent leading to a stable dispersion of the polymer-nanotube complex, Fig. 5(d). A number of polymers can be used so long as they have a suitably polar side chain [168]. Some of these nanotube-polymer complexes have shown liquid crystalline behavior.

However a word of caution here. Using surfactant and/or non-surfactant mediated techniques alone is not always a successful affair, because coating of individual tubes is much harder than it seems. Many groups reported successes

with dispersing SWNTs but in truth only managed to separate out the bundles and not the individual tubes themselves, resulting only in partial exfoliation. This remark applies to both the covalent and non-covalent methods. The techniques are more successfully applied to MWNTs but even then, attempts at coating the tubes can sometimes backfire, with aggregates being coated instead and making it even more difficult to disperse the tubes. Indeed, there appears to be a limit to the percentage of tubes, of around 1%, that is possible to be dispersed in a solvent using surfactants. Consideration must also be given to the polymers and surfactant adsorbed onto the nanotube surface and their possibly reduced compatibility with the host matrix in a composite.

Disentangling single-walled nanotube ropes in bulk quantities has only more recently been successfully achieved [166, 169, 170, 171]. However the techniques have still employed rather harsh conditions to achieve the dispersion goals. Does the ends justify the means? It depends really on the types of tubes required. The major problem here is that the tubes produced tend to be much shorter due to nanotube fragmentation, between 80-200nm. For some applications this may well be acceptable but perhaps not for all. High length carbon nanotubes (i.e. $> 1\mu$m) would be beneficial for nanotube-reinforced composites due to the improved reinforcing effect.

To this end, more recent work by Paredes and Burghard [172] modifies a technique developed by Islam *et al.* [170]. In this approach, SWNTs are dispersed in water by means of the surfactant sodium dodecylbenzene sulfonate (SDBS). A physical process of ultrasonication starts with using a tip (five pulses with 0.5s on/0.5s off cycles at $\sim$40W/cm^2), centrifugating at 20,200g for 30 minutes, decanting the upper 80% supernatant and placing in a ultrasonic bath for 30 minutes more. It is thought that the final step of gentle bath ultrasonication for a relatively short period of time is the crucial step in achieving individually

dispersed tubes *while* retaining their lengths [172]. However, the technique still has the limitations indigenous to surfactant use already outlined above.

New work by Iijima *et al.* [173] suggests using highly positively charged nanoparticles of ZrO_2 to help disperse SWNTs in water and other solvents. The stabilization mechanism is most likely due to the high level of charge repulsion between the nanoparticles that coat the nanotubes. However, no direct evidence of this effect has been reported to date. What is also evident about this technique is that the researchers also apply physical methods of dispersion such as the ultrasonic tip in conjunction with chemical ones.

It is clear that the issue of dispersion is not a simple matter and has yet to be fully solved for SWNTs. There is as yet no simple and effective method of dispersing nanotubes in a hydrophobic polymer matrix. Compromises need to be made to effectively distribute the tubes. Furthermore, dispersion of single-walled tubes has only been achieved on the laboratory scale and many of the scalable chemical methods outlined here are limited to around 1% loaded dispersions. Clearly much more work needs to be concluded in this area. A sizeable research effort is underway. No one dispersion route has been found to be successful on its own but rather a carefully planned recipe of procedures needs to be adopted to obtain the best results. Many groups have demonstrated recipes that include both physical and chemical techniques. For MWNTs, a brighter horizon is closer at hand, with dispersion in viscous polymers proving successful for particular systems.

One final remark returns to the earlier made point about preventing tube re-aggregation, after the initial dispersion is achieved. This is less of an issue when the tube surface is modified by one of the chemical methods, which aim to stabilize the dispersion in the same way as in colloid science: by creating a short-range repulsion potential between nanotubes, due to either (screened)

charge or the steric effect of surfactant molecules. However, even with classical stabilized colloid suspensions, the long-term dispersion is a real challenge – with highly polarizable nanotubes the problem of suspension stabilization is further compounded. When dispersion is achieved by mechanical methods, no specific stabilization mechanism is offered and re-aggregation will occur at a rate allowed by the viscosity of the suspending matrix. The only practical way of preserving the homogeneous composite is by immobilizing the tubes: chemical crosslinking of the polymer matrix [170, 174, 175], or bringing it below glass transition.

5 Nanotube Alignment

Having picked one or a few (from a number) of the dispersion choices surveyed in section 4, alignment of the tubes embedded in the polymer matrix becomes the next critical issue. The purpose of aligning anisotropic embedded objects in the matrix depends on the application of the composite in question. Some applications will prefer zero orientational order of the nanotube filler; this maybe useful for composites requiring lower elastic modulus but higher conductivity. However, most engineering composites will need to maximize their strength, in particular, loading directions. Moreover, transport properties such as conductivity or heat transfer may only be required in a particular direction hence the need for orientational control of the nanotubes.

The requirement for anisotropic properties at the nanometer level highlights the driving motivation and significant contribution made by the polymer-nanotube composite field to the wider nanoscience community. Control and manipulation of nanometer sized objects to affect macroscopic properties is at the very heart of modern nanotechnology. With this in mind, control over orientation of nanotubes in a matrix is of significant importance in tailoring the composite performance. We shall see, later in this review, specific examples of

the critical role the orientational order of nanotubes plays in the macroscopic properties of nanocomposites, for instance, leading to a complete reversal in the material behavior.

5.1 Orientational Order

Some questions arise here as we try to define what is meant by alignment and also the processes that should be considered for such alignment. The direction, known as the *director*, $\boldsymbol{n}$, is usually defined as the average direction along which nanotubes can and do align [131, 176]. This is a local property of the system obtained as a result of averaging of individual particle axes, $\boldsymbol{u}_i$, over the macroscopically infinitesimal volume. The corresponding local orientational order parameter is a second-rank tensor $Q_{\alpha\beta}$ which for the uniaxial alignment (quadrupolar symmetry) is defined as:

$$Q_{\alpha\beta} \equiv \tfrac{3}{2}Q(n_\alpha n_\beta - \tfrac{1}{3}\delta_{\alpha\beta}) = \langle \tfrac{3}{2}u_\alpha u_\beta - \tfrac{1}{2}\delta_{\alpha\beta}\rangle, \tag{4}$$

$$\text{or in matrix form :} \quad Q_{\alpha\beta} \equiv \begin{pmatrix} -\frac{1}{2}Q & 0 & 0 \\ 0 & -\frac{1}{2}Q & 0 \\ 0 & 0 & Q \end{pmatrix},$$

where the principal axes are aligned with z along the ordering direction $\boldsymbol{n}$, cf. Fig. 8(a). The value of local scalar order parameter is indeed the average $Q = \langle P_2(\cos\theta)\rangle$, with $(\boldsymbol{n}\cdot\boldsymbol{u}_i) \equiv \cos\theta_i$ (cf. the classical literature for detail [131]). Full alignment of the components/material requires $\boldsymbol{n}$ to extend uniformly over the entire system. In some instances, by applying an external force, an induced re-orientation of the director occurs.

We shall concentrate on nanotubes in polymeric systems as we look at alignment. One immediate concern should be the choice of technique, with which to characterize this alignment quantitatively. The classical cases of uniaxial

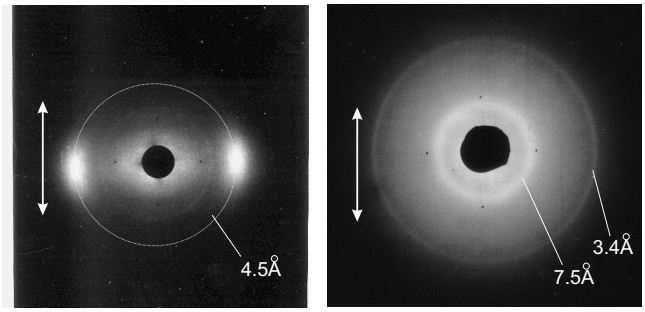

Figure 6: **X-ray images with azimuthal intensity bias at different scattering angles.** (a) The typical X-ray image from the aligned nematic liquid crystal, showing the strong azimuthal bias at the scattering angle corresponding to the molecular thickness. (b) The image from the nanotubes embedded in PDMS matrix, showing key scattering reflexes; the outer ring of $3.4\mathring{A}$ is from the nanotubes. The inner ring is indicative of the correlation length of PDMS mesh size. The arrows show the direction of the uniaxial ordering.

order are the nematic liquid crystals, where the wide angle X-ray scattering of rod-like molecules provides a characteristic peak at the scattering angle Θ, with $\sin(\Theta/2) = \lambda_x/2d_m$ (where $\lambda_x \sim 1.54\mathring{A}$ is the wavelength of X-rays and $d_m \sim 4.5\mathring{A}$ the thickness of the typical molecule. The azimuthal bias in the scattering plane, see Fig. 6(a) and Fig. 7(a), is a signature of uniaxial order. When the alignment of larger objects, such as clay plates or carbon fibers, embedded in polymer matrix is considered – the light scattering often provides the tool with the appropriate wavelength (of a few hundred nm). However, with carbon nanotubes one is placed strictly in between the characteristic ranges accessible to X-rays or to light. Electron microscopy (the real-space imaging technique, as opposed to the reciprocal-space scattering) is most frequently used to visualize nanotubes – but it is an essentially surface technique, not applicable when the tubes are embedded in a matrix.

One of the possible answers to this problem lies in the wide angle X-ray diffraction, used in a more delicate way, utilizing the internal periodicity of

graphene layers lining the multi-wall nanotubes. Figure 6(b) shows characteristic features of the diffraction halos produced by an aligned nanocomposite. This example is for a 7wt% sample, uniaxially stretched by ∼50% along the axis shown by the arrow to induce the tube alignment. The Bragg peak around $3.40\mathring{A}$ corresponds to the (002) scattering plane which describes the inter-shell spacing periodicity within the MWNT, see e.g. [31]. The contrast is weak, when compared to the classical liquid crystal scattering imaged in (a), but it gives the distinct azimuthal bias and allows the accurate detection of multi-wall nanotube alignment, in this particular case with $Q \approx 0.23$, see Fig. 7 below.

A question must arise about the bright scattering ring corresponding to the length scale $\sim 7.5\mathring{A}$. This is a feature very interesting in itself, and is exactly the same in the pristine PDMS rubber prepared in the same batch. In the polymer network, with no solvent, the only X-ray contrast arises due to the difference between the chains and crosslinks. A very clear scattering length must be an indication of crosslink density fluctuations (in other terminology called clustering). As the extensive theory of this phenomenon suggests [177], at the given chain lengths and crosslinking density the network is well below the 'crosslink saturation threshold' and the correlation length of clustering should be of the order of mesh size. The length scale of $\sim 7.5\mathring{A}$ is very accurately this size and, accordingly, we believe this scattering to be produced by very small scale crosslink density fluctuations. These should not affect macroscopic properties, or even the local MWNT embedding. The bright inner ring at $\sim 7.5\mathring{A}$ is an inherent feature of the PDMS network at given crosslink density and does not affect the physics described in this work.

Analysis of uniaxial orientational ordering is a tool commonly used in a different fields of physics and engineering. The azimuthal bias of X-ray intensity scattered at the characteristic angle in the detection plane, illustrated in Fig. 6,

contains this information. However, the quantitative extraction of although the original formulation of the order parameter Q from the intensity variation $I(\beta)$ remains a delicate and complicated issue. Since the original formulation of this problem by Leadbetter [178], a number of practical approaches have been used, involving various levels of approximation. The simplest is to treat the azimuthal variation of the intensity $I(\beta)$ as the (non-normalized) probability distribution and write

$$\begin{aligned} Q &= \frac{3}{2N}\int_{-\pi/2}^{\pi/2}\cos^2\beta\, I(\beta)\sin\beta d\beta - \frac{1}{2} \\ &\text{with} \qquad N = \int_{-\pi/2}^{\pi/2} I(\beta)\sin\beta d\beta. \end{aligned} \tag{5}$$

However, there are many uncontrolled assumptions in this approach, not the least being the problem of the background intensity level in the scattering image. The most rigorous treatment of this problem is that of Deutsch [179]. Not going into details of quite involved analysis, we only quote the final result,

$$\begin{aligned} Q &= 1 - \frac{3}{2N}\int_0^{\frac{\pi}{2}} I(\beta)\left\{\sin^2\beta + \sin\beta\,\cos^2\beta\,\ln\left[\frac{1+\sin\beta}{\cos\beta}\right]\right\}d\beta \\ &\text{with} \qquad N = \int_0^{\frac{\pi}{2}} I(\beta)d\beta. \end{aligned} \tag{6}$$

With nanocomposites in mind, we need to compare these results with a model of tube alignment. The experimental data shown in Fig. 7(b) represents the sequence of calculations (by the Deutsch method, as explained above) of the order parameter induced in the initially non-aligned composite of MWNTs in crosslinked PDMS matrix, at 7wt% loading. As the sample is uniaxially stretched by a increasing factor $\lambda = 1 + \varepsilon$ (ε being the extension zz-strain), the induced alignment of embedded tubes is evident. The experimental data (in which the dotted line is just a guide to the eye) may be compared with the

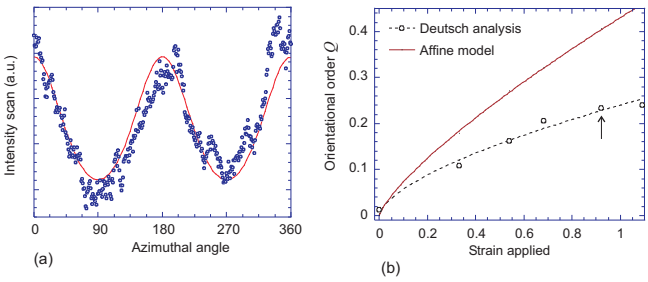

Figure 7: **Analysis of orientational order from X-ray images.** (a) Azimuthal scan of intensity scattered from the nanotubes, obtained from Fig. 6(b) (b) The orientational order parameter Q determined with the help of Eq.(6) and the theoretical prediction of the affine model, for 7wt% MWNT-PDMS rubber composite sample subjected to uniaxial strain, see text. [The arrow labels the sample imaged in Fig. 6(b).]

affine theoretical model, which assumes rigid rods embedded in a continuum matrix and rotating according to its volume-preserving deformation, Fig. 8(b). The argument is straightforward: The initial orientational distribution of rods (with no strain applied, $\varepsilon = 0$) is isotropic

$$P_0(\theta, \phi) = \frac{1}{4\pi} \sin\theta \, d\theta \, d\phi.$$

Take a rod that initially had an orientation θ with respect to the stretching axis, and thus the components $L_z = L\cos\theta$ and $L_\perp = L\sin\theta$ (with L the constant length of the rod).

The uniaxial extension of the incompressible elastic body is described by the matrix of strain tensor

$$\mathbf{\Lambda} = \begin{pmatrix} 1/\sqrt{\lambda} & 0 & 0 \\ 0 & 1/\sqrt{\lambda} & 0 \\ 0 & 0 & \lambda \end{pmatrix} \tag{7}$$

where the axis of stretching is taken as 3 (or z) and the magnitude of stretching

is $\lambda = 1 + \varepsilon = L/L_0$. This tensor describes the affine change of shape, which could be visualized as locally transforming a sphere into the ellipsoid of the same volume (incompressibility) and the aspect ratio $R_\parallel/R_\perp = \lambda^{3/2}$.

After such a deformation, every element of length in the body changes according to the matrix product $\boldsymbol{L}' = \boldsymbol{\Lambda} \cdot \boldsymbol{L}$, which in our case of uniaxial incompressible extension means that $L'_z = \lambda L_z$ and $L'_\perp = (1/\sqrt{\lambda})L_\perp$. This corresponds to the new angle of the rod, θ' such that $\tan\theta' = L'_\perp/L'_z = (1/\lambda^{3/2})\tan\theta$. Therefore, to obtain the new (now biased) orientational distribution function we need to convert the variable θ in $P_0(\theta)$ into the new (current) variable θ', which gives (after some algebraic manipulation)

$$\theta \to \mathrm{ArcTan}(\lambda^{3/2}\tan\theta'); \quad \sin\theta\,\mathrm{d}\theta \to \frac{\lambda^3}{(\cos^2\theta' + \lambda^3\sin^2\theta')^{3/2}}\sin\theta'\mathrm{d}\theta'.$$

This produces the final expression for the normalized orientational distribution

$$P(\theta', \phi) = \frac{\lambda^3}{4\pi(\cos^2\theta' + \lambda^3\sin^2\theta')^{3/2}}\sin\theta' d\theta' d\phi, \tag{8}$$

which is an explicit function of the uniaxial strain applied to the body ($\varepsilon = \lambda - 1$) and can be used to calculate the induced order parameter Q:

$$Q(\varepsilon) = \frac{3}{2}\int \cos^2\theta' \frac{[1+\varepsilon]^3}{4\pi(\cos^2\theta' + [1+\varepsilon]^3\sin^2\theta')^{3/2}}\sin\theta' d\theta' d\phi - \frac{1}{2}. \tag{9}$$

The exact analytical result for $Q(\varepsilon)$ is a cumbersome function, which plotted as solid line in Fig. 7(b). At relatively small strains, its approaches the linear regime: $Q \approx \frac{3}{5}\varepsilon - \frac{6}{35}\varepsilon^2 + ...$ The induced order parameter has all the expected qualitative features, and the appropriate order of magnitude. However, it is obvious that the real MWNT composite aligns slightly less under uniaxial extension. This is natural: we cannot expect nanotubes to behave exactly as rigid

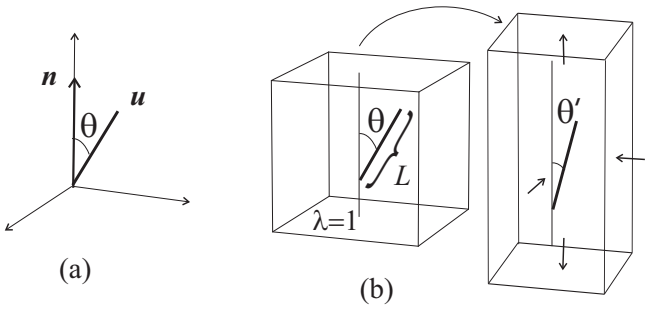

Figure 8: **Geometry of uniaxial ordering.** (a) Unit vectors $\boldsymbol{u}$ have a preference in aligning along the ordering direction $\boldsymbol{n}$, providing the frame for identifying the order parameter Q, Eq.(4). (b) The model of affine deformation and orientational order induced on the embedded rods on uniaxial stretching the matrix by a factor $\lambda = 1 + \varepsilon$, see text.

rods affinely embedded in the matrix – both the tube flexibility and the defects would contribute to the reduction of strain-induced alignment. Nevertheless, the fact that experimentally observed ordering of nanocomposite is relatively close to the affine model means that much of the affine idea is in fact valid.

There is an issue, well argued in the literature [140, 180], about whether a truly isotropic nanotube dispersion can be obtained. Regarding the tubes as rigid rods with extremely high aspect ratio, well dispersed in an amorphous medium, the Onsager transition to the steric orientational ordering should start at very low concentrations. However, the tube flexibility may play a role in softening this condition quite significantly. Currently, there is growing evidence of nematic behavior of nanotube-polymer composites and it is believed that this area of research could be a fertile scientific region to explore in the near future [140, 141, 174, 181].

5.2 Shear Alignment

There were many approaches to achieving nanotube alignment, dependent on the way in which they have been incorporated in a polymer matrix. Given below

is a coarse summary of some of the most significant works to date. The first attempt to control nanotube orientation in a polymer host matrix was reported by Ajayan *et al.* [24]. In that work, grounbreaking at the time, the authors observed tube alignment along the shear direction in the cutting planes, when preparing their samples for TEM.

More successful alignment was achieved by Deheer *et al.* [52]. In this work, the first real attempt to demonstrate alignment of nanotubes and associated properties of their aggregates was made. Arc-discharge nanotubes ($\sim$ 10nm and 1-5μm length) were ultrasonically dispersed in ethanol and centrifuged before being drawn through an 0.2μm-pore-ceramic filter leaving a uniform black deposit on the filter. The tube-coated side of the filter was pressed onto the polymer (Delrin or Teflon) and lifted off to reveal a grey surface which, with further rubbing with Teflon sheet or Aluminum foil, became silver and was shown to have high nanotube orientation along the direction of rubbing. The anisotropic nature of the film (birefringence and electrical properties) were demonstrated [52]. A production of aligned MWNT samples by the CVD injection method has been reported in [182]. However, all these studies only focused on the alignment of nanotubes in their bulk aggregates and did not deal with any aspect of polymer composition.

An important contribution to understanding the nature of nanotube alignment within a continuous polymer matrix was made by Jin *et al.* [183]. They obtained an anisotropic distribution of MWNTs in poly(hydroxy aminoether) by stretching cast films to a draw ratio of $\sim$5. Of great interest was the interpretation of the alignment of the nanotubes, described by analyzing 2D X-ray scattering data to determine the azimuthal full width at half maximum (FWHM) of the intershell correlation (002) within the multi-walled tubes, cf. Fig. 6(b). They demonstrated that a 50 wt% composite stretched to $\sim$3.3 exhibited a

FWHM of 46.4°. Although this is not a proper quantitative characteristic of uniaxial order, which would require a proper analysis of X-ray imaging data discussed in detail above, the results of [183] unambiguously confirm the tube alignment.

It is well-known in the field of classical polymer and composite alignment that the most effective way to achieve high shear alignment is the process of fiber drawing. Haggenmueller *et al.* [138] applied this technique, of melt-mixing SWNTs to promote nanotube dispersion and then subsequently spin-drawing fibers with extension ratios (λ up to 3600) to align the SWNTs along the fiber axis. As with alignment of carbon- or glass fibers in drawn composite fibers, the tube alignment was very strong, with the mosaic distribution FWHM$\sim 4°$.

Wood *et al.* [184] focused on aligning the tubes in a polymer matrix and characterizing the anisotropy through the D*-peak Raman signatures of longitudinally and transversely aligned nanotube-polymer composites. The alignment was achieved by spreading a dispersed nanotube-polymer viscous fluid onto a glass slide and shearing twice with a blade to induce flow orientation. The resulting thin films ($\sim$150μm thick) were immediately cured by UV-initiated crosslinking. The use of Raman spectroscopy as a viable tool to measure the degree of alignment of nanotubes in a polymer was then demonstrated. It also indicated the potential of using nanotubes as Raman active sensors. However, absorption and re-emission on consecutive layers makes this interesting technique only fully applicably to the single-walled nanotubes, in contrast to the X-ray analysis that relies on the scattering from the layers in MWNTs. Since the use of Raman techniques on MWNTs is not well defined, such work is rarely mentioned in the literature. The reader interested in the use of Raman spectroscopy for studying nanocomposites should refer to the recent detailed review [185].

Other groups have also reported mechanical orientation of nanocomposites through melt spinning [148, 186] and extrusion processes [187, 188, 189, 190, 191]. The work of Hobbie *et al.* [192] has been particularly important in understanding the shear alignment properties of nanotubes. They were able to demonstrate the full analogy between the nanotube orientation with the behavior of fibers aligned in a polymer melt under simple shear. When the shear stress is less than a certain critical value, $\sigma < \sigma_c$, the tubes are thought to broadly align along the direction of flow. For $\sigma > \sigma_c$, a transition occurs with the tubes aligning along the vorticity axis. This response is analogous to the semi-dilute fibre suspensions in purely viscous fluids [193, 194].

5.3 Electric Field

The shear flow, and in particular the melt spinning, are obvious routes to obtain uniaxially aligned nanocomposite samples. However, other routes have also recently become viable. Recent work has shown the possibility of using surface acoustic waves to align MWNTs [195]. Electric and magnetic fields can be used to induce tube alignment due to the very high anisotropy of their polarizability. This anisotropy originates from the delocalized π electrons along the nanotube axis, thus producing a substantial dielectric torque when they are exposed to an external field.

Electric fields can be applied at different times during the composite processing cycle. For example, aligned nanotubes can be obtained on their own via various processing routes or by directed growth using an electric field and inducing dipole moments [196, 197] (dielectrophoresis). Local alignment of individual nanotubes can also be accomplished using electric fields to initiate electrophoresis (charging induced mobility) [198, 199] or directed growth off surfaces [200]. With carefully aligned nanotube growth during processing, it has been shown

that a polymer such as polystyrene can then be introduced across the vertical tubes to form a well-aligned composite [201]. Nanotubes have also been dispersed and aligned in low-viscosity ethanol using an AC field [202, 203]. Larger nanofibres have been aligned in the same way in an epoxy resin during its curing [204, 205].

An interesting method was demonstrated by Dierking *et al.* [206], in which SWNTs and MWNTs were dispersed in a nematic liquid crystal, and by Courty *et al.* [174], who worked with crosslinked nematic elastomers. The inherent self-ordering properties of the liquid crystal, and its easy re-aligning upon application of an electric field, were used to manipulate nanotube orientation. Dispersing nanotubes in an anisotropic host material whose orientation can be manipulated by external fields can lead to possible applications for nanotubes as molecular switches [206], although their alignment mechanisms still relies on reorientation in the liquid state.

Only two groups have thus far reported results from experiments involving direct electric field alignment of nanotubes within a polymer matrix. Even then, both groups were investigating novel electromechanical actuator effects as oppose to actual permanent alignment states. Courty *et al.* [174] demonstrated the realignment of MWNTs in a nematic elastomer upon application of an electric field. The resulting novel electrically driven mechanical actuator response is discussed in detail in section 7. However, the initial alignment of the tubes in the elastomer was achieved through mechanical means, by uniaxial stretching before crosslinking. The second report on electric field effects on nanotubes embedded within a polymer matrix is that of Koratkar *et al.* [207]. They demonstrate the ability of a SWNT-polymer composite to mechanically actuate when a voltage is applied. In this case, the sample was grounded with respect to an Al electrode and cantilever-style actuation was observed. This area of research is very new

and requires substantial development. One of the reasons for the scarce amount of studies on the topic of electric field alignment (and electro-mechanical actuation) is perhaps because the experimental technique can sometimes prove very difficult and achieving such high fields (∼1-10MV/m) is also not trivial.

Electrospinning is a more recent technique that has shown some interesting results in terms of producing aligned nanotube composites. The method uses electrostatic forces to draw a jet of the polymer solution, which experiences high extension due to an electrostatically driven bending instability forming thin fibers [208]. The technique is better suited to produce very thin yarn fibers, especially when compared to the analogous technique of mechanical fiber drawing, because elongation can be achieved through a contactless scheme employing an electric field [209]. The composite fibers were obtained by converging an electric field on a rotating disk with a tapered edge. During processing, air pressure of 0.1-0.3kg/cm^2 was used to force the solution out of a syringe 0.5mm in diameter at a voltage difference of 15kV with respect to the collector. Later work has confirmed the viability of aligning SWNTs using this technique [208, 210, 211], but much development is required to achieve the full scalability of this method [212].

5.4 Magnetic Fields

Magnetic fields have recently shown promise in encouraging nanotube alignment along specific directions. Theory suggests that carbon nanotubes should have an anisotropic magnetic susceptibility [213]. Metallic tubes are calculated to be paramagnetic in the direction of their long axis. Paramagnetic character causes such tubes to align parallel to the applied field. All other nanotube variations are thought to be diamagnetic. The diamagnetic susceptibility is most negative in the direction perpendicular to the tube axis, causing tubes with

these chiralities to also align parallel to **B** [213]. Interestingly, the alignment energy is proportional to the overall amount of carbon. Hence, a rope of SWNTs or a multi-walled nanotube requires less magnetic field for alignment, than an individual single-walled nanotube of the same length [214].

The first group to produce a sample of aligned SWNTs using a magnetic field was led by Smalley [214, 215]. Their technique involved initially using a 25T field to align small quantities of tubes surfactant-stabilized in a solvent. The suspension was then filtered, while still under the strong field, to produce very well aligned aggregate structures. The method was further refined to produce larger macroscopic objects of aligned SWNTs [216]. Recent studies have shown that good alignment can also be garnered under similar processing conditions but with a much lower field strength, 7T [216, 217]. However, once again, this approach relies on the low-viscosity solvent, not presenting high resistance to the magnetic torque of nanotubes.

Kimura *et al.* [218] were the first to characterize a composite made using magnetic field alignment. The work was significant in that it treated the method of magnetic alignment as a viable future route toward large-scale industrial alignment processing. To this end, particular care was taken in selecting MWNTs produced via CVD processes, which were then further annealed at 2000-3000°C in Ar to enhance crystallinity. The so-called graphitiznment needed to occur, as the magnetic anisotropy has to be high enough to overcome thermal motion and the resistance against the viscous monomer solution. A field of 10T was used. Kimura *et al.* argue that other more physical techniques, such as mechanical stretching and melt processing, are limited to manufacturing composites in thin-film or fiber form. They go on to show that high magnetic fields can be used as an efficient, completely homogenous and direct means to align nanotubes [218].

Further work concentrating on SWNTs has since appeared, focusing on the

magnetically induced realignment of the polymer matrix itself to assist nanotube alignment [219, 220]. Where high viscosity polymer hosts are employed, it is thought that the reorientation of the nanotubes occurs due to a cooperative effect of the magnetic torque exerted by the **B**-field and the hydrodynamic torque and viscous shear exerted on the tubes by the polymer chains themselves. The cooperative mechanisms occur for many polymer-nanotube systems including those tested by Kimura *et al.* [218]. More specifically in the case of materials produced by Garmestani *et al.* the reorientation of the SWNT is related to a local stretching effect that the magnetic field exerts on the cross-linked epoxy network [219]. Thus, the self-organizing process of the polymeric system leads to enhanced SWNT alignment under high magnetic fields [220]. Naturally, this sort of mechanism can only occur for certain polymeric systems that respond to the magnetic field in a particular way.

At the time of writing, no single method of alignment dominates over any other. A vast array of techniques have been employed with new ones being invented seemingly every other month. The mechanical methods of manipulating nanotube orientation in a polymer are clear front-runners in terms of successful alignment regimes but it should be noted that these methods have received the most scientific attention. This is probably due to the fact that mechanical techniques are relatively simple to set-up and implement, and have been previously used on many systems prior to the advent of polymer-nanotube composites. New approaches based on magnetic alignment have shown a great deal of promise primarily due to the native scalability and flexibility of forming different composite shapes. Surprisingly, little research has been published on the ability of electric fields to align nanotubes embedded in composites.

6 Properties of Polymer-Nanotube composites

6.1 Mechanical Properties

So now our polymer-nanotube composite is made! Here, a brief review is given of the specialized properties that have so far been discovered.

It has already been mentioned that the first work to demonstrate the 'proof of concept' of nanotube-polymer composites was published by Ajayan *et al.* [24]. The group was primarily looking for a method of nanotube alignment, as opposed to characterizing composite properties. It took a few years before the efficacy of nanotube based composites was demonstrated. Amongst the first real attempts to characterize mechanical properties of nanocomposites came from Wagner *et al.* [25]. The team primarily looked at the interface between the MWNTs and a polymeric matrix and found that the composite could have an interfacial strength (a measure of stress transfer ability) an order of magnitude larger than other known advanced composites at the time. The multi-walled tubes were able to "telescopically" rupture, i.e. each layer breaking in succession. The precise nature of the stress transfer mechanism has yet to be verified but the work highlighted some important experimental observations regarding nanotube polymer interaction.

In the study of the nature of deformation and fracture modes of embedded nanotubes, compressive strengths of MWNTs were found to be $\sim$2 orders of magnitude higher than the compressive strength of any known fiber at the time [26]. It is important to note that this study focused on nanotubes within a polymeric matrix and *not* individual isolated tubes.

Shaffer and Windle were among the first to look at mechanical properties of nanocomposites systematically. Their polyvinyl-alcohol (PVA)/nanotube films were prepared by tube acid treatment, aqueous dispersion, and then mixing with aqueous polymer and casting the mixtures as films while evaporating the

water. Testing using dynamic mechanical thermal analyzer (DMTA) provided data on the tensile modulus and damping properties, as a function of nanotube concentration and temperature [221]. A modulus of 150MPa was obtained from the experimental data using a short-fiber composite approximation. This value compares poorly with data reported for an isolated MWNT (∼30GPa for a highly defective catalytically grown tube [91]). The discrepancy is thought to be caused by the poor stress transfer ability in the composite system [97, 222], as well as a contribution from the high defect density of the tubes – a consequence of the nanotube production method. Contrastingly, Cadek *et al.* revisited the PVA-nanotube system in 2002 [223], achieving seemingly better results from the nanocomposite. MWNTs (arc produced, hence lower defect density) were mixed with solution and cast on glass substrates. Young's modulus values of a 1wt% nanotube-PVA composite were higher by a factor of 1.8 over the pristine polymer; hardness was up by 1.6 [223]. Strong interfacial bonding was evidenced by TEM images and is thought to have originated due to local crystallization of the polymer nucleating off the nanotube surface. Further studies demonstrated fracture of the polymer rather that the polymer-nanotube interface verifying the strong interface [223]. Comparison of these two works [221, 223] demonstrates the importance of strong interfacial bonding and the benefits of superior quality nanotubes.

The study of mechanical behavior of epoxy/MWNT composites in both tension and compression [28] established that the compression modulus is higher than the tensile modulus, suggesting load transfer to the nanotubes in the matrix was much higher in compression. The Raman peak position, which is a measure of the strain experienced by the C–C bonds under loading, shifted significantly under compression but not in tension. This indicates that during load transfer to multi-walled nanotubes, only the outer layers are stressed in tension whereas

all the layers respond in compression [28]. This phenomenon is attributed to the inner layers sliding within the outer shell, thus the load not being effectively transmitted to all layers in the MWNT assembly during tension [90].

Qian *et al.* studied a polystyrene-nanotube composite system to better understand the fracture mechanisms. The presence of 1wt% MWNTs in the polymer raised the elastic stiffness by 36 and 42% for short and long tubes respectively. Theoretic arguments supported the experimental findings to within ∼10% accuracy [146, 224, 225]. At higher nanotube loadings, especially above 10vol%, large increases in the Young modulus were seen. Conversely, at concentrations ≤10vol% tensile strength *decreased* from the pristine polymer value of ∼40MPa. The tensile strength of the pristine polymer was only exceeded when nanotube loading was >15vol% [224]. The fracture mechanisms leading to such non-linear behavior were elucidated by performing deformation studies inside a TEM. Using the electron beam to create local thermal stresses leading to crack nucleation and propagation, the *in situ* TEM experiment showed that cracks would nucleate in a low nanotube density region and then propagate along weak nanotube-polymer interfaces or low nanotube density areas. Furthermore, the MWNTs became aligned perpendicular to the crack vector/direction and thus bridged the crack faces in the wake [224, 225, 222], in full analogy to the crazing effect in classical polymer science. Beyond a critical crack opening displacement (in this case, ∼800nm), nanotube breakage and tube pull-out occurs. A similar study by Watts and Hsu [226] verified these findings with one exception: nanotube breakage was not observed, probably due to their MWNTs being of higher quality. Fiber pull-out is also observed in epoxy-MWNT composite films [227, 228]. In particular, Gojny *et al.* used functionalized arc-produced MWNTs, demonstrating their enhanced bonding within the epoxy. This leads to the outer shells of the tubes remaining behind in the matrix after nanotube

pull-out has taken place [228].

Trying to understand fracture behavior in a MWNT-polymer composite is further complicated by the buckling behavior observed in multi-walled tubes under strain [229]. By analysis of a large number of bent nanotubes, Bower *et al.* showed that the onset buckling strain to be ≈5% and fracture strain ≈18% in MWNTs. Buckling was found to be a reversible deformation, at least at moderate strain. Plastic deformation of the tubes was observed at larger strains (30%-50%). Nanotube 'kinking' at fracture surfaces (by up to 20°–40°) was observed in the TEM. It is thought that topological defects, such as pentagon and heptagon pairs in the hexagonal layers, were formed under large strains, giving rise to the sharp bending geometry [229, 230]. Other more theoretical work has since appeared trying to describe nanotube deformations [231, 232, 233], but these treatments remain limited and a rigorous theory has yet to be developed.

All of these studies have concentrated their efforts on the mechanical behavior of multi-walled nanotubes in polymer matrices. Polymer composites with single-walled tubes appear to possess different properties. SWNT-epoxy composite were used to test elastic behavior and load transfer in the matrix [234]. The SWNTs were dispersed as prepared and thus were embedded into the matrix in rope-bundle form, a common arrangement for single-walled tubes. Experiment showed the tube bundles to be either pulled out of the matrix during fracture or stretched between two fracture surfaces, as with polymer crazing. Micro-Raman analysis supported the notion that individual tubes were not being significantly stretched. Thus, load transfer was not found to be effectively taking place. In essence, the data indicates that it is the low-modulus features of the nanotube bundles, and *not* the high axial modulus of individual SWNTs, that dominates the mechanical stability and strength of the composite. Im-

portant methods of improving the composite strength include breaking down SWNT bundles to form the individual tubes prior to dispersion in the matrix, or cross-linking the tubes within the bundles to prevent tube slippage [234]. The interface between SWNTs and polymer matrices was also highlighted as another limiting factor. Further Raman spectroscopy work indicates that stress transfer between SWNTs and the epoxy matrix does occur [235]. The shift in the G' Raman band to a lower wavenumber was indicative of strain in the graphite structure for all MWNTs and SWNTs tested. With some additional modelling, using the experimental data as a guideline, the effective modulus of SWNTs and MWNTs in the matrix was shown to be as high as 1TPa and 0.3TPa, respectively [235].

The polymer-nanotube interface, which is a restrictive factor in strengthening the composite, could be modified by tube functionalization [236, 237, 238, 239] (the pros and cons of which are discussed in section 4.2). On the other hand, improved mechanical and thermal properties were reported by Biercuk *et al.* using SWNTs that had not been chemically functionalized [137]. Their work focused on the heat transfer ability of the composite and they argue that chemical functionalisation reduces the thermal transport ability of the composite, a view shared and confirmed by Padgett *et al.* [240]. The contrasting views effectively demonstrate the need for further understanding and standardization of testing practises. Additionally, the trade-off between functionalizing nanotubes and achieving enhanced properties needs to be better understood.

A more theoretical study of Lordi and Yao [241] focused on the molecular mechanics of binding in nanotube-polymer composites to help understand the factors governing interfacial adhesion. Using the force-field molecular mechanics calculations, the authors determined binding energies and sliding frictional stresses between pristine carbon nanotubes and a range of polymers. When the

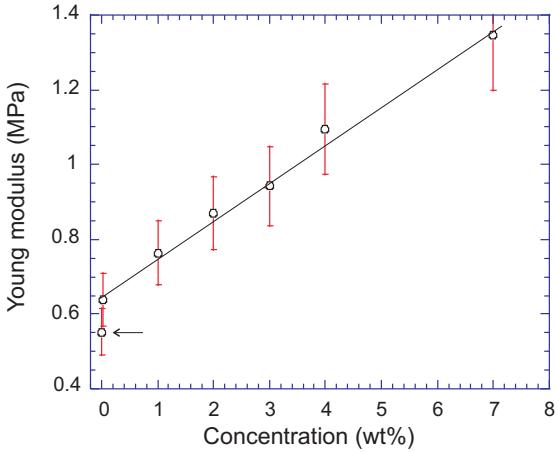

Figure 9: **Young modulus of nanocomposite rubber at low loading.** The plot shows the characteristic increase in the linear response modulus (here – the extensional Young modulus) on increasing the concentration of MWNTs embedded in a crosslinked PDMS rubber matrix. The line is the guide to an eye, while the arrow points at the pristine PDMS rubber value.

nanotubes are not chemically altered, hydrogen bond interactions with the π-bonded network on the nanotube surface were found to be strongest. However, and perhaps somewhat surprisingly, binding energies and frictional forces were found to play only a minor role in determining the strength of the interface. The significant factor in forming a strong interfacial bond is to have a helical polymer conformation around the nanotube. The authors suggested that the interface strength may originate from molecular-level entanglement of the two components, the tubes and the polymer chains, forcing long-range ordering of the polymer. A number of other simulations have also since appeared in the literature [242, 243, 244, 245] but their validity still requires experimental confirmation. Figure 9, illustrating the initial linear increase in the Young modulus values on increasing the nanotube concentration in a crosslinked PDMS elastomer matrix, also points at the interesting initial jump, when the first tube interfaces are added into the amorphous matrix.

This review has singularly focused on nanotubes within a continuous amorphous polymer matrix. It is perhaps worth considering the affect of nanotube addition on the polymer conformation. To date, very little work has appeared characterizing the influence nanotubes can have on the matrix. The work that is available concludes that the crystallization and morphology of a polymer can be strongly affected by nanotube inclusion. In particular, the presence of nanotubes provides additional surfaces which facilitate nucleation of crystalline lamellae in common polymers such as polypropylene [246, 247, 248]. Of great interest is the finding that the symmetries of the crystalline state of the polymer are directly determined by the underlying chirality of the nanotube [249]. Thus changes in crystal structure can be directly induced by the nanotubes [249, 250].

New methods are appearing all the time, showing promise in making composites with excellent mechanical properties. A layer-by-layer technique [251] has produced polymer-nanotube composite films with tensile strengths ∼220-325MPa. These values are several orders of magnitude greater than many industrially used plastics and approach the behavior of hard ceramics. Coating was achieved by alternate dipping of a glass slide or Si-wafer (substrates) into an acid treated SWNT dispersion and polymer solution. Once this procedure was complete, the films were heated to 120°C to promote cross-linking. Free standing membranes could then be lifted off the substrate. A similar method can be used to construct multi-layered films [252]. Recent advances with irradiation of SWNT bundles to promote cross-linking between individual tubes also offer the possibility of increased mechanical performance from composites made from such bundles [237, 253].

6.2 Electrical and Optical Properties

Many groups have studied the effects of incorporating nanotubes in a polymer matrix with the aim of modifying electrical properties. Different fabrication routes and potential end uses have been investigated. Here, we present only a summary of the vast amount of information on the subject, which we feel is significant to the subfield.

Looking to fabricate a novel material for molecular optoelectronics, Curran *et*.al. [27] designed a composite of carbon nanotubes and conjugated poly(m-phenylene vinylene-co-2,5-dioctoxy-p-phenylene vinylene) (PmPV). MWNTs and the polymer were mixed together in toluene and sonicated briefly. The authors believe that the polymer might have coiled around individual nanotubes, allowing π-π interactions to occur due to close intermolecular proximity. Nanotubes (MWNTs, arc produced) embedded in the polymer were found to increase the native conductivity by up to eight orders of magnitude as well as acting as 'nanometric' heat sinks, preventing the build up of large thermal effects, which can degrade these conjugated systems [27, 254]. The authors also demonstrated the ability of the composite to behave as an emissive layer in an organic light-emitting diode suggesting possible applications in optoelectronics. Why is this important, when many optoelectronic properties of conjugated polymers are successfully utilized already? The answer is in the doping mechanism. In a typical light-emitting polymer, exciton generation is vital hence the transport of charge is a key limiting factor in improving luminescence. Doping of such polymers introduces states within the polymer bandgap that can reduce and/or even quench luminescence. A polymer treated with nanotubes remains chemically undoped. Electronic processes such as radiative decay remain unaltered but the charge transport is still increased [27, 254]. The work illustrated the use of nanotubes in light-emitting polymers to improve the overall luminescence to

a very appreciable degree.

Another electric-based application for nanotube composites is for electrostatic dissipation, a property in much demand in the computing, automotive and aerospace industries. With electrostatic dissipation in mind, Sandler *et al.* [255] investigated conductivities of nanotube-epoxy composites. The macroscopic conductivity, $\sigma = 10^{-2}\mathrm{Sm}^{-1}$ with filler volume fraction ≈ 0.1 vol% was achieved [256]. By comparison with carbon black, an established filler used in polymers for electrostatic uses, these figures were a vast improvement especially considering the very low loadings of nanotubes. These findings (see also [228, 257]) suggest nanotubes have potential in replacing existing technologies when it comes to reducing electrostatic charging in bulk polymers. It is thought that a great deal of commercial work has already been undertaken, outside the public domain, with some automotive manufacturers already making use of nanotube-polymer composites in external body parts to encourage electrostatic painting [14].

The use of nanotubes to enhance the conducting ability or even *create* a conducting ability has also achieved widespread attention in the literature. A conducting (usually conjugated) polymer such as polyaniline has been shown to have its conductivity enhanced by the presence of nanotubes by an order of magnitude at room temperature: the nanotubes have a strong influence on the transport properties of the system [258, 259, 260]. It is interesting to note that the resistivity of the composites was much smaller than of the pure polyaniline, or even MWNTs alone. The authors suggest that *in situ* polymerization favors charge transfer between the nanotube and the polymer resulting in a composite conducting better than its constituents. A site-selective interaction between the tube and the quinoid ring of the conjugated polymer is responsible for the charge transfer process, as also shown by Raman spectroscopy [222, 258].

Considerable work has also focused on construction of photovoltaic devices. One of the earliest reports is the work by Romero *et al.* [261] in 1996. They deposited a layer of MWNTs on teflon, with a PPV derivative cast onto the structure, followed by a layer of Al on top to complete the sandwich device. The onset for nonlinear current injection was shown to occur at an applied electric field more than an order of magnitude lower than for semiconducting polymer/conducting oxide or metal heterojunction systems. However, only a small photocurrent was observed when stimulated by a He-Ne laser, possibly due to the relatively thick PPV active layer [222, 261]. Greater success was achieved by by Ago *et al.*, who constructed a similar photovoltaic device by depositing a PPV layer onto a glass-supported MWNT film [262]. Exciton separation was inferred as being enhanced due to experimental measurements showing reduced photoluminescence. Photoluminescence is the result of radiative recombination of the electron-hole pairs. The reduction in photoluminescence is an indication of a reduction in the recombination process. This directly implies that exciton (electron-hole pair) separation is improved, which is the desired effect in photovoltaic devices. Diode characteristics were demonstrated without light. Illumination of the sandwich structure through an Al electrode produced a photocurrent with a quantum efficiency twice that of standard indium tin oxide (ITO) electrode [262]. Enhancement of photovoltaic effects were also observed in polymer-SWNT films made by Kymakis *et al.* [263, 264, 265]. They used a spin/drop casting technique to deposit a polymer solution containing dispersed nanotubes onto ITO and quartz substrates. These authors have also recently shown an ability to tailor optical properties of these composites by varying nanotube volume fraction [266].

Only little work has so far been undertaken in the area of non-linear optical properties of the composites. Notably, the report of Chen *et al.* [267]

demonstrated third order optical non-linearity in a SWNT/polyimide composite. O'Flaherty *et al.* [268, 269] have demonstrated the use of polymer-nanotube composites as optical limiters (at loadings>3.8wt%) when dispersed in toluene.

Very recent work has also demonstrated the ability to form ultrathin, transparent, optically homogeneous, electrically conducting films of pure single-walled carbon nanotubes and the transfer of those films to various substrates [270]. The films exhibit optical transmittance comparable to that of commercial ITO in the visible spectrum. More importantly, far superior transmittance in the technologically relevant 2-5μm infrared spectral band is observed. This is an exciting development with the characteristics indicating broad applicability of the films for electrical coupling in photonic devices. As an example, the authors construct an electric field-activated optical modulator using the nanotube films. One of the other key advances in this work is the processing technique which allows the films to be deposited on any kind of substrate, polymer or otherwise.

It is difficult to formulate concluding remarks on the electrical and mechanical properties of nanotube-polymer composites because the field still remains in such a rapidly developing state. One can can see that recent reports are beginning to effectively demonstrate the real ability of carbon nanotubes to enhance and/or influence polymer behavior over and above commercially available advanced composites such as those based on carbon fibers. Although agreement on "numbers" is still difficult to achieve regarding mechanical properties, the state-of-the-art research displays an unambiguous trend towards ever improved composite behavior. With advances in nanotube production, as well as dispersion and alignment within a matrix, it is hoped that a standardized processing method can evolve, from which, gathering mechanical, electrical and optical data may prove far more routine.

7 Polymer-Nanotube Actuators

Recent work on nanotube-polymer composites has emerged that focuses on the functionalization ability the nanometer-scale objects bring to the polymer host. The nanotubes can have a differing response to specific stimuli, when compared to the host matrix. This can lead to non-linear mechanical behavior of the "transistor" nature, when an active system placed on the verge of spontaneous instability generates a large response under only a very small stimulus. That can be further tailored to produce some new and interesting actuator properties. This makes for an important case study as manipulation of the nanometer–scale architecture leads to direct influence on active actuator material behavior: a phenomenon at the very heart of modern nanoscience. Here, we discuss some recent advances in the field of nanotube-polymer composite actuators in some detail.

Of course, we first need to define what is meant by an actuator. The conversion of energy from an external source to mechanical work in a single solid state structure is of key importance for many potential applications. It is the ability of certain actuator materials to change their dimensions upon application of a given stimulus, such as heat, electric voltage or light, that makes them such attractive systems to study. Actuators with differing characteristics and mechanisms have been widely adopted by industry to fill each given technological requirement; see the comprehensive review [271] for detail. Some actuator systems have a one-way response, while others are based on an equilibrium, reversible response to the stimulus. Some (often called 'smart') materials exhibit a latent ability to actuate under the right conditions, such as shape-memory alloys [272] or liquid crystal elastomers [176]. Other systems require the blending of two (or more) distinctly different materials to impart a new physical response leading to the actuation process. Some of the work presented here focuses on the

second class of equilibrium mechanical actuation employing the use of carbon nanotubes embedded in a polymer matrix.

As has been illustrated in this review, interest in carbon nanotube based structures has increased exponentially since the first nanotube-polymer composite was reported a decade earlier by the group of Ajayan [24]. Since then, much attention has been given over to improve the mechanical and electrical properties of such composites. Very little information is available on the actuation properties of the nanotubes themselves, and almost none on the affect they can have on material actuation properties when embedded in a polymer film.

In studies of mechanical transformations induced in MWNTs, an interesting insight into the possibility of designing nanoelectromechanical (NEMS) systems has been obtained [273]. The bending of individual MWNTs under an applied electric field has been reported [73]. The torsional actuation has also been seen [274, 275]. All these studies focused on individual MWNTs and not a collection of tubes, nor their composite in a continuous matrix.

The polymer nanocomposite only very recently appeared as the subject of the mechanical actuation studies, with first reports demonstrating mechanical deformation under stimulus in nanocomposites [175, 276, 277]. However, with the exception of [174] where the electrically stimulated response of MWNTs embedded and aligned in a nematic elastomer matrix is considered, most of these studies have concentrated on accentuating the already present features of the host matrix by adding nanotubes. The nanotubes, in essence, exaggerate actuator behavior by either *improving* electromechanical responses or heating the sample more efficiently due to their inherent high conductivity [278].

7.1 Actuation Driven by Electric Field

The work of Courty *et al.* [174] was unique in that it reports a novel actuator response due to the presence of MWNTs, which otherwise would not occur in the host system. It is solely the presence of nanotubes within the matrix, that accounts for the effect observed. By controlling the type, concentration and alignment of tubes during fabrication, the actuator response could essentially be tailored – a novel development in the nanoscience field as a whole. For this reason, we now discuss this work in some detail, focusing on its experimental findings.

Nematic elastomers [176] have only recently entered the actuator arena; with strains of up to 400% and characteristic stress of up to 1 MPa, nematic elastomers offer a range of new engineering possibilities. In all cases studied so far, the mechanism of actuation, represented as spontaneous uniaxial extension/contraction of the nematic rubber along the director axis, has been the coupling of the elastic network to the underlying nematic order parameter Q, see [176] for details. Changing the order can be achieved by heating the material, leading to thermal actuators [279, 280, 281], by light in photochromic materials [282, 283], or by other means such as dilution by solvents. Although manipulation by electric fields is a common approach in physics of liquid crystals, electrically-driven actuation in nematic elastomers has been impossible, for a very simple reason. Assuming the electric field E interacts with dielectrically anisotropic nematic medium, causing the director to rotate, the characteristic energy density could be estimated as $\sim \varepsilon_o \Delta\varepsilon\, E^2$ [131]. For a field $E \sim 10^6$ V/m and typical dielectric parameters of nematic liquid crystals, this gives a density of $\sim 10^3$ J/m^3. The rubbery elastic network resists any such rotation with a characteristic energy density of the order of rubber modulus $\mu \sim 10^5$ J/m^3 or higher; clearly, no effect in response to a manageable electric field could be ex-

pected. A new approach to this problem produced a composite material with embedded and aligned nanotubes, presumably resulting with an effective dielectric anisotropy many orders of magnitude higher than in usual liquid crystals. As a result, a significant electromechanical response was demonstrated in such nematic nanocomposites.

Preparation of Nematic Nanocomposites

The side-chain polysiloxane nematic polymers and their elastomer networks, aligned in the uniaxial monodomain orientation, were prepared following the procedure pioneered by H. Finkelmann [176, 284]. The polysiloxane backbone chains with mesogenic rod-like side groups was vulcanized with the 10% crosslinking density. The multi-walled nanotubes were dispersed at very low concentration (between 0 and 0.05wt%) in polymer melt before crosslinking, using the shear-mixing technique. The crosslinking agent and initiator were added at the last stage of dispersion and the weak gel network was formed. This gel was uniaxially stretched and then crosslinked further, to freeze in the monodomain orientation of the nematic director by the subsequent completion of network crosslinking (this is a famous two-step crosslinking technique used in the field of liquid crystal elastomers). The MWNTs were aligned in this stretching direction as well. As we shall see below, the degree of tube alignment on uniaxial stretching of affine rubber is not very good – but it was much improved by the uniaxial nematic order in these materials. Figure 10 shows the scanning electron microscopy (SEM) images of freeze-fractured composite samples. Two fractured planes shown in Fig. 10(a,b) illustrate the low tube concentration and their good alignment. Image (b) shows several nanotubes protruding perpendicularly out of the fracture surface, while image (a) gives an opportunity to see a few nanotubes that showed out of the fractured polymer surface, nearly parallel or at a small angle to it.

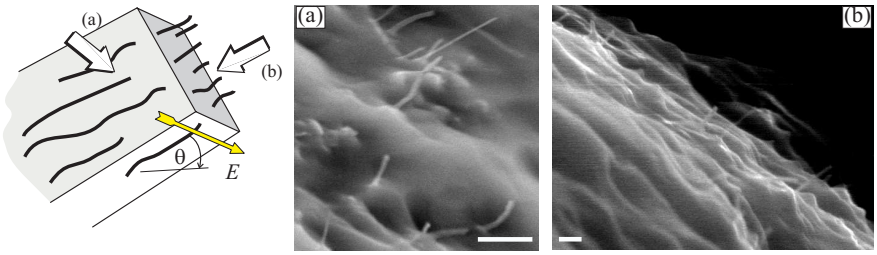

Figure 10: **A plane strip of nematic elastomer with embedded aligned MWNTs**. Applying electric field E across the sample causes a local torque and a small nanotube rotation. Arrows indicate two planes of freeze-fracture, shown in scanning electron microscopy images of the sample with 0.02wt% nanotubes: (a) in the plane parallel to the nematic director and the nanotube alignment axis, viewed from the top; (b) in the plane perpendicular to this axis, viewed edge-on. The scale bar in both images is 0.5 μm.

After this preparation, the samples of nematic elastomer-nanotube composite were subjected to a constant and an alternating electric field perpendicular to the initial director/CNT alignment, Fig. 10. Experiments were conducted such that no electric contact has been made with the sample, and no current flow has occurred. At such low amount of loading, shown by conductivity measurements to be well below the percolation limit, $\sim$0.1% [255], one should expect each nanotube to act on its own, embedded in a rubber elastic medium and providing a very strong local anchoring to the nematic director. As a result of strong dielectric torque on individual nanotubes, the whole polymer network structure experienced a significant mechanical shape change [174]. In the fixed-length (isostrain) conditions, the actuator force of sample contraction along the initial alignment axis was registered.

All mechanical measurements were carried out at a room temperature, sufficiently far from the glass or nematic-isotropic transition points. The tensile stress was calculated as the force divided by the fixed cross-section area. At the low tube concentrations used in this study, the Young modulus remained within the same order of magnitude as in the pristine rubber, $Y \sim 1$ MPa. The elec-

tric field was generated between two aluminium plates separated by 1.56 mm and surrounding the flat strip of clamped elastomer sample, with no contact. However, there seems to be no inherent argument against using the flexible electrodes attached directly to the polymer surface, as long as the composite remains insulating below the tube percolation threshold.

Electromechanical Response.

The samples, mounted on an insulating (thermally and electrically) frame which keeps the natural length of the sample fixed but measures the contractile force exerted on the clamps, were subjected to a constant electric field perpendicular to the initial director (and tube) orientation. With the applied voltage of 3000 V, the field was $E \approx 1.9 \cdot 10^6 \mathrm{V/m}$. Figure 11(a) shows a typical sequence of "field-on" and "field-off" cycles applied in a successive 1-hour sequence, demonstrating the dependence of actuation stress on the elapsed time. The response is clearly significant. The on-cycle shows an immediate steep rise in exerted stress, which then reaches a plateau level $\sigma_{\max}$ that depends on tube concentration as well as the field strength; the latter is illustrated in Fig. 11(b). There is no electromechanical response in the elastomer without nanotubes, which confirms estimates about the relative strength of dielectric and elastic torques.

The mechanism of the electromechanical response seems to be clear: the highly polarisable nanotubes experience a high torque to rotate towards the direction of constant field, proportional to $\Delta\varepsilon_{\mathrm{CNT}} E^2$. Nanotubes respond, and take the elastic network with them, causing the measurable stress on the clamped sample. It could be argued that, at high enough field, the nanotubes would rupture the local polymer network in their vicinity – however, the high reproducibility of data after many cycles suggests the effect remained equilibrium and no significant degradation has occurred. In these experiments the actual rotation of nanotubes is small, which is indicated by the field dependence of

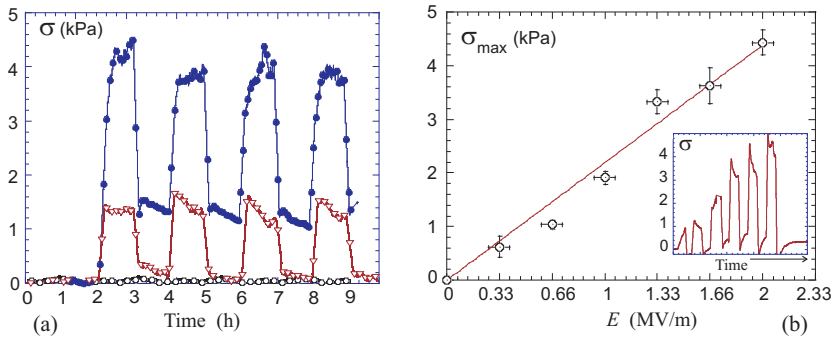

Figure 11: **Static electromechanical actuation in nematic nanocomposite**. (a) On- and Off- cycles of constant electric field ($E \approx 1.9$ MV/m), for samples with increasing MWNT concentration: 0% (non-filled elastomer, $\circ$), 0.0085% ($\triangledown$) and 0.02% ($\bullet$). (b) Dependence of the plateau stress $\sigma_{\max}$ on the applied field strength, for the 0.02% composite sample. The inset shows the elapsed time dependence, with each cycle at increasing constant field E.

plateau stress $\sigma_{\max}$, Fig. 11(b). If a full 90°-rotation was achieved one would see a plateau, whereas the linear increase $\sigma_{\max} = \text{const} \cdot E$ clearly indicates the regime of "small fields".

An important feature of any actuator is the reproducibility and the speed of its response. Figure 12 demonstrates the effect, for the 0.02wt% nanocomposite, under a field of $1.9 \cdot 10^6$V/m [as in Fig. 11(a)] switching on and off every 30 seconds. Clearly the stress responds very fast, to both "on" and "off" cycles. The initial spike at each cycle is an artefact of the power supply electronics that produces a voltage surge before settling at the required constant value. Both the short-time and the long-time representations in plots (a) and (b) illustrate a good reproducibility of response speed and the plateau stress amplitude $\sigma_{\max}$. This is practically useful for any actuator application.

The response stress is demonstrated to follow a linear dependence on applied field, at least in the range of fields studied. This, in fact, is puzzling because if one assumes the angle of local tube rotation, θ, to be linearly proportional to the dielectric torque (which in turn is $\propto \Delta\varepsilon_{\rm CNT} E^2$), then the uniaxial strain induced

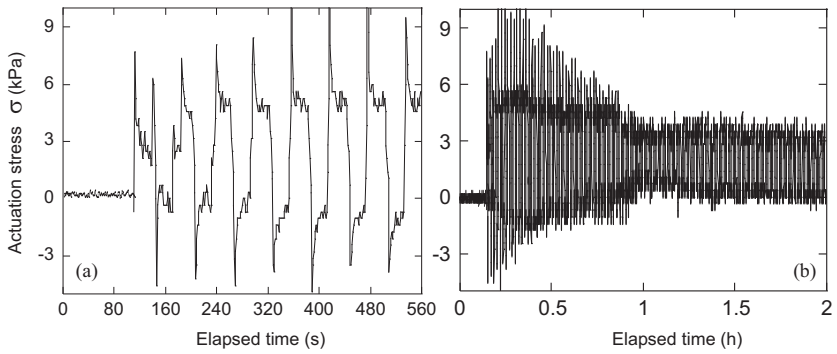

Figure 12: **The response of nematic nanocomposite to an alternating field**. The plots show, with different magnification, the response to a constant amplitude field switching on and off every 30 seconds. The short initial period of this test, plot (a), illustrates the high speed of the stress response which closely follows the field spike produced by the power supply on both switching on and off. The long-time representation (b) cannot resolve each individual cycle, but demonstrates the overall stability of the response.

in the rubbery network along the initial director axis should be $\propto (1 - \cos\theta) \propto \theta^2$, which means the strain (or in the isostrain conditions of the experiments, the exerted stress $\sigma_{\max}$) could be expected to follow $\propto E^4$; this is very clearly not the case. The observed linear field dependence of the response resembles the sop-called Fredericks effect in liquid crystals [131], where the externally imposed torque is opposed by an internal barrier in the system. In electrooptical cells of nematic liquid crystals (used in LCD displays) this barrier is provided by the anchoring on cell surfaces, while in these nanocomposites it is likely to be the bulk resistance. The barrier generates a threshold response, such that $\theta \propto \sqrt{|E - E_c|}$ (see [131, 285] for detail). This would explain the linear $\sigma_{\max}(E)$ dependence in Fig. 11(b), although would raise a question whether the data actually has a threshold.

Another effect which is difficult to explain is the stress not returning to zero after the field is switched off. It is only one of several unclear aspects of this phenomenon and an indication of how much is still not understood about the

underlying response of nanocomposite systems. This particular aspect is most likely a result of complex relaxation of the polymer network with embedded MWNTs, after spending a long time [1 hour in Fig. 11] under the applied field. However, simply claiming the slow relaxation as the explanation of non-zero "off"-stress may not be enough: if the nanotubes start each subsequent field-on cycle with a non-relaxed pre-tilt angle, one might expect the "on"-stress to increase. The results of Fig. 11 clearly demonstrate that this is not the case and that $\sigma_{\max}$ is a unique and reproducible function of applied field, but not the field application history. Note that in the fast-alternating field experiment on the same material under the same field, Fig. 12, the authors see no residual stress in the field-off state. If anything, the "off"-stress is below zero during the first hour of testing, perhaps due to a reactive effect in the elastic network. Figure 12(b) shows that after the initial settling period, the response becomes very regular, returning to zero on every 30-second cycle.

Courty *et al.* [174] conclude that, notwithstanding many shortcomings in their preparation techniques, sample characterization and understanding of the underlying fundamental physical mechanisms, the effect of large electromechanical actuation is demonstrated unambiguously and its speed and reproducibility make it an attractive system for new applications. The uniaxial stress, of the order ~ 1 kPa (or the corresponding actuation strain of 0.1%, from the rubber modulus $\mu \sim 1$ MPa), is induced by electric field of the order ~ 1 MV/m, in a nematic nanocomposite that was clearly not optimized in any way for better performance. It must be remembered that there are many systems that generate higher stress, and strains well above 50% are common in nematic elastomers. However, the ability to produce a mechanical response by an electrical stimulus is invaluable for many practical applications. Carbon nanotubes provide such a capacity in liquid crystal elastomers.

7.2 IR Driven Actuation

Very recent investigations have yielded a new but simple polymer nanocomposite system (comparing with nematic elastomer nanocomposites of [174]) which, by the presence of MWNTs, produces a mechanical response to the infrared (IR) irradiation [175]. Remarkably, a more detailed investigation has reported that both compressive *and* expansive[4] response modes exist in the same material depending on the externally uniaxial strain. The effect is thought to be dependent on the induced nanotube orientation within a homogenous polymer matrix, thus the orientational order parameter information summarized in section 5.1 will be relevant here. Here we shall test a basic theoretical model that predicts the opposite mechanical response of the composite at low, and at high degree of MWNT alignment. It is thought that no other materials of any class (metal, polymer, ceramic) can display so diverse behavior and to such large effect, thus, the study of the underlying physics of such systems is of clear scientific and commercial importance.

The typical materials include multi-walled nanotubes with a core diameter between 5-10nm, outer diameter of 60-100nm and length between 5-15 microns were used in these studies. They were produced using a catalytic CVD process and were thus fairly pure in the as-produced form with verified purity of >95%. These nanotubes were not surface-modified at any time during processing. As discussed earlier in this review, it is expected that chemical functionalisation of the tube walls would degrade their electronic and photonic properties due to the introduction of sp^3 hybridized carbon defects [118, 119].

The polymer matrix is PDMS (polydimethylsiloxane). In pristine condition this crosslinks with hydrosilane crosslinker, forming a uniform solvent-free elastomer. It was verified in these studies (with SEM on microtomed and freeze-

[4]Meaning that the sample spontaneously contracts or elongates on irradiation.

fractured surfaces) that the resulting polymer network is pure crosslinked PDMS with no other filler particles, as sometimes could be the case with supplied elastomer mixes. The nanotube-polymer composites are fabricated by shear mixing the tubes until the dispersion is achieved and then casting the viscous suspension and initiating the fast crosslinking by raising the temperature to 80°C. With no additional aligning treatment one obtains an almost completely isotropic nanotube dispersion in a homogeneous elastomer matrix.

Samples discussed below are identified by the wt% of MWNTs mixed with the PDMS. Most experiments have been conducted on the 0, 0.02, 0.5, 1, 4 and 7wt% MWNTs in PDMS elastomer films. The standard quantitative experiment consists of clamping the sample in the dynamometer frame so that its physical dimensions are not changed during the test. This isostrain configuration achieves two important purposes: avoiding complex issues of long-time stress relaxation after deforming the rubbery network and allowing unambiguous calculation of stress from the measured tensile force and the (fixed) transverse sample dimensions. As part of the experimental protocol, the samples (with natural length L_0 ∼5cm) were stretched in the frame before irradiation, so that different degrees of nanotube alignment could be imposed [cf. Fig. 7(b) and the details of the alignment analysis]. The imposed extensional strain is calculated by $\varepsilon = (L - L_0)/L_0$, with L provided from the micrometer reading after stretching. The materials were equilibrated in their 'natural' pre-strained state, and then the IR source was switched on to full intensity. In a typical protocol, after 15 minutes of exposure, the light source was switched off and further relaxation data was collected. Exactly the same protocol was then repeated for the same sample but at a different applied pre-strain ε.

With the IR irradiation, the question is always posed, whether the response is due to photon absorption or trivial heating of the materials (which does take

place during irradiation). As a comparison the same experiment was carried out with the infrared source replaced by a heater. The results indicate that although thermo-mechanical response was present in PDMS-nanocomposites, it was at least an order of magnitude smaller than the direct irradiation effect, suggesting that direct photon absorption by nanotubes is the origin of the nanocomposite mechanical response.

Infrared Actuation - Observations

The intriguing response of one sample to infrared stimuli is shown in Fig. 13, presenting the data on stress measured in the 1wt% PDMS-MWNT sample, initially non-aligned. It is important to spend some time and fully appreciate and expand upon the information provided in this complex plot. At the start of the experiment the sample has a very low, 2%, pre-strain ($\varepsilon = 0.02$) applied to it on mounting in the frame, after which the sample has been allowed to settle. Let us follow the first data set, which represents the 2% strain line labelled by $\circ$ in Fig. 13(a). The plot shows the raw data of measured stress as a function of time of the experiment. The initial stress reading is simply the measure of Young modulus $Y \approx 1.15$ MPa (cf. Fig. 9), and this point is transferred as an open symbol to the plot (b). At a certain moment of time ($t = 16$s) the IR light source is switched on and the stress reading changes. In this case (for 2% pre-strain) the change is downwards, meaning that the sample natural length has expanded on actuation. The new (IR-on) stress reading is transferred as a filed symbol to the plot (b). After a period of constant irradiation, of $\sim$2 min, the light source is switched off – and the stress reading returns to its original value. This experiment is then repeated with the same sample pre-strained at different values, up to 40%, as shown by the sequence of stress-reading curves in Fig. 13(a), and the corresponding pairs of stress-strain points, with and without IR stimulation, in the plot (b).

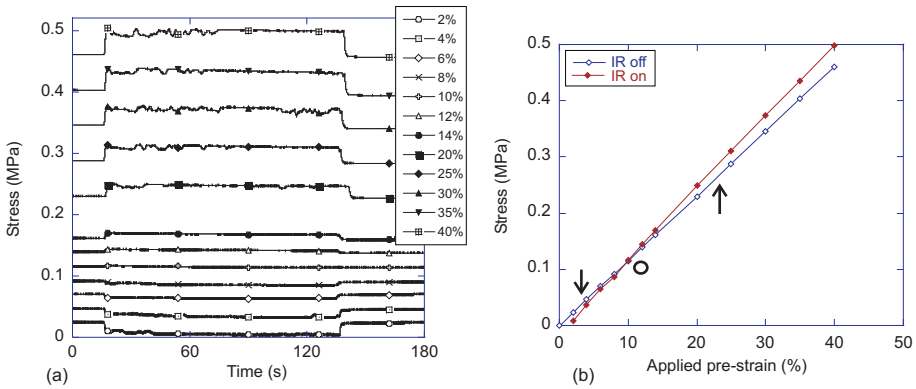

Figure 13: **The response of a nanocomposite to IR radiation**. The 1wt%-loaded sample is tested at different degrees of pre-strain ε: (a) raw data on stress measured at fixed sample length (different pre-strain curves labelled on the plot); (b) the stress-strain data – open symbols: in equilibrium, filled symbols: on IR actuation, highlighting the opposite direction of actuation at different extensions evident in plot (a).

A question of possible sample degradation may be asked: this type of experiment was deliberately conducted in the random sequence of pre-strain/equilibration cycles. The evidently consistent trend proves the reversibility of the sample state. The first main conclusion that can be made is the unambiguous and significant photo-actuation response of PDMS nanocomposites. However, the immediate next step is the observation of this response changing sign at a certain level of pre-strain. In other words, equilibrium or weakly stretched composites show the reversible *expansion* on irradiation, while highly stretched ones show the stronger tendency to *contract* (hence the increase in the measured stress). There are two main questions thus arising: what is the mechanism of photo-mechanical response, and why does it change its macroscopic signature on sample extension?

Figure 14 summarizes the actuation effect by plotting the magnitude of stress step in the IR-on state, at different levels of pre-strain and for samples with increasing MWNT loading. Although this is not explicitly measured in the

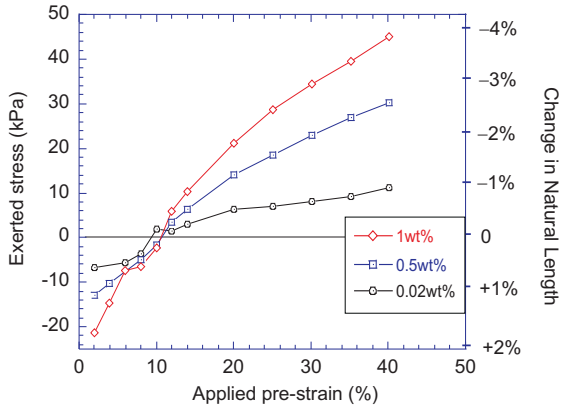

Figure 14: **Summary of photo-actuation response in PDMS nanocomposite.** The magnitude (in kPa) of exerted actuation stress (the height of steps in Fig. 13), as function of pre-strain, for samples with increasing MWNT loading. The right y-axis shows the corresponding actuation stroke: the change in the natural length L_0 on IR irradiation.

(isostrain) experiment, one can directly calculate the change of the underlying natural length of the samples on actuation. This is shown on the right axis of the same plot, explicitly illustrating the regions of expansion and contraction. Remarkably, all samples with different nanotube loading appear to have a crossover at the same point, around 10% pre-strain (the increase in the effect amplitude is to be expected). For comparison, the pristine PDMS rubber in the same experiment, shows a very minor stress response, of 2 orders of magnitude smaller than in Fig. 13, which is attributed entirely to the sample temperature change on IR irradiation.

Model of Actuation Mechanism

What is happening with carbon nanotubes (multi- or, presumably, single-wall as well) on absorption of infrared photons is not obviously clear. It is believed that the reason behind change of actuation direction on increasing sample extension is due to the nanotube alignment, described in section 5.1. At relatively low

pre-strains, the orientational order induced in the MWNT distribution is, to a good approximation, a linear function of the strain: $Q \approx 0.6\varepsilon$, cf. Eq.(9). At the crossover point $\varepsilon^* \approx 0.1$, giving $Q^* \sim 0.06$. Experiment suggests that at lower order parameter the nearly isotropic nanocomposite expands under IR-irradiation; as the order increases – the response becomes the photo-induced contraction with a magnitude increasing with order parameter. Now let us apply the same affine ideas about the induced orientational bias and averaging of the (hypothetical) individual nanotube response.

We have to assume that this individual response of a single MWNT after the photon absorption is, in essence, a contraction – because this is what better-aligned composite response is. It is easy to imagine why this could be for an initially rod-like tube: on absorption of an energy quantum it may generate kink-instabilities, thus decreasing its net length. Let us simply assume that each nanotube, on IR-stimulus, undergoes a contraction by a factor $\Delta < 1$ (certainly proportional to radiation intensity, which was kept constant in experiments we describe), accompanied by a transversely-isotropic volume conserving expansion $1/\sqrt{\Delta}$. This means that a local strain is created with the principal axes along the current nanotube orientation (at angle θ to the macroscopic z-axis), see Fig. 15(a):

$$\mathbf{\Lambda}(\mathrm{IR}) = \begin{pmatrix} 1/\sqrt{\Delta} & 0 & 0 \\ 0 & 1/\sqrt{\Delta} & 0 \\ 0 & 0 & \Delta \end{pmatrix}.$$

The projection of this local strain on the macroscopic axis of sample extension (and force measurement) is

$$\lambda_z(\mathrm{IR}) = \Delta \cos^2\theta + (1/\sqrt{\Delta}) \sin^2\theta. \tag{10}$$

When we average this local contribution with the probability to find the nan-

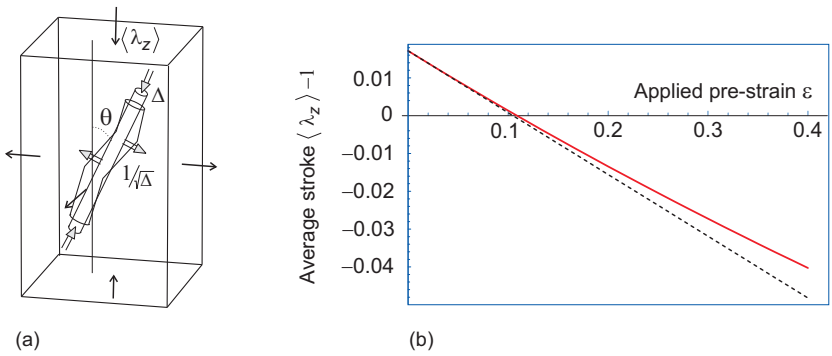

Figure 15: **Model of mechanical actuation.** (a) The scheme of local and macroscopic strains, illustrating how the distortion (kinking) of an individual tube, lying at an angle θ to the alignment axis, projects on the z-axis to contribute to the macroscopically uniaxial strain, Eq. (10). (b) The result of theoretical model, Eq. (11); the dashed line shows the linear approximation at small pre-strain ε. To achieve these values, the nanotube contraction factor is required to be $\Delta = 0.8$, as suggested by the crossover strain value $\varepsilon^* \sim 0.1$.

otube at this orientation, $P(\theta)$, from the Eq.(8), it will produce an estimate of the effective stroke of actuation $(\lambda_z - 1)$ or, if multiplied by the corresponding Young modulus, the exerted stress of Fig. 14. Such a model is very crude indeed, ignoring a large number of undoubtedly important and delicate factors of continuum elasticity, the interface features and the nanotube morphology. However, it is elastically self-consistent and has only one parameter Δ that carries all the underlying complexity of the nanotube problem in it.

The orientational averaging is straightforward:

$$\begin{aligned} \langle \lambda_z \rangle &= \int_0^\pi \frac{[\Delta \cos^2\theta + (1/\sqrt{\Delta})\sin^2\theta]\ (1+\varepsilon)^3}{4\pi(\cos^2\theta + [1+\varepsilon]^3 \sin^2\theta)^{3/2}} \sin\theta d\theta d\phi \\ &\approx \tfrac{1}{3}\left(\Delta + 2/\sqrt{\Delta}\right) - \tfrac{2}{5}\varepsilon\left(1/\sqrt{\Delta} - \Delta\right) \end{aligned} \tag{11}$$

Although the integral above has a full analytic form, it is more transparent to give its limit at small imposed pre-strain ε. This shows the key point: at very low pre-strain, $\varepsilon \to 0$, the average actuation stroke of the disordered nanocomposite

is a positive $(\lambda_z - 1)$, i.e. the expansion of its natural length. However, above the threshold pre-strain ε^* this average deformations becomes negative, i.e. the contraction. It is easy to find

$$\varepsilon^* \approx \frac{5(2 - \Delta^{1/2} - \Delta)}{6(1 + \Delta^{1/2} + \Delta)}, \tag{12}$$

so that the prediction would be to observe the crossover at $\varepsilon^* \sim 0.1$ if the nanotube response factor $\Delta \sim 0.8$, that is, on IR-irradiation the nanotube itself contracts overall by ∼20%. The value is higher than one might expect, considering reports in the literature of nanotube strains of only 1-2%. However, as Fig. 15(a) indicates, our proposition is not that of the lattice strain of nanotube walls but a contortion of the tube as a whole. This has not been seen, but one must appreciate that all existing experiments with individual tubes are carried out on (conducting) substrates, in totally different conditions. In any case, we found no reports about the MWCNT response under IR radiation.

Figure 15(b) plots the full (non-expanded) result of orientational averaging of actuation stroke $(\langle\lambda_z\rangle - 1)$ from the Eq.(11) to illustrate the points discussed here. The qualitative behavior (as summarized in Fig. 14) is reproduced here almost exactly, including the magnitude of the predicted actuation stroke (that is, the ratio $L_0(\mathrm{IR})/L_0(0) - 1$). Therefore, it is very likely that the orientational feature of the effect, with its change of actuation direction at a critical level of induced alignment, is captioned correctly, while much more work is required to understand the individual nanotube response to IR radiation generating the phenomenological factor Δ used in this analysis.

The rubber nanocomposite material described in this section shows the ability to change its actuation direction, from expansive to contractive response. The suggested simple model attributes this crossover to the orientational ordering imposed on nanotubes by uniaxial extension; a number of other experimental

funding support this conclusions. The strength of photo-actuator response, at a given radiation intensity, is of the order of tens-kPa. Translated into the stroke, this corresponds to actuation strains of $2 - 4\%$. As expected, the response increases at higher nanotube loading. Understanding the nature of the actuator mechanisms in this system certainly warrant further investigation. Many questions require clarification, in particular, the effect of using different types of nanotubes i.e. smaller multi-wall diameters, single-wall tubes, etc. Future investigations may also want to address the issue of using another host matrix and confirm its relatively neutral role in the actuation mechanism.

With actuating materials already used in widespread applications, from micromanipulators to vibration control, the systems that can respond to stimulus in both directions may open new possibilities and could mean an important new step toward finding applications for nanotube based materials above and beyond improvements in existing carbon fibre technologies.

8 Conclusions

In this review a survey of the polymer-nanotube composites has been given, with particular emphasis on the physics underpinning this new frontier of materials research. We have, in a sense, followed a recipe as possible production routes have been explored and potential properties discussed.

After an initial treatment of carbon nanotube fundamentals and their known mechanical and electrical properties, a full discussion on their production and purification has been given. Post production dispersion techniques along with alignment mechanisms have also been covered. Together, this represents an almost comprehensive catalogue of possible fabrication methods for polymer-nanotube composites.

Some effort has also been made to survey the properties these composites

can have. However, it is acknowledged that this is still a fast developing arena thus the focus has been on more widely accepted experimental data along with consideration of the physical models supporting such findings. Finally, considerable detail has been given over to the actuation properties and mechanisms which have recently been discovered in these systems.

So where do we stand? How far along are we in realizing nanotube-polymer composites in everyday use? Many of the manufacturing problems, such as dispersion and alignment as well as nanotube quality (i.e. defect distribution), are slowly being solved. This review gives state-of-the-art information on how this is being tackled. However, as we have seen, the solutions are not fully satisfactory as yet and thus commercial exploitation still requires much R&D work.

A huge international research effort is ongoing to quantify the properties and the science of polymer-nanotube composites. This is an exciting time to be involved in the field with new fundamental discoveries occurring regularly. It is hoped that this review will contribute in some small way to future discoveries and will inspire new research to augment an already fruitful discipline.

Acknowledgments

This work was carried out with the support of the Engineering and Physical Sciences Research Council (EPSRC), the EOARD (FA8655-04-1-3018), the ESA-ESTEC (18351/04) and a CASE award from Makevale Ltd. We thank S. Courty, G. Lagubeau, A.R. Tajbakhsh and A.M. Squires for useful discussions. The authors would also like to thank Aidan Craig and Karisma Patel for proofreading of the manuscript.

References

[1] R. P. Feynman, There's plenty of room at the bottom - An invitation to enter a new field of physics, Talk given at the annual meeting of the American Physical Society, 1959.

[2] K. E. Drexler, *Engines of Creation*, Anchor Books, NY, 1986.

[3] N. Taniguchi, *Nanotechnology*, Oxford University Press, Oxford, 1996.

[4] R. A. L. Jones, *Soft Machines*, Oxford University Press, Oxford, 2004.

[5] F. L. Mathews and R. D. Rawlings, *Composite Materials: Engineering and Science*, Chapman & Hall, 1994.

[6] G. W. Milton, *The Theory of Composites*, Cambridge University Press, 2002.

[7] M. S. Dresselhaus, G. Dresselhaus, K. Sugihara, I. L. Spain, and H. A. Goldberg, *Graphite Fibers and Fillaments*, Berlin: Springer, 1988, ed U Gonser, A Mooradian, K A Muller, M B Panish, and H Sakaki.

[8] H. J. Arpe, *Ullmann's Encyclopedia of Industrial Chemistry*, Wiley, 1998.

[9] N. M. Rodriguez, J. Mater. Res **8**, 3233 (1993).

[10] D. Chung, *Carbon Fiber Composites*, Butterworth-Heinemann, NY, 1994.

[11] P. M. Ajayan and T. W. Ebbesen, Rep. Prog. Phys. **60**, 1025 (1997).

[12] H. Kroto, J. R. Heath, S. Obrien, R. F. Curl, and R. E. Smalley, Nature **318**, 162 (1985).

[13] S. Iijima, Nature **354**, 56 (1991).

[14] H. G. Tennent, US Patent 4,663,230 (May 5th, 1987).

[15] M. Endo, Mechanisme de croissance en phase vapeur de fibres de carbone (the growth mechanisms of vapour-grown carbon fibers), PhD thesis, 1975, (In French).

[16] M. Dresselhaus, G. Dresselhaus, and R. Saito, Phys. Rev. B **45**, 6234 (1992).

[17] P. M. Ajayan and S. Iijima, Nature **358**, 23 (1992).

[18] S. Iijima and T. Ichihashi, Nature **363**, 603 (1993).

[19] D. Bethune, C. Kiang, M. Devries, G. Gorman, R. Savoy, J. Vazquez, and R. Beyers, Nature **363**, 605 (1993).

[20] R. Saito, G. Dresselhaus, and M. S. Dresselhaus, *Physical properties of carbon nanotubes*, Imperial College Press, London, 1998.

[21] S. Iijima, Physica B **323**, 1 (2002).

[22] Y. A. Krotov, D. H. Lee, and S. Louie, Phys. Rev. Lett. **78**, 4245 (1997).

[23] C. T. White, D. H. Robertson, and J. W. Mintmire, Phys. Rev. B **47**, 5485 (1993).

[24] P. M. Ajayan, O. Stephan, C. Colliex, and D. Trauth, Science **265**, 1212 (1994).

[25] H. D. Wagner, O. Lourie, Y. Feldman, and R. Tenne, Appl. Phys. Lett. **72**, 188 (1998).

[26] O. Lourie, D. M. Cox, and H. D. Wagner, Phys. Rev. Lett. **81**, 1638 (1998).

[27] S. A. Curran, P. M. Ajayan, W. J. Blau, D. L. Carroll, J. N. Coleman, A. B. Dalton, A. P. Davey, A. Drury, B. McCarthy, S. Maier, and A. Strevens, Advan. Mater. **10**, 1091 (1998).

[28] L. S. Schadler, S. C. Giannaris, and P. M. Ajayan, Appl. Phys. Lett. **73**, 3842 (1998).

[29] W. de Heer, MRS Bull. **29**, 281 (2004).

[30] Y. K. Zhou, B. L. He, W. J. Zhou, J. Huang, X. H. Li, B. Wu, and H. I. Li, Electrochim. Acta **49**, 257 (2004).

[31] J. C. Charlier and J. P. Michenaud, Phys. Rev. Lett. **70**, 1858 (1993).

[32] X. F. Zhang, X. B. Zhang, G. Vantendeloo, S. Amelinckx, M. O. Debeeck, and J. Vanlanduyt, J. Cryst. Growth **130**, 368 (1993).

[33] H. B. Harris, R. D. Kamien, and T. C. Lubensky, Rev. Mod. Phys. **71**, 1745 (1999).

[34] M. Bretz, B. G. Demczyk, and L. Q. Zhang, J. Cryst. Growth **141**, 304 (1994).

[35] M. Endo, K. Takeuchi, K. Kobori, K. Takahashi, H. W. Kroto, and A. Sarkar, Carbon **33**, 873 (1995).

[36] C. H. Kiang, W. A. Goddard, R. Beyers, and D. S. Bethune, Carbon **33**, 903 (1995).

[37] S. Datta, *Electronic Transport in Mesoscopic Systems*, Cambridge University Press, 1st edition, 1997.

[38] S. J. Tans, M. H. Devoret, H. J. Dai, A. Thess, R. E. Smalley, L. J. Geerligs, and C. Dekker, Nature **386**, 474 (1997).

[39] S. J. Tans, A. R. M. Verschueren, and C. Dekker, Nature **393**, 49 (1998).

[40] S. J. Tans, M. H. Devoret, R. J. A. Groeneveld, and C. Dekker, Nature **394**, 761 (1998).

[41] M. Bockrath, D. H. Cobden, P. L. McEuen, N. G. Chopra, A. Zettl, A. Thess, and R. E. Smalley, Science **275**, 1922 (1997).

[42] P. L. McEuen, M. S. Fuhrer, and H. K. Park, IEEE. Trans. Nanotechnol. **1**, 78 (2002).

[43] C. Dekker, Phys. Today **52**, 22 (1999).

[44] P. Avouris, J. Appenzeller, R. Martel, and S. J. Wind, Proc. IEEE. **91**, 1772 (2003).

[45] A. Jorio, R. Saito, T. Hertel, R. B. Weisman, G. Dresselhaus, and M. S. Dresselhaus, MRS Bull. **29**, 276 (2004).

[46] J. W. Mintmire, B. I. Dunlap, and C. T. White, Phys. Rev. Lett. **68**, 631 (1992).

[47] P. L. McEuen and J. Y. Park, MRS Bull. **29**, 272 (2004).

[48] J. W. Mintmire and C. T. White, Carbon **33**, 893 (1995).

[49] L. Langer, L. Stockman, J. P. Heremans, V. Bayot, C. H. Olk, C. Vanhaesendonck, Y. Bruynseraede, and J. P. Issi, J. Mater. Res **9**, 927 (1994).

[50] Y. Nakayama, S. Akita, and Y. Shimada, Jpn. J. Appl. Phys. Pt. 2 **34**, L10 (1995).

[51] W. A. Deheer, A. Chatelain, and D. Ugarte, Science **270**, 1179 (1995).

[52] W. A. Deheer, W. S. Bacsa, A. Chatelain, T. Gerfin, R. Humphreybaker, L. Forro, and D. Ugarte, Science **268**, 845 (1995).

[53] M. Terrones, W. K. Hsu, A. Schilder, H. Terrones, N. Grobert, J. P. Hare, Y. Q. Zhu, M. Schwoerer, K. Prassides, H. W. Kroto, and D. R. M. Walton, Appl. Phys. A-Mat. Sci. process **66**, 307 (1998).

[54] G. Baumgartner, M. Carrard, L. Zuppiroli, W. Bacsa, W. A. deHeer, and L. Forro, Phys. Rev. B **55**, 6704 (1997).

[55] S. Frank, P. Poncharal, Z. L. Wang, and W. A. de Heer, Science **280**, 1744 (1998).

[56] W. J. Liang, M. Bockrath, D. Bozovic, J. H. Hafner, M. Tinkham, and H. Park, Nature **411**, 665 (2001).

[57] J. Kong, E. Yenilmez, T. W. Tombler, W. Kim, H. J. Dai, R. B. Laughlin, L. Liu, C. S. Jayanthi, and S. Y. Wu, Phys. Rev. Lett. **8710**, art. no. 106801 (2001).

[58] H. J. Dai, E. W. Wong, and C. M. Lieber, Science **272**, 523 (1996).

[59] T. W. Ebbesen, H. J. Lezec, H. Hiura, J. W. Bennett, H. F. Ghaemi, and T. Thio, Nature **382**, 54 (1996).

[60] A. Thess, R. Lee, P. Nikolaev, H. J. Dai, P. Petit, J. Robert, C. H. Xu, Y. H. Lee, S. G. Kim, A. G. Rinzler, D. T. Colbert, G. E. Scuseria, D. Tomanek, J. E. Fischer, and R. E. Smalley, Science **273**, 483 (1996).

[61] M. Terrones, W. K. Hsu, J. P. Hare, H. W. Kroto, H. Terrones, and D. R. M. Walton, Phil. Trans. Roy. Soc. London A **354**, 2025 (1996).

[62] P. Lambin, A. Fonseca, J. P. Vigneron, J. B. Nagy, and A. A. Lucas, Chem. Phys. Lett. **245**, 85 (1995).

[63] P. Lambin, J. P. Vigneron, A. Fonseca, J. B. Nagy, and A. A. Lucas, Synthet. Metal. **77**, 249 (1996).

[64] V. Meunier, L. Henrard, and P. Lambin, Phys. Rev. B **57**, 2586 (1998).

[65] L. Chico, V. H. Crespi, L. X. Benedict, S. G. Louie, and M. L. Cohen, Phys. Rev. Lett. **76**, 971 (1996).

[66] M. Terrones, Annu. Rev. Mater. Res. **33**, 419 (2003).

[67] A. Hashimoto, K. Suenaga, A. Gloter, K. Urita, and S. Iijima, Nature **430**, 870 (2004).

[68] D. H. Robertson, D. W. Brenner, and J. W. Mintmire, Phys. Rev. B **45**, 12592 (1992).

[69] B. I. Yakobson, C. J. Brabec, and J. Bernholc, Phys. Rev. Lett. **76**, 2511 (1996).

[70] V. M. Harik, Computational Materials Science **24**, 328 (2002).

[71] R. S. Ruoff and D. C. Lorents, Carbon **33**, 925 (1995).

[72] M. M. J. Treacy, T. W. Ebbesen, and J. M. Gibson, Nature **381**, 678 (1996).

[73] P. Poncharal, Z. L. Wang, D. Ugarte, and W. A. de Heer, Science **283**, 1513 (1999).

[74] M. Endo, K. Takeuchi, S. Igarashi, K. Kobori, M. Shiraishi, and H. W. Kroto, J. Phys. Chem. Solids **54**, 1841 (1993).

[75] B. I. Yakobson and R. E. Smalley, American Scientist **85**, 324 (1997).

[76] B. I. Yakobson, Appl. Phys. Lett. **72**, 918 (1998).

[77] M. F. Yu, B. S. Files, S. Arepalli, and R. S. Ruoff, Phys. Rev. Lett. **84**, 5552 (2000).

[78] M. B. Nardelli, B. I. Yakobson, and J. Bernholc, Phys. Rev. Lett. **81**, 4656 (1998).

[79] M. F. Yu, T. Kowalewski, and R. S. Ruoff, Phys. Rev. Lett. **86**, 87 (2001).

[80] K. Okahara, K. Tanaka, H. Aoki, T. Sato, and T. Yamabe, Chem. Phys. Lett. **219**, 462 (1994).

[81] K. Harigaya, Phys. Rev. B **45**, 13676 (1992).

[82] B. Friedman, Phys. Rev. B **45**, 1454 (1992).

[83] K. Harigaya and M. Fujita, Synthet. Metal. **56**, 3196 (1993).

[84] K. Harigaya, Synthet. Metal. **56**, 3202 (1993).

[85] K. Harigaya and M. Fujita, Phys. Rev. B **47**, 16563 (1993).

[86] M. Ichida, S. Mizuno, Y. Saito, H. Kataura, Y. Achiba, and A. Nakamura, Phys. Rev. B **65**, art. no. 241407 (2002).

[87] M. T. Figge, M. Mostovoy, and J. Knoester, Phys. Rev. B **65**, art. no. 125416 (2002).

[88] V. Robert and J. P. Malrieu, J. Chemical Physics **120**, 8853 (2004).

[89] J. P. Salvetat, J. M. Bonard, N. H. Thomson, A. J. Kulik, L. Forro, W. Benoit, and L. Zuppiroli, Applied Physics a-Materials Science & Processing **69**, 255 (1999).

[90] M. F. Yu, O. Lourie, M. J. Dyer, K. Moloni, T. F. Kelly, and R. S. Ruoff, Science **287**, 637 (2000).

[91] J. P. Salvetat, A. J. Kulik, J. M. Bonard, G. A. D. Briggs, T. Stockli, K. Metenier, S. Bonnamy, F. Beguin, N. A. Burnham, and L. Forro, Advan. Mater. **11**, 161 (1999).

[92] M. S. Dresselhaus, G. Dresselhaus, and A. Jorio, Annual Review of Materials Research **34**, 247 (2004).

[93] M. F. Yu, J. Eng. Mater. Technol. **126**, 271 (2004).

[94] C. Journet, W. K. Maser, P. Bernier, A. Loiseau, M. L. delaChapelle, S. Lefrant, P. Deniard, R. Lee, and J. E. Fischer, Nature **388**, 756 (1997).

[95] A. G. Rinzler, J. Liu, H. Dai, P. Nikolaev, C. B. Huffman, F. J. Rodriguez-Macias, P. J. Boul, A. H. Lu, D. Heymann, D. T. Colbert, R. S. Lee, J. E. Fischer, A. M. Rao, P. C. Eklund, and R. E. Smalley, Applied Physics a-Materials Science & Processing **67**, 29 (1998).

[96] Z. F. Ren, Z. P. Huang, D. Z. Wang, J. G. Wen, J. W. Xu, J. H. Wang, L. E. Calvet, J. Chen, J. F. Klemic, and M. A. Reed, Appl. Phys. Lett. **75**, 1086 (1999).

[97] E. T. Thostenson, Z. F. Ren, and T. W. Chou, Composites Sci. Technol. **61**, 1899 (2001).

[98] M. N. R. Ashfold, P. W. May, C. A. Rego, and N. M. Everitt, Chemical Society Reviews **23**, 21 (1994).

[99] C. E. Snyder, H. Mandeville, H. G. Tennent, L. K. Truesdale, and J. J. Barber, US Patent 5,877,110 (March 2nd, 1999).

[100] G. G. Tibbetts, Appl. Phys. Lett. **42**, 666 (1983).

[101] H. D. Buckley and D. D. Edie, *Carbon-Carbon Materials and Composites*, Noyes Publications, Park Ridge, NJ, 1993.

[102] J. Liu, S. S. Fan, and H. J. Dai, MRS Bull. **29**, 244 (2004).

[103] Y. Saito, K. Nishikubo, K. Kawabata, and T. Matsumoto, J. Appl. Phys. **80**, 3062 (1996).

[104] Z. J. Shi, Y. F. Lian, F. H. Liao, X. H. Zhou, Z. N. Gu, Y. Zhang, S. Iijima, H. D. Li, K. T. Yue, and S. L. Zhang, J. Phys. Chem. Solids **61**, 1031 (2000).

[105] P. Nikolaev, M. J. Bronikowski, R. K. Bradley, F. Rohmund, D. T. Colbert, K. A. Smith, and R. E. Smalley, Chem. Phys. Lett. **313**, 91 (1999).

[106] A. M. Cassell, J. A. Raymakers, J. Kong, and H. J. Dai, J. Phys. Chem. B **103**, 6484 (1999).

[107] H. J. Dai, J. Kong, C. W. Zhou, N. Franklin, T. Tombler, A. Cassell, S. S. Fan, and M. Chapline, J. Phys. Chem. B **103**, 11246 (1999).

[108] S. Maruyama, R. Kojima, Y. Miyauchi, S. Chiashi, and M. Kohno, Chem. Phys. Lett. **360**, 229 (2002).

[109] H. Igarashi, H. Murakami, Y. Murakami, S. Maruyama, and N. Nakashima, Chem. Phys. Lett. **392**, 529 (2004).

[110] Y. M. Li, D. Mann, M. Rolandi, W. Kim, A. Ural, S. Hung, A. Javey, J. Cao, D. W. Wang, E. Yenilmez, Q. Wang, J. F. Gibbons, Y. Nishi, and H. J. Dai, Nano Lett. **4**, 317 (2004).

[111] L. X. Zheng, M. J. O'Connell, S. K. Doorn, X. Z. Liao, Y. H. Zhao, E. A. Akhadov, M. A. Hoffbauer, B. J. Roop, Q. X. Jia, R. C. Dye, D. E. Peterson, S. M. Huang, J. Liu, and Y. T. Zhu, Nat. Mater. **3**, 673 (2004).

[112] R. C. Haddon, J. Sippel, A. G. Rinzler, and F. Papadimitrakopoulos, MRS Bull. **29**, 252 (2004).

[113] J. Liu, A. G. Rinzler, H. J. Dai, J. H. Hafner, R. K. Bradley, P. J. Boul, A. Lu, T. Iverson, K. Shelimov, C. B. Huffman, F. Rodriguez-Macias, Y. S. Shon, T. R. Lee, D. T. Colbert, and R. E. Smalley, Science **280**, 1253 (1998).

[114] T. W. Ebbesen, P. M. Ajayan, H. Hiura, and K. Tanigaki, Nature **367**, 519 (1994).

[115] I. W. Chiang, B. E. Brinson, A. Y. Huang, P. A. Willis, M. J. Bronikowski, J. L. Margrave, R. E. Smalley, and R. H. Hauge, J. Phys. Chem. B **105**, 8297 (2001).

[116] I. W. Chiang, B. E. Brinson, R. E. Smalley, J. L. Margrave, and R. H. Hauge, J. Phys. Chem. B **105**, 1157 (2001).

[117] A. R. Harutyunyan, B. K. Pradhan, J. P. Chang, G. G. Chen, and P. C. Eklund, J. Phys. Chem. B **106**, 8671 (2002).

[118] A. Garg and S. B. Sinnott, Chem. Phys. Lett. **295**, 273 (2002).

[119] S. B. Sinnott, J. Nanosci. Nanotechnol. **2**, 113 (2002).

[120] E. Farkas, M. E. Anderson, Z. H. Chen, and A. G. Rinzler, Chem. Phys. Lett. **363**, 111 (2002).

[121] S. K. Doorn, R. E. Fields, H. Hu, M. A. Hamon, R. C. Haddon, J. P. Selegue, and V. Majidi, J. Am. Chem. Soc. **124**, 3169 (2002).

[122] B. L. Chen and J. P. Selegue, Anal. Chem. **74**, 4774 (2002).

[123] Y. J. Chen, M. L. H. Green, J. L. Griffin, J. Hammer, R. M. Lago, and S. C. Tsang, Advan. Mater. **8**, 1012 (1996).

[124] J. Chen, M. A. Hamon, H. Hu, Y. S. Chen, A. M. Rao, P. C. Eklund, and R. C. Haddon, Science **282**, 95 (1998).

[125] Z. Gu, H. Peng, R. H. Hauge, R. E. Smalley, and J. L. Margrave, Nano Lett. **2**, 1009 (2002).

[126] P. X. Hou, S. Bai, Q. H. Yang, C. Liu, and H. M. Cheng, Carbon **40**, 81 (2002).

[127] M. E. Itkis, S. Niyogi, M. E. Meng, M. A. Hamon, H. Hu, and R. C. Haddon, Nano Lett. **2**, 155 (2002).

[128] M. E. Itkis, D. E. Perea, S. Niyogi, S. M. Rickard, M. A. Hamon, B. Zhao, and R. C. Haddon, Nano Lett. **3**, 309 (2003).

[129] R. Sen, S. M. Rickard, M. E. Itkis, and R. C. Haddon, Chem. Mater. **15**, 4273 (2003).

[130] D. L. Shi, X. Q. Feng, Y. G. Y. Huang, K. C. Hwang, and H. J. Gao, J. Eng. Mater. Technol. **126**, 250 (2004).

[131] de Gennes P.-G. and P. J., *Physics of Liquid Crystals*, Oxford University Press, Oxford, 1994.

[132] J. Hilding, E. A. Grulke, Z. G. Zhang, and F. Lockwood, J. Disper. Sci. Tech. **24**, 1 (2003).

[133] K. L. Lu, R. M. Lago, Y. K. Chen, M. L. H. Green, P. J. F. Harris, and S. C. Tsang, Carbon **34**, 814 (1996).

[134] Y. A. Kim, T. Hayashi, Y. Fukai, M. Endo, T. Yanagisawa, and M. S. Dresselhaus, Chem. Phys. Lett. **355**, 279 (2002).

[135] N. Pierard, A. Fonseca, Z. Konya, I. Willems, G. Van Tendeloo, and J. B. Nagy, Chem. Phys. Lett. **335**, 1 (2001).

[136] Y. B. Li, B. Q. Wei, J. Liang, Q. Yu, and D. H. Wu, Carbon **37**, 493 (1999).

[137] M. J. Biercuk, M. C. Llaguno, M. Radosavljevic, J. K. Hyun, A. T. Johnson, and J. E. Fischer, Appl. Phys. Lett. **80**, 2767 (2002).

[138] R. Haggenmueller, H. H. Gommans, A. G. Rinzler, J. E. Fischer, and K. I. Winey, Chem. Phys. Lett. **330**, 219 (2000).

[139] P. G. Petrov, S. V. Ahir, and E. M. Terentjev, Langmuir **18**, 9133 (2002).

[140] M. F. Islam, A. M. Alsayed, Z. Dogic, J. Zhang, T. C. Lubensky, and A. G. Yodh, Phys. Rev. Lett. **92**, 088303 (2004).

[141] W. H. Song, I. A. Kinloch, and A. H. Windle, Science **302**, 1363 (2003).

[142] P. Potschke, T. D. Fornes, and D. R. Paul, Polymer **43**, 3247 (2002).

[143] S. Lin-Gibson, J. A. Pathak, E. A. Grulke, H. Wang, and E. K. Hobbie, Phys. Rev. Lett. **92**, art. no. 048302 (2004).

[144] R. G. Larson, *The Structure and Rheology of Complex Fluids*, Oxford University Press, Oxford, 1999.

[145] S. B. Kharchenko, J. F. Douglas, J. Obrzut, E. A. Grulke, and K. B. Migler, Nat. Mater. **3**, 564 (2004).

[146] R. Andrews, D. Jacques, M. Minot, and T. Rantell, Macromol. Mater. Eng. **287**, 395 (2002).

[147] P. Potschke, S. M. Dudkin, and I. Alig, Polymer **44**, 5023 (2003).

[148] M. Sennett, E. Welsh, J. B. Wright, W. Z. Li, J. G. Wen, and Z. F. Ren, Appl. Phys. A - Mat. Sci. Process. **76**, 111 (2003).

[149] P. Potschke, A. R. Bhattacharyya, and A. Janke, Eur. Polym. J. **40**, 137 (2004).

[150] A. Hirsch, Angew. Chem. Int. Ed. **41**, 1853 (2002).

[151] A. Hirsch, Principles of fullerene reactivity, in *Fullerenes and Related Structures*, volume 199 of *Topics in Current Chemistry*, pages 1–65, 1999.

[152] M. A. Hamon, H. Hu, P. Bhowmik, S. Niyogi, B. Zhao, M. E. Itkis, and R. C. Haddon, Chem. Phys. Lett. **347**, 8 (2001).

[153] M. A. Hamon, J. Chen, H. Hu, Y. S. Chen, M. E. Itkis, A. M. Rao, P. C. Eklund, and R. C. Haddon, Advan. Mater. **11**, 834 (1999).

[154] M. Holzinger, O. Vostrowsky, A. Hirsch, F. Hennrich, M. Kappes, R. Weiss, and F. Jellen, Angew. Chem. Int. Ed. **40**, 4002 (2001).

[155] V. Georgakilas, K. Kordatos, M. Prato, D. M. Guldi, M. Holzinger, and A. Hirsch, J. Am. Chem. Soc. **124**, 760 (2002).

[156] V. Georgakilas, D. Voulgaris, E. Vazquez, M. Prato, D. M. Guldi, A. Kukovecz, and H. Kuzmany, J. Am. Chem. Soc. **124**, 14318 (2002).

[157] P. J. Boul, J. Liu, E. T. Mickelson, C. B. Huffman, L. M. Ericson, I. W. Chiang, K. A. Smith, D. T. Colbert, R. H. Hauge, J. L. Margrave, and R. E. Smalley, Chem. Phys. Lett. **310**, 367 (1999).

[158] S. Banerjee and S. S. Wong, Nano Lett. **2**, 49 (2002).

[159] M. S. P. Shaffer, X. Fan, and A. H. Windle, Carbon **36**, 1603 (1998).

[160] S. Bandow, A. M. Rao, K. A. Williams, A. Thess, R. E. Smalley, and P. C. Eklund, J. Phys. Chem. B **101**, 8839 (1997).

[161] V. Krstic, G. S. Duesberg, J. Muster, M. Burghard, and S. Roth, Chem. Mater. **10**, 2338 (1998).

[162] G. S. Duesberg, M. Burghard, J. Muster, G. Philipp, and S. Roth, Chem. Commun. , 435 (1998).

[163] R. J. Chen, Y. G. Zhan, D. W. Wang, and H. J. Dai, J. Am. Chem. Soc. **123**, 3838 (2001).

[164] Y. Sun, S. R. Wilson, and D. I. Schuster, J. Am. Chem. Soc. **123**, 5348 (2001).

[165] J. Kong and H. J. Dai, J. Phys. Chem. B **105**, 2890 (2001).

[166] M. Zheng, A. Jagota, E. D. Semke, B. A. Diner, R. S. McLean, S. R. Lustig, R. E. Richardson, and N. G. Tassi, Nat. Mater. **2**, 338 (2003).

[167] M. A. Hamon, M. E. Itkis, S. Niyogi, T. Alvaraez, C. Kuper, M. Menon, and R. C. Haddon, J. Am. Chem. Soc. **123**, 11292 (2001).

[168] M. J. O'Connell, P. Boul, L. M. Ericson, C. Huffman, Y. H. Wang, E. Haroz, C. Kuper, J. Tour, K. D. Ausman, and R. E. Smalley, Chem. Phys. Lett. **342**, 265 (2001).

[169] M. J. O'Connell, S. M. Bachilo, C. B. Huffman, V. C. Moore, M. S. Strano, E. H. Haroz, K. L. Rialon, P. J. Boul, W. H. Noon, C. Kittrell, J. P. Ma, R. H. Hauge, R. B. Weisman, and R. E. Smalley, Science **297**, 593 (2002).

[170] M. F. Islam, E. Rojas, D. M. Bergey, A. T. Johnson, and A. G. Yodh, Nano Lett. **3**, 269 (2003).

[171] N. I. Kovtyukhova, T. E. Mallouk, L. Pan, and E. C. Dickey, J. Am. Chem. Soc. **125**, 9761 (2003).

[172] J. I. Paredes and M. Burghard, Langmuir **20**, 5149 (2004).

[173] J. Zhu, M. Yudasaka, M. F. Zhang, and S. Iijima, J. Phys. Chem. B **108**, 11317 (2004).

[174] S. Courty, J. Mine, A. R. Tajbakhsh, and E. M. Terentjev, Europhys. Lett. **64**, 654 (2003).

[175] H. Koerner, G. Price, N. A. Pearce, M. Alexander, and R. A. Vaia, Nature Mater. **3**, 115 (2004).

[176] M. Warner and E. M. Terentjev, *Liquid Crystal Elastomers*, Oxford University Press, Oxford, 2003.

[177] S. Panyukov and Y. Rabin, Phys. Rep. **269**, 1 (1996).

[178] A. J. Leadbetter, in *The Molecular Physics of Liquid Crystals*, edited by G. R. Luckhurst and G. W. Gray, Academic Press, NY.

[179] M. Deutsch, Phys. Rev. A **44**, 8264 (1991).

[180] A. M. Somoza, C. Sagui, and C. Roland, Phys. Rev. B **6308**, art. no. 081403 (2001).

[181] V. A. Davis, L. M. Ericson, A. N. G. Parra-Vasquez, H. Fan, Y. H. Wang, V. Prieto, J. A. Longoria, S. Ramesh, R. K. Saini, C. Kittrell, W. E. Billups, W. W. Adams, R. H. Hauge, R. E. Smalley, and M. Pasquali, Macromolecules **37**, 154 (2004).

[182] C. Singh, M. Shaffer, I. Kinloch, and A. Windle, Physica B **323**, 339 (2002).

[183] L. Jin, C. Bower, and O. Zhou, Appl. Phys. Lett. **73**, 1197 (1998).

[184] J. R. Wood, Q. Zhao, and H. D. Wagner, Compos. Part A-Appl. Sci. Manuf. **32**, 391 (2001).

[185] Q. Zhao and H. D. Wagner, Phil. Trans. Roy. Soc. A **362**, 2407 (2004).

[186] J. K. W. Sandler, S. Pegel, M. Cadek, F. Gojny, M. van Es, J. Lohmar, W. J. Blau, K. Schulte, A. H. Windle, and M. S. P. Shaffer, Polymer **45**, 2001 (2004).

[187] C. A. Cooper, D. Ravich, D. Lips, J. Mayer, and H. D. Wagner, Composites Sci. Technol. **62**, 1105 (2002).

[188] B. Vigolo, P. Poulin, M. Lucas, P. Launois, and P. Bernier, Appl. Phys. Lett. **81**, 1210 (2002).

[189] E. T. Thostenson and T. W. Chou, J. Phys. D - Appl. Phys. **35**, L77 (2002).

[190] E. T. Thostenson, W. Z. Li, D. Z. Wang, Z. F. Ren, and T. W. Chou, J. Appl. Phys. **91**, 6034 (2002).

[191] R. E. Gorga and R. E. Cohen, J. Polym. Sci. B-Polym. Phys. **42**, 2690 (2004).

[192] E. K. Hobbie, H. Wang, H. Kim, S. Lin-Gibson, and E. A. Grulke, Phys. Fluids **15**, 1196 (2003).

[193] M. Rahnama, D. L. Koch, and E. S. G. Shaqfeh, Phys. Fluids **7**, 487 (1995).

[194] C. A. Stover, D. L. Koch, and C. Cohen, J. Fluid Mech. **238**, 277 (1992).

[195] C. J. Strobl, C. Schaflein, U. Beierlein, J. Ebbecke, and A. Wixforth, Appl. Phys. Lett. **85**, 1427 (2004).

[196] B. H. Fishbine, Fullerene Sci. Technol. **4**, 87 (1996).

[197] Y. G. Zhang, A. L. Chang, J. Cao, Q. Wang, W. Kim, Y. M. Li, N. Morris, E. Yenilmez, J. Kong, and H. J. Dai, Appl. Phys. Lett. **79**, 3155 (2001).

[198] K. Yamamoto, S. Akita, and Y. Nakayama, Jpn. J. Appl. Phys. Pt. 2 **35**, L917 (1996).

[199] E. Joselevich and C. M. Lieber, Nano Lett. **2**, 1137 (2002).

[200] A. Ural, Y. M. Li, and H. J. Dai, Appl. Phys. Lett. **81**, 3464 (2002).

[201] B. J. Hinds, N. Chopra, T. Rantell, R. Andrews, V. Gavalas, and L. G. Bachas, Science **303**, 62 (2004).

[202] K. Bubke, H. Gnewuch, M. Hempstead, J. Hammer, and M. L. H. Green, Appl. Phys. Lett. **71**, 1906 (1997).

[203] X. Q. Chen, T. Saito, H. Yamada, and K. Matsushige, Appl. Phys. Lett. **78**, 3714 (2001).

[204] T. Prasse, J. Y. Cavaille, and W. Bauhofer, Composites Sci. Technol. **63**, 1835 (2003).

[205] G. Kim and Y. M. Shkel, J. Mater. Res **19**, 1164 (2004).

[206] I. Dierking, G. Scalia, P. Morales, and D. LeClere, Advan. Mater. **16**, 865 (2004).

[207] N. Koratkar, A. Modi, J. Kim, B. Q. Wei, R. Vajtai, S. Talapatra, and P. M. Ajayan, J. Nanosci. Nanotechnol. **4**, 69 (2004).

[208] D. Li and Y. N. Xia, Advan. Mater. **16**, 1151 (2004).

[209] Y. Dror, W. Salalha, R. L. Khalfin, Y. Cohen, A. L. Yarin, and E. Zussman, Langmuir **19**, 7012 (2003).

[210] F. Ko, Y. Gogotsi, A. Ali, N. Naguib, H. H. Ye, G. L. Yang, C. Li, and P. Willis, Advan. Mater. **15**, 1161 (2003).

[211] C. Seoul, Y. T. Kim, and C. K. Baek, J. Polym. Sci. B-Polym. Phys. **41**, 1572 (2003).

[212] R. Sen, B. Zhao, D. Perea, M. E. Itkis, H. Hu, J. Love, E. Bekyarova, and R. C. Haddon, Nano Lett. **4**, 459 (2004).

[213] J. P. Lu, Phys. Rev. Lett. **74**, 1123 (1995).

[214] J. Hone, M. C. Llaguno, N. M. Nemes, A. T. Johnson, J. E. Fischer, D. A. Walters, M. J. Casavant, J. Schmidt, and R. E. Smalley, Appl. Phys. Lett. **77**, 666 (2000).

[215] B. W. Smith, Z. Benes, D. E. Luzzi, J. E. Fischer, D. A. Walters, M. J. Casavant, J. Schmidt, and R. E. Smalley, Appl. Phys. Lett. **77**, 663 (2000).

[216] D. A. Walters, M. J. Casavant, X. C. Qin, C. B. Huffman, P. J. Boul, L. M. Ericson, E. H. Haroz, M. J. O'Connell, K. Smith, D. T. Colbert, and R. E. Smalley, Chem. Phys. Lett. **338**, 14 (2001).

[217] M. J. Casavant, D. A. Walters, J. J. Schmidt, and R. E. Smalley, J. Appl. Phys. **93**, 2153 (2003).

[218] T. Kimura, H. Ago, M. Tobita, S. Ohshima, M. Kyotani, and M. Yumura, Advan. Mater. **14**, 1380 (2002).

[219] H. Garmestani, M. S. Al-Haik, K. Dahmen, R. Tannenbaum, D. S. Li, S. S. Sablin, and M. Y. Hussaini, Advan. Mater. **15**, 1918 (2003).

[220] E. S. Choi, J. S. Brooks, D. L. Eaton, M. S. Al-Haik, M. Y. Hussaini, H. Garmestani, D. Li, and K. Dahmen, J. Appl. Phys. **94**, 6034 (2003).

[221] M. S. P. Shaffer and A. H. Windle, Advan. Mater. **11**, 937 (1999).

[222] P. J. F. Harris, Int. Mater. Rev. **49**, 31 (2004).

[223] M. Cadek, J. N. Coleman, V. Barron, K. Hedicke, and W. J. Blau, Appl. Phys. Lett. **81**, 5123 (2002).

[224] D. Qian, E. C. Dickey, R. Andrews, and T. Rantell, Appl. Phys. Lett. **76**, 2868 (2000).

[225] D. Qian and E. C. Dickey, J. Microscopy **204**, 39 (2001).

[226] P. C. P. Watts and W. K. Hsu, Nanotechnol. **14**, L7 (2003).

[227] X. J. Xu, M. M. Thwe, C. Shearwood, and K. Liao, Appl. Phys. Lett. **81**, 2833 (2002).

[228] F. H. Gojny, J. Nastalczyk, Z. Roslaniec, and K. Schulte, Chem. Phys. Lett. **370**, 820 (2003).

[229] C. Bower, R. Rosen, L. Jin, J. Han, and O. Zhou, Appl. Phys. Lett. **74**, 3317 (1999).

[230] J. Han, M. P. Anantram, R. L. Jaffe, J. Kong, and H. Dai, Phys. Rev. B **57**, 14983 (1998).

[231] M. Wong, M. Paramsothy, X. J. Xu, Y. Ren, S. Li, and K. Liao, Polymer **44**, 7757 (2003).

[232] T. Xiao and K. Liao, Compos. Part B-Eng. **35**, 211 (2004).

[233] M. Terrones and H. Terrones, Phil. Trans. Roy. Soc. London A **361**, 2789 (2003).

[234] P. M. Ajayan, L. S. Schadler, C. Giannaris, and A. Rubio, Advan. Mater. **12**, 750 (2000).

[235] C. A. Cooper, R. J. Young, and M. Halsall, Compos. Part A-Appl. Sci. Manuf. **32**, 401 (2001).

[236] J. Zhu, J. D. Kim, H. Q. Peng, J. L. Margrave, V. N. Khabashesku, and E. V. Barrera, Nano Lett. **3**, 1107 (2003).

[237] P. M. Ajayan and F. Banhart, Nat. Mater. **3**, 135 (2004).

[238] L. W. Qu, Y. Lin, D. E. Hill, B. Zhou, W. Wang, X. F. Sun, A. Kitaygorodskiy, M. Suarez, J. W. Connell, L. F. Allard, and Y. P. Sun, Macromolecules **37**, 6055 (2004).

[239] H. T. Ham, C. M. Koo, S. O. Kim, Y. S. Choi, and I. J. Chung, Macromol. Res. **12**, 384 (2004).

[240] C. W. Padgett and D. W. Brenner, Nano Lett. **4**, 1051 (2004).

[241] V. Lordi and N. Yao, J. Mater. Res **15**, 2770 (2000).

[242] S. J. V. Frankland, A. Caglar, D. W. Brenner, and M. Griebel, J. Phys. Chem. B **106**, 30468 (2002).

[243] S. J. V. Frankland, V. M. Harik, G. M. Odegard, D. W. Brenner, and T. S. Gates, Composites Sci. Technol. **63**, 1655 (2003).

[244] C. Y. Li and T. W. Chou, J. Nanosci. Nanotechnol. **3**, 423 (2003).

[245] H. R. Lusti and A. A. Gusev, Model. Simul. Mater. Sci. Eng. **12**, S107 (2004).

[246] K. Lozano and E. V. Barrera, J. Appl. Polym. Sci. **79**, 125 (2001).

[247] L. Valentini, J. Biagiotti, J. M. Kenny, and S. Santucci, Composites Sci. Technol. **63**, 1149 (2003).

[248] J. Sandler, P. Werner, M. S. P. Shaffer, V. Demchuk, V. Altstadt, and A. H. Windle, Compos. Part A - Appl. Sci. Manufac. **33**, 1033 (2002).

[249] R. Czerw, Z. X. Guo, P. M. Ajayan, Y. P. Sun, and D. L. Carroll, Nano Lett. **1**, 423 (2001).

[250] B. P. Grady, F. Pompeo, R. L. Shambaugh, and D. E. Resasco, J. Phys. Chem. B **106**, 5852 (2002).

[251] A. A. Mamedov, N. A. Kotov, M. Prato, D. M. Guldi, J. P. Wicksted, and A. Hirsch, Nature Mater. **1**, 190 (2002).

[252] J. H. Rouse and P. T. Lillehei, Nano Lett. **3**, 59 (2003).

[253] A. Kis, G. Csanyi, J. P. Salvetat, T. N. Lee, E. Couteau, A. J. Kulik, W. Benoit, J. Brugger, and L. Forro, Nat. Mater. **3**, 153 (2004).

[254] S. Curran, A. P. Davey, J. Coleman, A. Dalton, B. McCarthy, S. Maier, A. Drury, D. Gray, M. Brennan, K. Ryder, M. L. de la Chapelle, C. Journet, P. Bernier, H. J. Byrne, D. Carroll, P. M. Ajayan, S. Lefrant, and W. Blau, Synthet. Metal. **103**, 2559 (1999).

[255] J. Sandler, M. S. P. Shaffer, T. Prasse, W. Bauhofer, K. Schulte, and A. H. Windle, Polymer **40**, 5967 (1999).

[256] J. K. W. Sandler, J. E. Kirk, I. A. Kinloch, M. S. P. Shaffer, and A. H. Windle, Polymer **44**, 5893 (2003).

[257] K. Lozano, J. Bonilla-Rios, and E. V. Barrera, J. Appl. Polym. Sci. **80**, 1162 (2001).

[258] M. Cochet, W. K. Maser, A. M. Benito, M. A. Callejas, M. T. Martinez, J. M. Benoit, J. Schreiber, and O. Chauvet, Chem. Commun. , 1450 (2001).

[259] J. G. Deng, X. B. Ding, W. C. Zhang, Y. X. Peng, J. H. Wang, X. P. Long, P. Li, and A. S. C. Chan, Eur. Polym. J. **38**, 24971 (2002).

[260] H. Zengin, W. S. Zhou, J. Y. Jin, R. Czerw, D. W. Smith, L. Echegoyen, D. L. Carroll, S. H. Foulger, and J. Ballato, Advan. Mater. **14**, 1480 (2002).

[261] D. B. Romero, M. Carrard, W. DeHeer, and L. Zuppiroli, Advan. Mater. **8**, 899 (1996).

[262] H. Ago, K. Petritsch, M. S. P. Shaffer, A. H. Windle, and R. H. Friend, Adv. Mater. **11**, 1281 (1999).

[263] E. Kymakis, I. Alexandou, and G. A. J. Amaratunga, Synthet. Metal **127**, 59 (2002).

[264] E. Kymakis and G. A. J. Amaratunga, Appl. Phys. Lett. **80**, 112 (2002).

[265] E. Kymakis, I. Alexandrou, and G. A. J. Amaratunga, J. Appl. Phys. **93**, 1764 (2003).

[266] E. Kymakis and G. A. J. Amaratunga, Synth. Metals **142**, 161 (2004).

[267] Y. C. Chen, N. R. Raravikar, L. S. Schadler, P. M. Ajayan, Y. P. Zhao, T. M. Lu, G. C. Wang, and X. C. Zhang, Appl. Phys. Lett. **81**, 975 (2002).

[268] S. A. O'Flaherty, R. Murphy, S. V. Hold, M. Cadek, J. N. Coleman, and W. J. Blau, J. Phys. Chem. B **107**, 958 (2003).

[269] S. M. O'Flaherty, S. V. Hold, M. E. Brennan, M. Cadek, A. Drury, J. N. Coleman, and W. J. Blau, J. Opt. Soc. Am. B - Opt. Physics **20**, 49 (2003).

[270] Z. C. Wu, Z. H. Chen, X. Du, J. M. Logan, J. Sippel, M. Nikolou, K. Kamaras, J. R. Reynolds, D. B. Tanner, A. F. Hebard, and A. G. Rinzler, Science **305**, 1273 (2004).

[271] J. E. Huber, N. A. Fleck, and M. F. Ashby, Proc. Roy. Soc London Ser. A. **453**, 2185 (1997).

[272] K. Battacharya, *Microstructure of Martensite*, Oxford University Press, Oxford, 2004.

[273] J. Cumings and A. Zettl, Science **289**, 602 (2000).

[274] P. A. Williams, S. J. Papadakis, A. M. Patel, M. R. Falvo, S. Washburn, and R. Superfine, Phys. Rev. Lett. **89**, art. no. 255502 (2002).

[275] A. Fennimore, T. Yuzvinsky, W. Han, M. Fuhrer, J. Cumings, and A. Zettl, NATURE **424**, 408 (2003).

[276] B. J. Landi, R. P. Raffaelle, M. J. Heben, J. L. Alleman, W. VanDerveer, and T. Gennett, Nano Lett. **2**, 1329 (2002).

[277] M. Tahhan, V. T. Truong, G. M. Spinks, and G. G. Wallace, Smart Mater. Struct. **12**, 626 (2003).

[278] J. Naciri, A. Srinivasan, H. Jeon, N. Nikolov, P. Keller, and B. R. Ratna, Macromolecules **36**, 8499 (2003).

[279] H. Finkelmann and H. Wermter, Abstr. Pap. Amer. Chem. Soc. **219**, 189 (2000).

[280] A. R. Tajbakhsh and E. M. Terentjev, Eur. Phys. J. E **6**, 181 (2001).

[281] D. L. Thomsen, P. Keller, J. Naciri, R. Pink, H. Jeon, D. Shenoy, and B. R. Ratna, Macromolecules **34**, 5868 (2001).

[282] H. Finkelmann, E. Nishikawa, G. G. Pereira, and M. Warner, Phys. Rev. Lett. **87**, art. no. 015501 (2001).

[283] P. M. Hogan, A. R. Tajbakhsh, and E. M. Terentjev, Phys. Rev. E **65**, art. no. 041720 (2002).

[284] J. Kupfer and H. Finkelmann, Makromol. Chem.-Rap. Comm. **12**, 717 (1991).

[285] E. M. Terentjev, M. Warner, R. B. Meyer, and J. Yamamoto, Phys. Rev. E **60**, 1872 (1999).

Photo-mechanical actuation in polymer-nanotube composites

Samit V. Ahir and Eugene M. Terentjev*

Cavendish Laboratory, University of Cambridge,
Cambridge CB3 0HE, U.K.

* E-mail: emt1000@cam.ac.uk

February 12, 2005

Abstract

For some systems, energy from an external source can trigger changes in the internal state of the structure, leading to a mechanical response much larger than the initial input. The ability to unlock this *internal* work in a solid state structure is of key importance for many potential applications. We report a novel phenomenon of photo-induced mechanical actuation observed in a polymer-nanotube composite when exposed to infrared radiation. At small strains the sample tends to expand, when stimulated by photons, by an amount which is orders of magnitude greater than the pristine polymer. Conversely, at larger applied pre-strain, it will contract under identical infrared excitation. The behavior is modelled as a function of orientational ordering of nanotubes induced by the uniaxial extension. It is thought that no other materials can display this continuously reversing response and of so large magnitude, making rubber nanocomposites important for actuator applications.

It is the ability of certain actuator materials to change their dimensions upon application of a given stimulus, such as heat, electric voltage or light, that makes them such attractive systems to study. Actuators with differing characteristics and mechanisms have been widely adopted by industry to fill a variety of technological requirements [1]. Some actuators have a one-way response, while others are based on an equilibrium, reversible response to the given stimulus. Some (smart) materials exhibit a latent ability to actuate under the right conditions, such as shape-memory alloys [2] or liquid crystal elastomers [3]. Other systems require the blending of two (or more) distinctly different materials to impart a new physical response leading to the actuation process. The work presented here focuses on the second class of equilibrium mechanical actuation employing the use of carbon nanotubes embedded in a polymer matrix.

The sometimes complex behavior of multi-walled carbon nanotubes (MWCNTs) has heralded some interesting insight into the possibility of designing nanoelectromechanical

(NEMS) systems [4]. The actuator properties of individual bending MWCNTs under an applied electric field have been studied experimentally [22]. Their torsional actuator properties have also been reported [6, 7]. It is interesting to note that all these studies focus on individual MWCNTs and not a collection of tubes, nor their composite in a continuous elastic matrix. Little information is available on the actuation properties of nanotube assemblies or the effect they can have on material actuation properties when embedded in a polymer.

A few studies have recently appeared in the literature which attempt to look at the actuation behavior of polymer-nanotube composites [8, 9, 10]. However, important as they are, many of these studies have concentrated on accentuating the already present features of the host matrix by adding nanotubes. The nanotubes, in essence, exaggerate actuator behavior by either *improving* electromechanical responses or heating the sample more efficiently due to their inherent high conductivity [11]. Particularly new and important is the case of electrically stimulated mechanical contraction of MWCNTs embedded in liquid crystal elastomers [12]. The work of Courty *et al.* [12] was unique in that it details a novel electro-actuator response due to the presence of MWCNTs which otherwise would not occur in that system.

The present work introduces a new but simple polymer composite system (comparing with nematic elastomer composites of [12]) which, by the presence of MWCNTs, produces a mechanical response to the infrared (IR) irradiation. Remarkably, we obtain both a compressive and an expansive response modes depending on the external uniaxial strain applied to the composite sample. We assert that this behavior is dependent on nanotube orientation within a homogenous polymer matrix.

Multi-walled nanotubes (Nanostructured & Amorphous Materials, Inc.) are uniformly dispersed in polydimethylsiloxane (PDMS) at concentrations of 0.02, 0.5, 1, 4 and 7wt%. A schematic of the apparatus is given in fig. 1(a). For characterization purposes, the linear mechanical response of our nanocomposites have been tested for different nanotube loadings in the crosslinked PDMS matrix. As the concentration of MWCNTs is increased from zero to 4wt% loading, the rubbery network becomes stiffer and the Young modulus Y increases by a factor of two. This is expected and in line with literature findings [13, 14]. A detailed account for subtle variations in measured moduli can be garnered if consideration is given to the polymer-nanotube interface and relaxation of local stress in the composites, to be published elsewhere.

It is important to characterize nanotube alignment quantitatively. Wide angle X-ray diffraction is used as a method to determine the average tube orientation as a function of increasing applied uniaxial strain. Fig 1(b) shows characteristic features of the diffraction halos. This example is for a 7wt% sample, initially non-aligned, stretched by $\varepsilon = 0.33$ (33%). The Bragg peak around $3.40\mathring{A}$ corresponds to the (002) scattering plane which describes the inter-shell spacing periodicity within the multiwall tubes, see e.g. [15].

A question must arise about the bright scattering ring corresponding to the length scale $\sim 7.5\mathring{A}$. This is an interesting feature and is exactly the same in the pristine PDMS rubber prepared in the same batch. In the pristine PDMS network, with no solvent, the only X-ray contrast arises due to the difference in crosslink distribution. A very clear scattering length must be an indication of crosslink density fluctuations (in other terminology called clustering). As the extensive theory of this phenomenon suggests [16], at the given chain

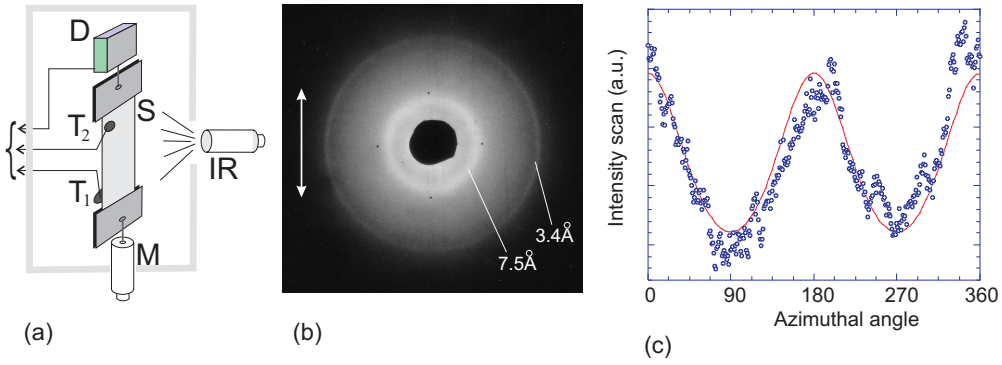

Figure 1: **Scheme of apparatus, X-ray scattering image and the azimuthal intensity scan. a.** The sample (S) is clamped in the frame with its length (e.g. pre-strain) controlled by the micrometer (M) and the exerted force measured by the dynamometer (D). Thermocouples (T_1 and T_2) are placed in front and behind, close to the sample surface. The actuation is provided by the light source (IR) uniformly illuminating the sample. The whole rig is enclosed in the thermally controlled compartment. A similar setup is employed when taking WAXS measurements. **b.** The X-ray image showing key scattering reflexes; the outer ring corresponding to $3.4\mathring{A}$ is the signal from the multiwall nanotubes. The inner ring is indicative of the correlation length of mesh size, see text. The arrow shows the direction of the aligning strain. **c.** The typical azimuthal intensity variation, $I(\beta)$, at a scattering angle corresponding to the outer (MWCNT, $3.4\mathring{A}$) ring. The data is fitted by the theoretical model of [17].

lengths and crosslinking density our PDMS network is well below the 'crosslink saturation threshold' and the correlation length of clustering should be of the order of mesh size. The length scale of $\sim 7.5\mathring{A}$ is very accurately this size and, accordingly, we believe this scattering to be produced by small scale crosslink density fluctuations (for comparison, same conditions of scattering from a non-crosslinked PDMS melt showed no such reflection). These should not affect macroscopic properties, or even the local MWCNT embedding.

As the applied uniaxial strain increases, the $3.4\mathring{A}$ (MWCNT) ring develops an increasing azimuthal bias [$I(\beta)$ in fig. 1(c)] indicating the orientational ordering of tubes. For instance, at the pre-strain value of $\varepsilon = 0.6$ (60%) this induced order reaches as high as $Q \sim 0.29$. As a comparison, samples which had been accidentally pre-stressed during preparation are shown to have a very low orientational order parameter, $Q \leq 0.005$. Therefore, composites with no significant initial alignment, on subsequent stretching reached much higher values of induced orientational order. We assume this is due to a much more rigid network surrounding the tubes and attempting to deform affinely, thus imposing significant orientational bias than a loosely crosslinked gel under similar deformation. Furthermore, the change in orientation on stretching is reversible, i.e. equilibrium. The details of this study of nanotube *reorientation* in a rubbery matrix are given in the Supplementary material.

There is an issue, well argued in the literature [18, 19], about whether a truly isotropic nanotube dispersion can be obtained. Regarding the tubes as rigid rods with extremely high aspect ratio, well dispersed in an amorphous medium, the Onsager transition to the sterically enforced orientational ordering could start at very low concentrations. We have as yet observed no clear indication of truly nematic liquid crystalline architecture in our system, although this could be due to a number of factors including matrix viscosity at sample preparation stage.

The intriguing response of our nanocomposite samples to infrared radiation is shown in fig. 2, presenting the data on stress measured in the 1wt% sample, initially non-aligned. It is important to spend some time and fully appreciate the information provided in this complex plot. At the start of experiment the sample has a 2% pre-strain ($\varepsilon = 0.02$) applied to it initially and has been allowed to mechanically equilibrate. Let us follow the first data set, which represents the 2%-strain line (the lowest curve in fig. 2). The plot shows the raw data of measured stress as a function of time of the experiment. The initial stress reading is simply the measure of Young's modulus $Y \approx 1.15$ MPa, and this value of stress is transferred as an open symbol to the plot in fig. 3. At a certain moment of time the IR light source is switched on and the stress reading changes. In this case (for 2% pre-strain) the change is downwards, meaning that the sample natural length has expanded on actuation. The new (IR-on) stress reading is transferred to the plot in fig. 3 as a filled symbol corresponding to the applied pre-strain of 2%. After a period of constant irradiation, during which the stress reading remains stable, the light source is switched off – and the stress reading returns to its original value. This experiment is then repeated with the same sample pre-strained at different values, up to 40%, as shown by the sequence of stress-reading curves, fig. 2, and the corresponding pairs of stress-strain points, with and without IR stimulation, in fig. 3. A question of possible sample degradation may be asked: we have deliberately conducted this type of experiment in the random sequence of pre-strain/equilibration cycles. The evidently consistent trend proves the reversibility of the sample state.

The first main conclusion we make is the unambiguous and significant photo-actuation response of PDMS nanocomposites. However, the immediate next question is this photo-

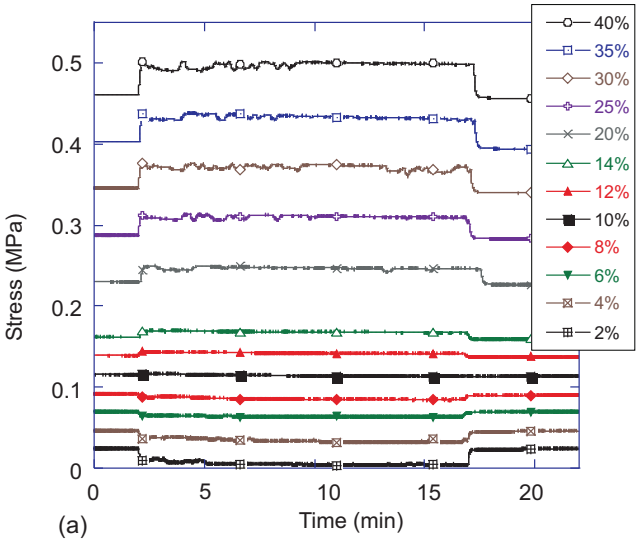

Figure 2: **Response to IR radiation at different values of pre-strain:** raw data on stress measured at fixed sample length of a 1wt% nanocomposite (different pre-strain curves labelled on the plot). A fixed pre-strain is applied to each given sample, which is then allowed to relax for a minimum of 10 minutes. Readings of stress are taken for 2 minutes and then the IR source is switched on to full intensity. After 15 minutes of exposure, the light source is switched off and further relaxation data is collected. This protocol is repeated for the same sample but at a different applied pre-strain ε after it has been equilibrated. Each sample is tested under a range of applied pre-strains between 2% and 40%.

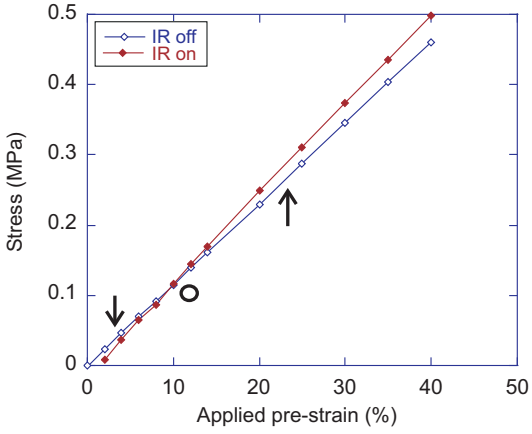

Figure 3: **Stress-strain variation under IR irradiation.** The data from fig. 2 for 1wt% nanocomposite – ○: in equilibrium, ●: on IR actuation, highlighting the opposite direction of actuation at different pre-strains, evident in fig. 2, and the crossover at $\varepsilon^* \approx 0.1$ (10%).

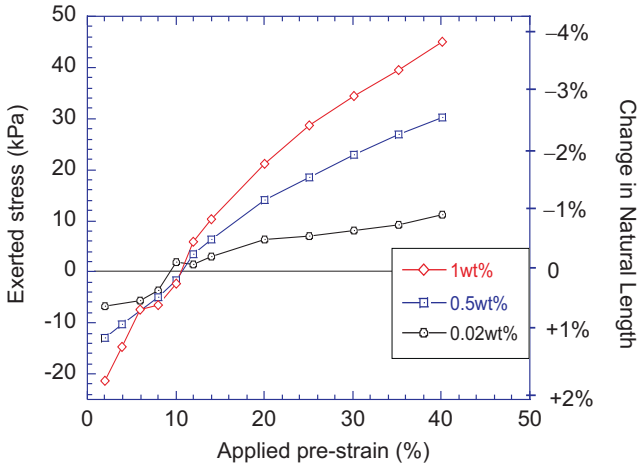

Figure 4: **Summary of IR response.** The magnitude (in kPa) of exerted actuation stress (the height of steps in fig. 2), as a function of pre-strain, for samples with increasing MWCNT loading. The right y-axis shows the corresponding actuation stroke: the change in natural length L_0 on IR irradiation.

mechanical response changing sign at a certain level of uniaxial pre-strain. In other words, equilibrium or weakly stretched composites show the reversible *expansion* on irradiation, while highly stretched ones show the much stronger tendency to *contract* (hence the increase in the measured stress). This is the central result of this paper and we shall spend some time discussing and analyzing it. There are two main questions: what is the mechanism of photo-mechanical response, and why does it change its macroscopic signature on sample extension?

Figure 4 summarizes the actuation effect by plotting the magnitude of stress step in the IR-on state, at different levels of pre-strain and for samples with increasing MWCNT loading. Although this is not explicitly measured in our (isostrain) experiment, we can directly calculate the change of the underlying natural length of the samples on actuation. This is shown on the right axis of the same plot, explicitly illustrating the regions of expansion and contraction. Remarkably, all samples with different nanotube loading appear to have a crossover at the same point, around 10% pre-strain (the increase in the effect amplitude with loading is to be expected).

There is no noticeable change in the reading of stress, fig. 2, with time after the IR source is switched on. This means that the heat transfer from the irradiated sample face into its bulk plays no significant role in the mechanism of mechanical actuation. The effect is highly reproducible, over many cycles of irradiation, which leads us to conclude no degradation due to non-radiative photon decay takes place in the nanocomposite samples. For comparison, the pristine PDMS rubber in the same experiment shows a very minor stress response, 2 orders of magnitude smaller than in fig. 2, which we attribute entirely to the sample temperature change on IR irradiation. The change in temperature by infrared heating is unavoidable and reaches $\Delta T \sim 15^{\circ}$C maximally, in our setting. This highlights

an important question as to whether the response is due to the photon absorption or the plain heat transfer. Though not presented in detail here, we have studied the mechanical response purely due to the temperature change. The temperature results are an order of magnitude smaller than in the case of IR-stimulation. The conclusion we reach is that such an effect does exist (i.e. the MWCNT-loaded composite has a stronger mechanical response than a pristine polymer on the same change ΔT) but its value is insignificant in comparison with the direct IR-photon absorption mechanism.

We believe the reason behind the change of actuation direction on increasing sample extension is due to the nanotube alignment. A simple affine model of induced orientational order gives the biased probability distribution of tube axes

$$P(\theta) = \frac{\lambda^{3/2}}{(\cos^2\theta + \lambda^{3/2}\sin^2\theta)^{3/2}}, \tag{1}$$

with uniaxial stretching factor $\lambda = 1 + \varepsilon$ (see Supplementary text for derivation). This corresponds to the data in fig. 1(c) and predicts the orientational order at relatively low pre-strains: $Q \approx \frac{3}{5}\varepsilon$. At the crossover point $\varepsilon^* \approx 0.1$, giving $Q^* \sim 0.06$. Let us now apply the same ideas about the induced orientational bias and averaging of the (hypothetical) individual nanotube response.

We assume this individual response is, in essence, a contraction – because this is what the better-aligned composite response is. It is easy to imagine why this could be for an initially rod-like tube: on photon absorption it may generate kink-instabilities, thus decreasing its net length. Let us simply assume that each nanotube, on IR stimulus, undergoes a contraction by a factor $\Delta < 1$ (certainly proportional to radiation intensity, which was kept constant in our work), accompanied by a transversely-isotropic volume conserving expansion $1/\sqrt{\Delta}$. This means that a local strain is created with the principal axes along the current nanotube orientation [at angle θ to the macroscopic z-axis, see fig. 5(a)]

$$\mathbf{\Lambda}(\mathrm{IR}) = \begin{pmatrix} 1/\sqrt{\Delta} & 0 & 0 \\ 0 & 1/\sqrt{\Delta} & 0 \\ 0 & 0 & \Delta \end{pmatrix}.$$

The projection of this local strain on the macroscopic axis of sample extension (and force measurement) is

$$\lambda_z(\mathrm{IR}) = \Delta\cos^2\theta + (1/\sqrt{\Delta})\sin^2\theta. \tag{2}$$

When we average this local contribution with the probability to find the nanotube at this orientation, $P(\theta)$, it will produce an estimate of the effective stroke of actuation $(\lambda_z - 1)$ or, if multiplied by the corresponding Young modulus, the exerted stress of fig. 4. Such a model is very crude indeed, ignoring a large number of undoubtedly important and delicate factors of continuum elasticity and nanotube morphology. However, it is elastically self-consistent and has only one parameter Δ that carries all the underlying complexity of the nanotube problem in it.

The orientational averaging is straightforward:

$$\begin{aligned} \langle\lambda_z\rangle &= \int_0^{\pi} [\Delta\cos^2\theta + (1/\sqrt{\Delta})\sin^2\theta] P(\theta)\, \tfrac{1}{4\pi}\sin\theta d\theta d\varphi \\ &\approx \tfrac{1}{3}\left(\Delta + 2/\sqrt{\Delta}\right) - \tfrac{2}{5}\varepsilon\left(1/\sqrt{\Delta} - \Delta\right) \end{aligned} \tag{3}$$

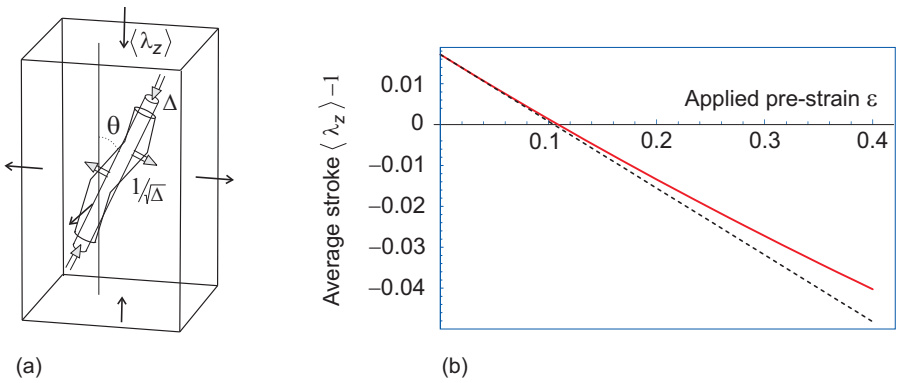

Figure 5: **Scheme of local and macroscopic strains, and the prediction of the actuation model. a.** The scheme illustrating how the distortion (kinking or undulation) of an individual tube, lying at an angle θ to the alignment axis, projects on the z-axis to contribute to the macroscopically uniaxial strain, eq. (2). **b.** The result of theoretical modelling based on orientational averaging of local deformations from each nanotube, eq. (3); the dashed line shows the linear approximation at small pre-strain ε. Nanotube contraction factor is chosen $\Delta = 0.8$, as suggested by the crossover strain value $\varepsilon^* \sim 0.1$.

Although the integral above has a full analytic form, it is more transparent to give its limit at small imposed pre-strain ε. This shows the key point: at very low pre-strain, $\varepsilon \to 0$, the average actuation stroke of the disordered nanocomposite is a positive $(\lambda_z - 1)$, i.e. the expansion of its natural length. However, above the threshold pre-strain ε^* this average deformations becomes negative, i.e. the contraction. It is easy to find

$$\varepsilon^* \approx \frac{5(2 - \Delta^{1/2} - \Delta)}{6(1 + \Delta^{1/2} + \Delta)}, \tag{4}$$

so that the prediction would be to observe the crossover at $\varepsilon^* \sim 0.1$ if the nanotube response factor $\Delta \sim 0.8$, that is, on IR-irradiation the nanotube itself contracts overall by ∼20%. The value is higher than one might expect, considering reports in the literature of nanotube strains of only 1-2%. However, as fig. 5(a) indicates, our proposition is not that of the lattice strain of nanotube walls but a contortion of the tube as a whole. Although this has not been yet directly observed and reported in the literature, a similar effect of resonant undulation has been seen (in simulation [21] and in experiment [22]) in response to distortion beyond the linear regime. Although in our system the tubes respond under totally different conditions, embedded in an elastic matrix under strain and absorbing the IR photons, the overall distortion factor of 20%, suggested by the model fit, is perhaps not altogether unreasonable.

Figure 5(b) plots the full (non-expanded) result of orientational averaging of actuation stroke $(\langle\lambda_z\rangle - 1)$ from eq.(3) to illustrate the points discussed here. The qualitative behavior (as summarized in fig. 4) is reproduced here almost exactly, including the magnitude of the predicted actuation stroke (that is, the ratio $L_0(\mathrm{IR})/L_0(0) - 1$). Therefore, it is very likely that the orientational feature of the effect, with its change of actuation direction

at a critical level of induced alignment, is captioned correctly, while much more work is required to understand the individual nanotube response to IR radiation generating the phenomenological factor Δ used in this analysis.

To summarize, this work describes a low-concentration composite of carbon nanotubes embedded in a crosslinked rubbery matrix, which exhibits rich actuation phenomena under infrared irradiation. The material shows the ability to change its actuation direction, from expansive to contractive response, as greater imposed strain is applied to the sample. The effect has not been seen before for any material and is thought to be completely novel. The suggested model attributes this crossover to the orientational ordering imposed on nanotubes by uniaxial extension; a number of other experimental findings support this conclusion.

The strength of photo-actuator response, at a given radiation intensity, is of the order of tens-kPa. Translated into the stroke, this corresponds to actuation strains of $2 - 4\%$. As expected, the response increases at higher nanotube loading. The similar (thermal actuation) behavior is also observed when the samples are heated by the same amount, but this has an order of magnitude lower amplitude.

Understanding the nature of the actuator mechanisms in this system certainly warrants further theoretical and experimental investigation. Many questions remain completely unclear, in particular, the response of an individual nanotube, embedded in a polymer matrix, to infrared photons. It is also not clear what the effect would be if different types of nanotube were used i.e. smaller multi-wall diameters, single-wall tubes, etc. Future investigations may also want to address the issue of using another host matrix and confirm its relatively neutral role in the actuation mechanism.

With actuating materials already used in such widespread applications, from micromanipulators to vibration control, the discovery of a structure that can respond to stimulus in both directions may open new possibilities and could mean an important new step toward finding applications for nanotube based materials above and beyond improvements in existing carbon fibre technologies.

Methods

Multi-walled nanotubes (Nanostructured & Amorphous Materials, Inc.) are used with purity verified (using SEM) as >95%. These nanotubes were not surface-modified at any time during processing.

The polymer matrix is PDMS (Polydimethylsiloxane) Sylgard 184^{TM} silicone elastomer from Dow Corning, USA. In pristine condition this crosslinks with hydrosilane crosslinker, the curing agent supplied with Sylgard 184^{TM} by Dow Corning, forming a uniform solvent-free elastomer. We have verified (with SEM on microtomed and on freeze-fractured surfaces) that the resulting polymer network is pure crosslinked PDMS with no filler particles, as sometimes is the case with supplied elastomer mixes.

The nanotube-polymer composites are fabricated by first carefully weighing the desired quantity of nanotubes and PDMS polymer. Calculations of weight percentage take into account the crosslinker, to be later used in the mixture. The viscous fluid is sheared using an Ika Labortechnik mixer for a minimum of 24 hours.

Crosslinker is added to the mixture after 24 hours. The ratio of cross-linker to PDMS is 1:10, according to Sylgard 184^{TM} specification, ensuring negligible sol fraction after preparation of pristine network. The sample is then further sheared for another 30 seconds before being placed in vacuum for 5 minutes, at all times remaining at ambient temperature to ensure little crosslinking reaction takes place in this time. This suitably removes the air cavities that unavoidably form during processing. It is then deposited in a specially designed reactor (centrifuge compartment with PTFE film strip lining its inner wall) and placed in a centrifuge at 5000rpm and 80°C. At this temperature the PDMS crosslinking is much faster.

The quality of nanotube dispersion is monitored throughout the processing with the use, initially, of optical microscopes and later with a High-Resolution Scanning Electron Microscope (HRSEM, Phillips XL 30 series) as aggregate sizes reduce well below optical resolution. We find that a shearing regime lasting 24 hours is suitable in removing nanotube aggregates due to the inherently high viscosity of the host polymer. Samples are identified by the wt% of MWCNTs mixed with the PDMS. Most experiments have been conducted on the 0, 0.02, 0.5, 1, 4 and 7wt% MWCNTs in PDMS elastomer films. In all cases the sample dimensions were kept approximately the same, 30× 1.5mm, with the film thickness 0.2mm, so that the area exposed to radiation was $\sim$0.45cm^2 and the cross-section area for calculating stress was $\sim 3 \cdot 10^{-6}$m^2.

A 25g Dynamometer (from Pioden Systems Ltd) was housed in a custom made thermal-control box with an open front end. The device, together with two independent thermocouples, outputs data via a DAQ card to a PC, see fig. 1(a). Distances between the clamps was controlled using a securely fitted micrometer with $\pm$0.001 mm accuracy. The rig is calibrated with weights to give a direct measure of stress and strain. The light source (Schott KL1500 LCD, maximum intensity at $\approx$675 nm, 702 μW cm^{-2}@1 m distance) was positioned 20 mm$\pm$0.02 mm from the sample surface. Calculation suggests that the total power of light delivered to the sample was of the order $\sim$ 0.008W. Additionally, the technique used to measure temperature involves placing the thermocouples on the sample surface itself. Hence, the $\sim$15°C increase in temperature is truly a measure of temperature change across the surface. This is not a microscopic measure of temperature throughout the sample, however, the same techniques have been repeated for every experimental run with the thermocouples manually placed at differing regions over the sample and the same relative change is always recorded.

Standardization across all samples is carried out through pre-experimental checks involving accurately finding the zero strain value of each experimental setup and calibrating the test rig from this point. Readings of stress are taken for 2 minutes, to verify that the material is equilibrated in its 'natural' pre-strained state, and then the IR source is switched on to full intensity. After 15 minutes of exposure, the light source is switched off and further relaxation data is collected for the remaining 15 minutes. This protocol is then repeated for the same sample but at a higher applied pre-strain ε. Each sample is tested under a range of applied pre-strains between 2% and 40% ($0.02 \leq \varepsilon \leq 0.4$) .

As a comparison the same experiment is carried out on the 1wt% MWCNT sample, but the infrared source is replaced by a mica-insulated heater (Minco Products Inc.) mounted approximately 10mm away from the sample.

Wide angle X-ray diffraction measurements were carried out on a Phillips PW1830 Wide Angle X-Ray generator (WAXS) using $Cu_{K_{\alpha 1}}$ radiation (=1.54$\mathring{A}$), running at 40 kV and

40 mA. Azimuthal curves, were generated as detailed in classical literature, as well as in more recent treatment [20] specifically for nanotubes. The azimuthal intensity variation of the arcs at the scattering angle corresponding to MWCNT (002) layer periodicity of $3.4\mathring{A}$ allows calculation of the degree of orientation.

Relative intensity along the azimuthal arcs, $I(\beta)$ (cf. fig. 1(c)), is the signature of the orientational distribution function; when approximated as a Legendre polynomial series in $\cos\beta$, it gives a direct measure of the (Herman's) orientational order parameter, in this context often called S_d, or $Q \equiv \langle P_2 \rangle = \frac{1}{2}(3\langle \cos^2 \beta \rangle - 1)$, where the averaging is performed with $I(\beta)$ as the distribution function. The more advanced method of orientational order parameter analysis [17] gives similar values. See Supplementary text for details.

Mechanical testing has been conducted on the same dynamometer rig, fig 1(a), finding the quasi-static stress-strain relationship on uniaxial stretching narrow strips of PDMS nanocomposites. In the linear regime of small strains this identifies the equilibrium Young modulus, from $\sigma = Y\,\varepsilon$.

References

[1] Huber, J. E., Fleck, N. A. and Ashby, M. F. The selection of mechanical actuators based on performance indices. *Proc. Roy. Soc. A*, 453(1965):2185–2205, 1997.

[2] Battacharya, K. *Microstructure of Martensite*. Oxford University Press, 2004.

[3] Warner, M. and Terentjev, E. M. *Liquid Crystal Elastomers*. Oxford University Press, 2003.

[4] Cumings, J. and Zettl, A. Low-Friction Nanoscale Linear Bearing Realized from Multiwall Carbon Nanotubes. *Science*, 289(5479):602–604, 2000.

[5] Poncharal, P., Wang, Z. L., Ugarte, D. and de Heer, W. A. Electrostatic deflections and electromechanical resonances of carbon nanotubes. *Science*, 283(5407):1513–1516, 1999.

[6] Williams, P. A., Papadakis, S. J., Patel, A. M., Falvo, M. R., Washburn, S. and Superfine, R. Torsional response and stiffening of individual multiwalled carbon nanotubes. *Phys. Rev. Lett.*, 89(25):art. no.–255502, 2002.

[7] Fennimore, A.M., Yuzvinsky, T.D., Han, W.Q., Fuhrer, M.S., Cumings, J. and Zettl, A. Rotational actuators based on carbon nanotubes. *Nature*, 424(6947):408–410, 2003.

[8] Landi, B.J., Raffaelle, R.P., Heben, M.J., Alleman, J.L., VanDerveer, W. and Gennett, T. Single wall carbon nanotube-nafion composite actuators. *Nano Letters*, 2(11):1329–1332, 2002.

[9] Koerner, H., Price, G., Pearce, N.A., Alexander, M. and Vaia, R.A. Remotely actuated polymer nanocomposites - stress-recovery of carbon-nanotube-filled thermoplastic elastomers. *Nature Materials*, 3(2):115–120, 2004.

[10] Tahhan, M., Truong, V.T., Spinks, G.M. and Wallace, G.G. Carbon nanotube and polyaniline composite actuators. *Smart Mater. Struct.*, 12(4):626–632, 2003.

[11] Naciri, J., Srinivasan, A., Jeon, H., Nikolov, N., Keller, P. and Ratna, B.R. Nematic elastomer fiber actuator. *Macromolecules*, 36(22):8499–8505, 2003.

[12] Courty, S., Mine, J., Tajbakhsh, A.R. and Terentjev, E.M. Nematic elastomers with aligned carbon nanotubes: New electromechanical actuators. *Europhys.Lett.*, 64(5):654–660, 2003.

[13] Gorga, R.E. and Cohen, R.E. Toughness enhancements in poly(methyl methacrylate) by addition of oriented multiwall carbon nanotubes. *J. Polym. Sci. B - Polym. Phys.*, 42(14):2690–2702, 2004.

[14] Harris, P.J.F. Carbon nanotube composites. *Int. Mater. Rev.*, 49(1):31–43, 2004.

[15] Charlier, J.C. and Michenaud, J.P. Energetics of multilayered carbon tubules. *Phys. Rev. Lett.*, 70:1858–1861, 1993.

[16] Panyukov, S.V. and Rabin, Y. Statistical physics of polymer gels. *Phys. Rep.*, 269(1-2):1–131, 1996.

[17] Deutsch, M. Orientational order determination in liquid-crystals by X-ray diffraction. *Phys. Rev. A*, 44(12):8264–8270, 1991.

[18] Somoza, A.M., Sagui, C. and Roland, C. Liquid-crystal phases of capped carbon nanotubes. *Phys. Rev. B*, 6308(8):art. no.–081403, 2001.

[19] Islam, M.F., Alsayed, A.M., Dogic, Z., Zhang, J., Lubensky, T.C. and Yodh, A.G. Nematic nanotube gels. *Phys. Rev. Lett.*, 92(8):art. no.–088303, 2004.

[20] Jin, L., Bower, C. and Zhou, O. Alignment of carbon nanotubes in a polymer matrix by mechanical stretching. *Appl. Phys. Lett.*, 73(9):1197–1199, 1998.

[21] Yakobson, B. I. and Bradec, C. J. and Bernholc, J. Nanomechanics of carbon tubes: instabilities beyond linear response. *Phys. Rev. Lett.*, 76(14):2511–2514, 1996.

[22] Poncharal, P. and Wang, Z. L. and Ugarte, D. and de Heer, W. A. Electrostatic deflections and electromechanical resonances of carbon nanotubes. *Science*, 283(5407):1513–1516, 1999.

Acknowledgments

We thank S. Courty, G. Lagubeau, A.R. Tajbakhsh, A.M. Squires and H. Körner for useful discussions. We also thank A. Hayer for assistance with calibration of the light source. This work was carried out with the support of the EPSRC, the EOARD (FA8655-04-1-3018), the ESA-ESTEC (18351/04) and a CASE award from Makevale Ltd.